Journal of the OPTICAL SOCIETY *of* AMERICA

VOLUME 30
No. 9

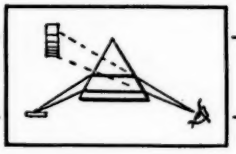

SEPTEMBER
1940

Editorial Comment: Opportunities for Research 367

Symposium on Optical Methods for Study of Molecular Structure:

I. The X-Ray Diffraction Method . . . . . B. E. WARREN 369

II. Electronic Diffraction Method . . . . . LOUIS R. MAXWELL 374

III. Raman Spectra Method . . . . . GEORGE M. MURPHY 396

Transmission of Infra-Red Light by Fog . . . . . J. A. SANDERSON 405

Refractive Index of Matter in Cylindrical Form . . . . . A. H. PFUND 410

Use of Step Weakeners in Photographic Photometry . . . . . GEORGE E. MOORE AND HAROLD W. WEBB 413

Properties of the Witch of Agnesi—Application to Fitting the Shapes of Spectral Lines . . . . . ROY C. SPENCER 415

Density of Silicate Glasses as a Function of Composition . . . . . MAURICE L. HUGGINS 420

Investigation of Thin Evaporated Silver Films on Glass . JOHN STRONG AND BARRY DIBBLE 431

The Prism and the Theory of Optical Resolution . . . . . B. P. RAMSAY, O. T. KOPPIUS AND E. L. CLEVELAND 439

Experiments to Test the Rebromination Theory of Photographic Solarization . . . . . J. H. WEBB AND C. H. EVANS 445

There is System in Color Preferences . . . . . J. P. GUILFORD 455

New Polaroid Study Lamp 460

Published monthly
at Prince and Lemon Sts., Lancaster, Pa.
by the
AMERICAN INSTITUTE OF PHYSICS
Incorporated
175 Fifth Avenue, New York, N. Y.
FOR AND UNDER THE EDITORIAL SUPERVISION OF
THE OPTICAL SOCIETY OF AMERICA

BOSTON UNIVERSITY
COLLEGE OF LIBERAL ARTS
LIBRARY

THE OPTICAL SOCIETY OF AMERICA

Officers of the Society

K. S. GIBSON, *President*
National Bureau of Standards
Washington, D. C.

A. G. WORTHING, *Vice President*
University of Pittsburgh
Pittsburgh, Pennsylvania

ARTHUR C. HARDY, *Secretary*
Massachusetts Institute of Technology
Cambridge, Massachusetts

HENRY F. KURTZ, *Treasurer*
Bausch & Lomb Optical Company
Rochester, New York

The Board of Directors consists of the above officers; the Editor of the Journal; the Past President; and five directors-at-large.

R. C. GIBBS, *Past President*
Cornell University
Ithaca, New York

GEORGE R. HARRISON, *Editor*
Massachusetts Institute of Technology
Cambridge, Massachusetts

Directors-at-Large

J. W. BEAMS
University of Virginia
Charlottesville, Virginia

H. P. GAGE
Corning Glass Works
Corning, New York

RUDOLF KINGSLAKE
Eastman Kodak Company
Rochester, New York

WILLIAM F. MEGGERS
National Bureau of Standards
Washington, D. C.

BRIAN O'BRIEN
University of Rochester
Rochester, New York

Rochester, New York, Section of the Optical Society of America

B. O'BRIEN, *President* R. B. HORSFALL, JR., *Vice President* D. L. MACADAM, *Secretary* J. W. GILLON, *Treasurer*
Councillors: H. F. KURTZ, J. H. MCLEOD, C. J. STAUD, T. R. WILKINS, R. E. BURROUGHS (*ex officio*)

Corporation Members of the Optical Society of America

AMERICAN OPTICAL COMPANY, Southbridge, Massachusetts
BAUSCH & LOMB OPTICAL COMPANY, Rochester, New York
BELL TELEPHONE LABORATORIES, INC., New York, New York
CORNING GLASS WORKS, Corning, New York
GAERTNER SCIENTIFIC CORPORATION, Chicago, Illinois
INTERCHEMICAL CORPORATION, New York, New York
KEUFFEL & ESSER COMPANY, Hoboken, New Jersey
SPENCER LENS COMPANY, Buffalo, New York
ARTHUR H. THOMAS COMPANY, Philadelphia, Pennsylvania

THE OPTICAL SOCIETY OF AMERICA was organized in 1916 "*to increase and diffuse the knowledge of optics in all its branches, pure and applied, to promote the mutual interests of investigators of optical problems, of designers, manufacturers and users of optical instruments and apparatus of all kinds and to encourage cooperation among them.*" It aims to serve the interests of all who are engaged in any branch of optics from fundamental research to the manufacture of optical goods.

MEMBERSHIP

Regular Members: "Any person who has contributed materially to the advancement of optics is eligible for regular membership."

Associate Members: "Any person who is interested in optics is eligible for associate membership."

Corporate Members: "Any corporation desirous of encouraging the work of the Society is eligible for corporation membership"

The Society cordially invites to membership all who are interested in any branch of optics, either in research, in instruction, in optical or illuminating engineering, in the manufacture and distribution of optical goods of all kinds or in physiological and medical optics.

ANNUAL DUES

Regular members, $7.50; Associate members, $5.00; Corporate members, $50.00. These dues include subscription to the Society's official journal, the *Journal of the Optical Society of America.*

MEETINGS

The Society holds two meetings per year: An annual meeting in the autumn and a midwinter meeting jointly with the American Physical Society.

All changes of address of members of the Optical Society of America should be communicated to the Secretary, Professor Arthur C. Hardy, Massachusetts Institute of Technology, Cambridge, Massachusetts.

Journal of the
OPTICAL SOCIETY *of* AMERICA

VOLUME 30 SEPTEMBER, 1940 NUMBER 9

Editorial Comment

OPPORTUNITIES FOR RESEARCH

THE Optical Society of America is fortunate in having come into existence at a time when it was unnecessary to overcome the indifference—not to say prejudice—formerly experienced by some of the older scientific societies. The whole world today recognizes its debt to the scientist. The graduates of our universities need no longer look forward to teaching as the only career open to them, for biologists, chemists, physicists are demanded by the industries in increasing numbers.

Realizing the extent to which the advances of applied science depend directly on the advances of pure science, the Optical Society may well consider the means available for actively promoting research in the several branches of Optics.

The Society itself cannot, as a society, engage directly in research. But there are several ways in which it can actively further the prosecution of research.

For example, there are, throughout the country, a large number of potential investigators who simply need encouragement, or the suggestion of some specific problem, to get a start on research. Many a promising young scientist, after graduation, has found a place as teacher in some smaller university, where, lacking the inspiration of co-workers, or perhaps of suitable apparatus, he has gradually lost his enthusiasm and has become content to use his full time in the routine duties of teaching. There are over 500 colleges in the United States, but only a very small proportion of them can be classed as contributors to the work of the several scientific societies. One of the most potent means for utilizing, to the full, our research facilities is to take active and immediate steps to enlist the services of these men who, not being required to do research, are content to sit aside and watch others.

It is true that the university is the home of pure science. But the average university regards the doing of research not as a duty but as a privilege, freely or grudgingly extended, as the case may be. There are many who regard this attitude as inadequate—perhaps even unworthy of the university of today. The doing of research should be a part of the duties of every university professor, on a par in every way with teaching. The Optical Society can further the general recognition of this principle by creating on the part of those (at present) scientifically inactive teachers a demand for research facilities.

What is needed is suitable machinery for

The Twenty-Fifth Annual Meeting
of the
Optical Society of America
will be held in
Rochester, New York,
October 3, 4, and 5,
1940

BOSTON UNIVERSITY
COLLEGE OF LIBERAL ARTS
LIBRARY

collecting a variety of specific research problems and placing them before potential investigators, either through the columns of the Journal or otherwise, with such individual encouragements as may be necessary to ensure a start on the work.

The collection of such problems should not be difficult in a society like the Optical Society, which is composed of both the pure science and the applied science groups of workers. We hear much today about the utilization of by-products. The by-product of any scientific investigation is a large number of problems more or less closely connected with the work in hand, but which must be absolutely passed by if the investigator is to proceed along the main lines of his investigation. These side issues, if they be followed out, frequently lead to results of quite as much importance as the original problem. The discovery of the phenomenon of photoelectricity by Hertz is a case in point. An important part of the report of any investigation should be a brief summary of such side problems as the investigator is willing to pass on to his fellow workers.

The increasing importance of the work of the scientist has imposed on him new obligations. What these obligations are, and how they can best be met, are questions which are being considered by a number of scientific societies and organizations at work on the problem of utilizing and organizing our research facilities. Whatever be the lines along which such organization takes place, due recognition must be given to the fact that advance in science is almost exclusively due to the insatiable curiosity of the individual; to his desire to "learn the truth" regardless of what its ultimate value measured in material standards may be. Any organization of research must therefore leave the individual worker, once started, free to follow paths of his own choosing. Perhaps in this connection the phrase "cooperation in research" is preferable to "organization of research." The latter implies a central agency directing research toward a definite end. The former suggests the banding together of individuals whose interests are mutual. It is the case of the monarchy as contrasted with the democracy.

In other words, the Optical Scoiety should not be content to hold meetings a few times a year and to publish a journal. Its opportunities extend far beyond these functions, which up to the present time have been the chief, if not the only, activities engaged in by many societies.

* * * * * *

The Editors point with pride to the above remarks as forming one of the most cogent editorials which have appeared in the Journal for a long time. They were written by F. K. Richtmyer. They constitute the first words printed in the newly founded *Journal of the Optical Society of America*, Volume 1, Number 1.

This editorial is reprinted almost verbatim, with a tense changed here and there to conform to the passage of time. Its inclusion is appropriate, not merely because these pages will appear shortly before the 25th annual meeting of the Optical Society, but because the opinions expressed are as timely today as they were when originally written.

Symposium on Optical Methods for Study of Molecular Structure

I. The X-Ray Diffraction Method*

B. E. WARREN
Massachusetts Institute of Technology, Cambridge, Massachusetts
(Received June 7, 1940)

I. INTRODUCTION

THE x-ray diffraction method for studying molecular structure is essentially an interference method. The direct information obtained is purely geometrical; interatomic distances, relative positions of the atoms, and in favorable cases the complete geometrical configuration of the molecule. Any other information such as the kind of bonding between two atoms must be deduced from the measured interatomic distances or the kind of neighboring atoms.

In the usual experimental arrangement, an approximately monochromatic x-ray beam is collimated by passing through two pinholes and allowed to fall upon the diffracting sample. The radiation used is generally the $K\alpha$ doublet partially monochromated by filtering or crystal reflection. A radiation used extensively is the Cu $K\alpha$ doublet $\lambda=1.54$A. Under the influence of the primary x-ray beam, the electrons in the diffracting sample are set into forced oscillation, giving rise to scattered radiation which is emitted by each atom in all directions. For the unmodified component of the scattered radiation from the various atoms, coherence exists, and accordingly there will be interference effects. In some directions the intensity of scattered radiation will be large and in other directions small. From observations of the intensity of scattering in various directions, we get information about the path differences for scattered radiation coming from the various atoms, and from the path differences we can draw conclusions about the spacial arrangement of the scattering atoms. By x-ray diffraction methods molecular structure can be studied in all three states; gaseous, liquid, and crystalline solid.

II. GASEOUS STATE

The x-ray diffraction study of molecular structure in the gaseous state was developed by Debye.[1] An x-ray beam is allowed to fall upon a gas held in a container, and the scattered radiation passing out through a thin window is recorded either photographically or with an ionization chamber. A scattering curve is obtained which shows peaks and dips, the amount of detail in the scattering curve corresponding to the amount of structure in the molecule.

Considering the molecule as a rigid array which takes with equal probability all possible orientations in space, the intensity of the scattered radiation per molecule is given by

$$I=\sum_m \sum_n f_n f_m \frac{\sin sr_{mn}}{sr_{mn}}, \qquad (1)$$

where I is the intensity in electron units, f_n is the atomic scattering factor of atom n,

$$s=4\pi \sin \theta/\lambda,$$

and r_{mn} is the distance from atom m to atom n.

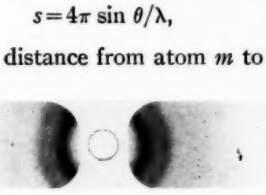

FIG. 1. X-ray diffraction pattern of water at 1.5°C.

The intensity is given as a function of the angle of scattering, through the variable s. The intensity depends upon the molecular structure through the interatomic distances r_{mn}. If one assumes a set of reasonable interatomic distances in the molecule, the intensity can be plotted out against $\sin \theta/\lambda$, using Eq. (1). This curve is then compared with the experimental curve, and

* Invited paper presented at the joint Symposium on Optical Methods for the Study of Molecular Structure, at the New York Meeting of the Optical Society of America and the American Physical Society, February 23, 1940.

[1] P. Debye, L. Bewilogua and F. Ehrhardt, Physik. Zeit. 30, 84 (1929).

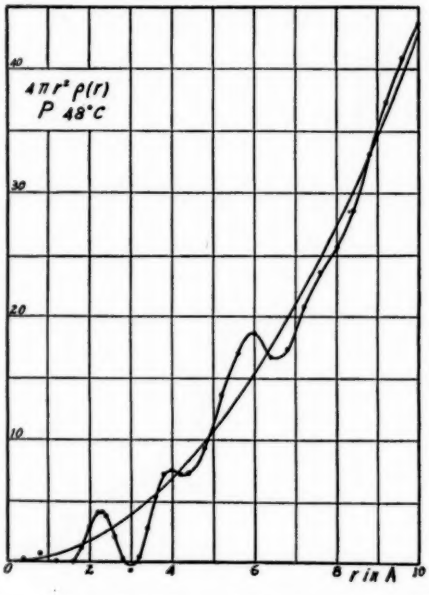

FIG. 2. The radial density distribution of atoms about any one atom in liquid yellow phosphorus at 48°C (Thomas and Gingrich).

changes made in the assumed interatomic distances until a satisfactory agreement is obtained between calculated and observed intensity curves.

It has turned out that for diffraction study of molecular structure in the gaseous state, electron diffraction is in many ways superior to x-ray diffraction. The electron diffraction methods are treated in another paper in this symposium. Very little x-ray diffraction work on molecular structure in gases has been done in recent years, and accordingly this method will be passed over.

III. LIQUIDS

The x-ray diffraction pattern of a liquid is a typical amorphous pattern consisting of several broad diffuse peaks. The diffraction pattern of water, shown in Fig. 1, is a typical liquid diffraction pattern. The interpretation of liquid patterns is usually done by the method of Fourier integral analysis.[2] By this method one obtains a radial distribution curve showing the number of atoms at any distance from each atom. In general there is serious confusion in distinguishing between intramolecular and intermolecular distances. However, it is usually the case that the peak corresponding to the shortest distance will be an intramolecular peak.

Figure 2 shows the radial distribution curve[3] obtained from the x-ray pattern of liquid phosphorus at 48°C. The first peak occurs at 2.25A, this value being interpreted as the P—P distance in the molecule. The area of the peak indicates that there are about 3 phosphorus neighbors at the distance 2.25A from each atom. These results are of course in excellent agreement with the idea of a P_4 molecule.

For very simple molecules considerable information about the molecular structure can be obtained from an x-ray study of the liquid. In general, however, there is so much overlapping of peaks and confusion of inter- and intramolecular effects that we must rule out liquid diffraction studies as a method of importance to the study of molecular structure.

IV. MOLECULAR CRYSTALS

It is in the study of molecular crystals that x-ray diffraction has made its greatest contributions to molecular structure determination. Before considering the subject, however, it might be well to discuss first what we mean by a molecular crystal. Rocksalt is an ionic crystal because it is made up of positive and negative ions Na^+ and Cl^-, each ion equidistantly surrounded by 6 ions of the opposite charge, there is no evidence of a molecule in the rocksalt structure. In a molecular structure such as that of ordinary sulphur, the molecule shows up as a clearly defined group of atoms in which the interatomic distances between nearest neighbors will be appreciably smaller than the shortest distances between atoms in different molecules. The short distances between atoms within the molecule correspond to strong bonding forces, while the larger distances between nearest atoms in different molecules indicate weaker bonding between the molecules, and corresponds to the generally low melting point of molecular crystals. Molecular crystals occur to limited extent among

[2] B. E. Warren, J. App. Phys. **8**, 645 (1937).

[3] C. D. Thomas and N. S. Gingrich, J. Chem. Phys. **6**, 659 (1938).

the elements and inorganic compounds, and are practically the general rule for organic materials.

The advantage to studying molecular structure in crystals is found in the fact that the molecule is tied down and can therefore be explored in three dimensions. One can determine not only interatomic distances but also the directions. Where it is possible to make a complete structure determination one finds the coordinates of each atom in the unit cell and has therefore a complete molecular configuration. For an average molecular crystal there are hundreds of diffracted beams and therefore sufficient data for a precise and unique determination of the molecular configuration.

Complete structure determinations for molecular crystals are usually made from rotation or oscillation patterns. A monochromatic x-ray beam falls upon a small single crystal of dimension 1 mm, or less, mounted so that it can be rotated continuously about a crystallographic axis. A typical example is the rotation pattern of quartz shown in Fig. 3. There are two steps in working out a crystalline structure; first the determination of the size and shape of the unit cell, and second the location of all the atoms within the unit cell. The first step is simple and straightforward, from a measurement of the positions of the spots on the diffraction pattern

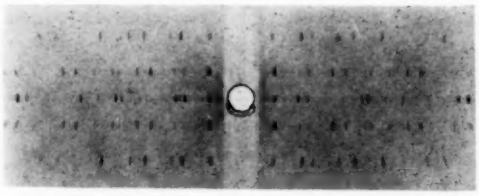

FIG. 3. X-ray rotation pattern of quartz, rotation about c axis, radiation Cu $K\alpha$.

the size of the unit cell is readily calculated. The positions of the atoms in the unit cell can be determined only from the intensities of the diffraction spots. For the diffracted beam of indices hkl, the amplitude of diffracted radiation per unit cell is given by

$$F_{hkl}=\sum_n f_n e^{2\pi i(hx_n/a+ky_n/b+lz_n/c)}, \qquad (2)$$

where x_n, y_n, z_n are the coordinates of atom n, f_n is the atomic scattering factor of atom n, and a, b, c are the crystal axes.

The intensities of the diffracted beams are given by

$$I_{hkl}=KF_{hkl}^2. \qquad (3)$$

For simple structures the old "trial and error" methods usually suffice. Using symmetry theory, known interatomic distances, and chemical information, it is possible to guess an approximate structure and thus determine a set of

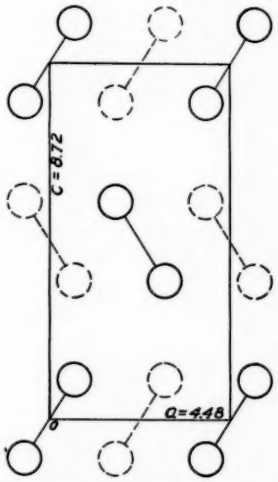

FIG. 4. Structure of crystalline bromine, showing Br_2 molecule. Dotted circles represent atoms above or below the plane of the paper by $b/2$.

tentative coordinates x, y, z, for all the atoms. The intensities of the diffracted beams are then calculated by Eqs. (2) and (3) and compared with the observed intensities. Small changes are then made in the assumed coordinates, until satisfactory agreement is obtained. In general the number of diffracted beams is many times the number of coordinates to be determined, and the structure is unique.

A simple molecular structure is that of bromine and iodine, shown in Fig. 4. Because of symmetry conditions two coordinates suffice to locate all the atoms in the unit cell. The Br_2 molecule stands out clearly in the figure. The Br—Br distance in the molecule is 2.27A while the closest approach of bromine atoms in different molecules is 3.3A.

Orthorhombic sulphur is another interesting

example of an element which forms a molecular crystal. The structure of the molecule is shown in Fig. 5. The unit cell contains 128 atoms but from symmetry considerations only 12 coordinates are involved and these are readily determined from the large number of intensities. The molecule is a puckered 8-atom ring with a S−S distance of about 2.12A and bond angle of 105°. Nearest atoms in neighboring molecules are at the larger distance of 3.3A.

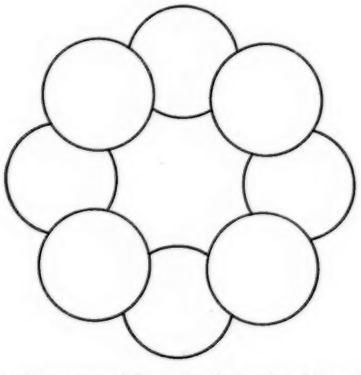

FIG. 5. Structure of S_8 molecule in rhombic sulphur.

An exceedingly simple organic molecular crystal is hexamethylenetetramine $C_6H_{12}N_4$. It crystallizes in the cubic system and with high enough symmetry so that only 2 parameters are needed to give the positions of all the carbon and nitrogen atoms in the molecule. The structure as determined by x-ray analysis is shown in Fig. 6. The positions of the hydrogens cannot be determined by x-ray methods. It is interesting to notice how clearly the molecules stand out in the structure, within the molecule the atoms are closely and tightly held together but the molecules themselves are well separated.

Another method of determining the atomic arrangement involves representing the electron density in the unit cell by a Fourier series.

$$\rho(x,y,z)=\frac{1}{V}\sum\sum_{-\infty}^{+\infty}\sum F_{hkl}e^{-2\pi i(hx/a+ky/b+lz/c)},$$
$$I_{hkl}=KF_{hkl}^2=KF_{hkl}\bar{F}_{hkl}. \tag{4}$$

The coefficients of the Fourier series are the structure factors F_{hkl}. The stumbling block of direct determination comes from the fact that the observed intensities determine only the square of the structure factor. In other words, we can determine experimentally the magnitude of the coefficients but not the phase. In general the series cannot be used.

In the phthalocyanines (free phthalocyanine $C_{32}H_{18}N_8$) studied by Robertson,[4] we have the interesting and unusual example of a complex molecular crystal for which all the phases can be determined and the Fourier series plotted out. This is because the cell has a center of symmetry and the F's are all real but either positive or negative. There is an isomorphous series of crystals with the free phthalocyanine and various metal derivatives. For the nickel derivative there is one Ni atom per molecule and the crystal symmetry requires this atom to be at a symmetry center, which can be taken at the origin. For the whole set of hOl reflections the Ni gives its full contribution with positive phase. The phase of all the hOl reflections can then be determined by comparing the measured F values for the free phthalocyanine with those for the nickel derivative.

Calling F_{Phth} the contribution to the structure factor due to the free phthalocyanine molecule alone, then assuming this to be the same for the free molecule and the nickel derivative, the following relations will hold.

$$\begin{array}{ll} \text{Free Phthalocyanine} & F_{hOl}=\pm F_{\text{Phth}} \\ \text{Ni Derivative} & F_{hOl}=F_{\text{Ni}}\pm F_{\text{Phth}}. \end{array} \tag{5}$$

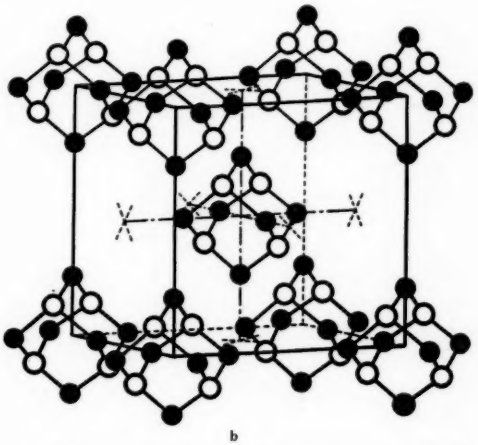

b

FIG. 6. Structure of hexa methylenetetramine $C_6H_{14}N_4$.

[4] J. M. Robertson, J. Chem. Soc. 1195 (1936).

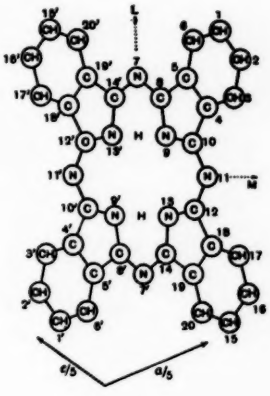

FIG. 7. Two-dimensional Fourier plot of electron density in a phthalocyanine molecule, compared with idealized molecular structure (Robertson).

By comparing the magnitudes of the measured F_{h0l} values for the free molecule and the nickel derivative it is obviously possible to determine the sign of the F_{h0l} values. Knowing both the magnitude and the sign of all the F_{h0l} coefficients, the two-dimensional Fourier series can be plotted out directly from experimental data. The plot is shown in Fig. 7, compared with an idealized molecular structure. With the exception of the hydrogens which cannot be detected by x-ray methods, every atom in the molecule is faithfully portrayed in the Fourier plot. From reflections involving the third dimension all the atomic coordinates and the orientation of the molecule are fixed. This is a very unusual case of a complex molecule being determined completely from x-ray data with no use being made of any chemical hunches as to the structural formula.

In general the phases cannot be determined. A Fourier series in which the coefficients are given by F_{hkl}^2 rather than F_{hkl} is one for which all necessary data could be directly detemined experimentally. Patterson[5] has recently shown that such an F^2 series has a physical significance. When plotted out it gives not the positions of atoms with respect to an origin but rather the displacement of each atom from every other atom. In such a series there is a great deal of overlapping of peaks and confusion in the interpretation. The Patterson plot does, however, represent all that the x-ray data alone can tell about the structure. By the use of the Patterson type series a number of complex molecular structures have been worked out which, without the Patterson method, would probably have been too difficult.

Having determined the interatomic distances in the molecule certain other conclusions can often be drawn from these distances. In general the stronger the bond between two atoms the closer they come together. In a system which may involve resonance between single bonding and double bonding the degree of single bond-double bond resonance can be estimated from the distance by comparing with the measured distances for simple substances.

A relatively new field is the application of x-ray diffraction studies to the crystalline proteins. The molecules are of course enormous and the number of coordinates needed to fix the position of each atom in the molecule is likewise enormous. Some of these complex biological materials, however, give diffraction patterns which are exceedingly rich in detail, and therefore contain a vast amount of information about these complex molecules. The work of interpretation will be slow and difficult, but the results will be of great interest, and the outlook is not by any means hopeless.

[5] A. L. Patterson, Phys. Rev. **46**, 372 (1934).

II. The Electronic Diffraction Method*

LOUIS R. MAXWELL
Bureau of Agricultural Chemistry and Engineering, Washington, D. C.
(Received July 9, 1940)

INTRODUCTION

IN this talk on the application of the electron diffraction method to a study of molecular structure, I shall be concerned entirely with gas molecules. Each molecule behaves as an independent diffracting unit so that the final analysis gives information on the structure of free molecules. First experiments showing electron interference phenomena by gas molecules were those by Mark and Wierl[1] and by Kirchner.[2] Since that time many investigators have taken advantage of this valuable tool for the determination of the structures of more than three hundred different molecules.[3] It has proved valuable to chemists in studies of the nature of the chemical bond by giving information concerning bond distances and the characteristic values of the bond angles which one atom makes with its neighbors. It has also proved useful in studies dealing with repulsive and attractive forces existing within particular molecules.

For the simpler types of molecules the electron diffraction results have had a direct bearing on the interpretation of band spectra. There have been opportunities for comparison between the electron and x-ray diffraction results in various instances.

THEORY

The electron diffraction method makes use of an early theory by Debye[4] and Ehrenfest[5] given for the scattering of x-rays from polyatomic gases. Each atom of the molecule is considered to have an electronic cloud which is spherically symmetrical about its nucleus, and in most cases the molecule is assumed to be a rigid configuration of these atoms. The theory has been developed to the point where this rigidity is not required so that the atoms may be considered as vibrating about their equilibrium positions in the usual manner as determined by the temperature of the gas. Atomic electron scattering is composed of two parts, the elastic and inelastic; the elastic scattering produces an interference pattern characteristic of the existing atomic configurations and the type of atoms present. The inelastic scattering, in which the electrons suffer energy losses at the time of collision, produces a general background whose intensity decreases rapidly with angle, resulting in a loss of definition in the interference pattern.

A general formulation of the complete intensity distribution is given by the following equations:

$$I(x)=N\left[\sum_{i=1}^{n}\sum_{j=1}^{n}\psi_i\psi_j e^{-A_{ij}}\frac{\sin x_{ij}}{x_{ij}}+\frac{k}{(\sin\frac{1}{2}\theta/\lambda)^4}\sum_{\nu=1}^{n}Z_\nu\cdot S_\nu\right], \quad (1)$$

$$x_{ij}=4\pi l_{ij}\frac{\sin\frac{1}{2}\theta}{\lambda} \text{ distance formula,} \quad (2)$$

$$\psi_{ij}=-\frac{1}{r}\frac{e^2\cdot m}{2h^2}\frac{(Z_i-F_i)}{(\sin\frac{1}{2}\theta/\lambda)^2} \text{ atomic scattering amplitude.} \quad (3)$$

Equation (1) gives $I(x)$ the number of electrons scattered at angle θ, per unit time per unit solid angle, per unit incident beam intensity, measured at a distance r from N randomly oriented molecules each composed of n atoms. The parameter x_{ij} is related to the angle of scattering and to the de Broglie wave-length λ through Eq. (2); l_{ij} is the distance between the ith and jth atoms. On the right-hand side of Eq. (1) the first term is the coherent part of the scattering composed of a series of $\sin x_{ij}/x_{ij}$

*Invited paper presented at the joint Symposium on Optical Methods for the Study of Molecular Structure at the New York Meeting of the Optical Society of America and the American Physical Society, February 23, 1940.

[1] H. Mark and R. Wierl, Naturwiss. **18**, 205 (1930).

[2] F. Kirchner, Physik. Zeits. **31**, 1025 (1930).

[3] For review articles on this subject covering publications up to 1939: L. O. Brockway, Rev. Mod. Phys. **8**, 231 (1936); J. Y. Beach, Pub. A. A. A. S. No. 7 (1939).

[4] P. Debye, Ann. d. Physik **46**, 809 (1915).

[5] P. Ehrenfest, Proc. Amst. Akad. Sci. **23**, 1132 (1915).

terms with amplitudes ψ_i and ψ_j. A temperature correction, $e^{-A_{ij}s}$ is frequently omitted for it gives only a gradual reduction in the intensity. The second term of Eq. (1) represents the incoherent scattering worked out by Morse,[6] using the Heisenberg S functions calculated for the analogous x-ray case, $k=e^4m^2/r^24h^4$. ψ_i stands for the atomic electron scattering amplitude given by Eq. (3) for the nonrelativistic case developed by Bethe[7] and Mott.[8] Z_i denotes the

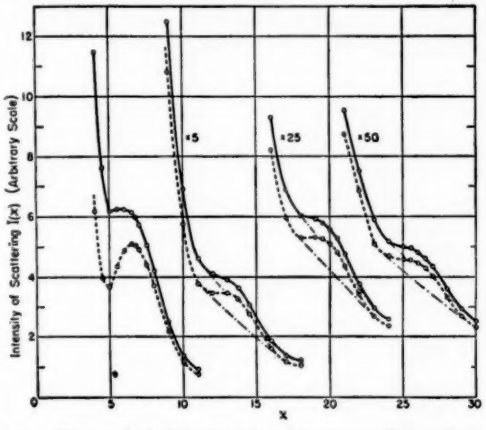

FIG. 1. Theoretical electron scattering curves of phosphorus (P_4) for a regular tetrahedron.

electron scattering by the nucleus while the scattering by the electron cloud is given by F_i, the well-known x-ray atom form factor. F_i decreases with $\sin\frac{1}{2}\theta/\lambda$ so that at large angles of scattering F_i is small compared to Z_i in which cases the formula reduces to the Rutherford scattering amplitude.

Procedures for determining the molecular structure are essentially trial and error methods. Various logical structures are considered and the intensity of scattering $I(x)$ is computed as a function of x according to Eq. (1). Experimental methods are then used to determine the intensity of scattering as a function of $\sin\frac{1}{2}\theta/\lambda$. Fitting of the two intensities by referring both to the same parameter, either x or $\sin\frac{1}{2}\theta/\lambda$, is permitted through the use of Eq. (2). Relative shapes of the molecules can be determined by comparing the relative positions of the various maxima or minima between theoretical and experimental curves while the atomic distances are given by Eq. (2).

In Fig. 1 is shown the theoretical intensity of scattering for the P_4 molecule[9] which has the form of a regular tetrahedron. The full curve gives the total scattering as a function of x while the broken curve represents only the coherent scattering, i.e., the first term in the scattering formula (Eq. (1)). It is noticed that with the exception of the first maximum the full curve shows humps rather than true maxima. For diatomic molecules these prominences are even less distinct. The worker is therefore confronted with a treatment of diffraction patterns which do not possess the sharp maxima found in x-ray and electron diffraction from crystalline solids.

EXPERIMENTAL

Electron diffraction photographs are usually obtained by the transmission of 20 to 60-kv electrons through a concentrated beam of gas molecules, a method introduced by Mark and

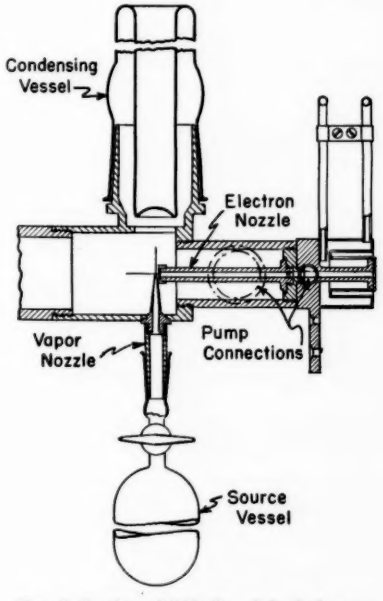

FIG. 2. Section of Wierl's original electron diffraction camera.

[6] P. M. Morse, Physik. Zeits. **33**, 443 (1932); see also, L. Bewilogua, Physik. Zeits. **33**, 688 (1932).
[7] H. A. Bethe, Ann. d. Physik **5**, 325 (1930).
[8] N. F. Mott, Proc. Roy. Soc. **A127**, 658 (1930).
[9] L. R. Maxwell, S. B. Hendricks and V. M. Mosley, J. Chem. Phys. **3**, 699 (1935).

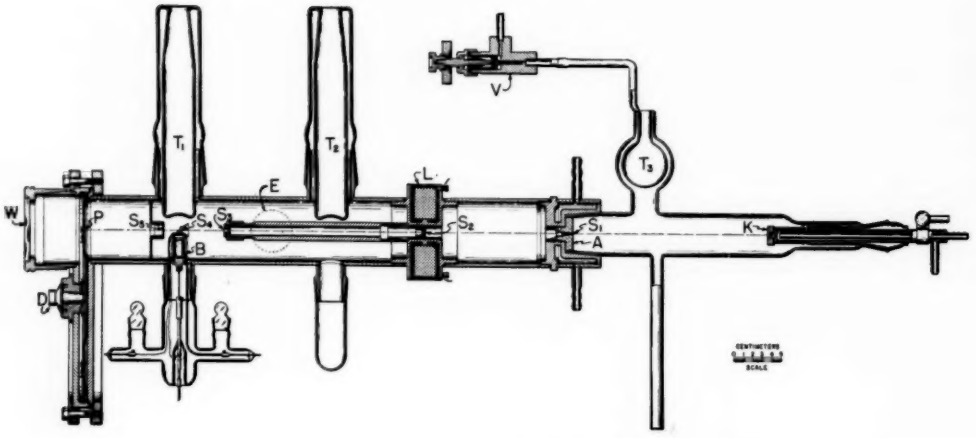

FIG. 3. Electron diffraction camera in use at the U. S. Department of Agriculture.

Wierl. Other investigators have used essentially the same method with various modifications and improvements.

A section of Wierl's apparatus[10] is shown in Fig. 2 where the electron beam moving from right to left along the axis of the tube is restricted to a fine ray colliding with gas molecules coming from the gas nozzle. A liquid-air trap condenses the gas molecules emitted and thereby maintains a low pressure in the diffraction chamber. The diffraction pattern is recorded on a photographic plate not shown in the figure. Figure 3 shows the type of apparatus used by the writer in the U. S. Department of Agriculture. Electrons originate from the cold aluminum cathode K in a low pressure discharge similar to that used by G. P. Thomson.[11] Cooling of the cathode is effected by a recirculating oil system while the cathode potential is supplied by a constant potential high voltage set through an x-ray tube acting as a current-limiting device. Air is admitted into the discharge through a special needle valve V over the surface of the liquid-air trap T_3 which stabilizes the operation of the tube. The water-cooled aluminum anode A has a small opening S_1 about 0.2 mm diameter. A slightly divergent electron beam emerges from S_1 and passes through an opening 1 mm in diameter in the diaphragm S_2 where the magnetic electron lens L renders the beam slightly convergent and produces an image of the opening S_1 on the recording photographic plate P. Figure 4 shows in more detail the arrangement of parts near the scattering region at S_4. An opening 0.1 mm diameter in the electron thimble C is in direct alignment with the gas stream coming from the gas boiler. Both openings can be properly aligned outside of the apparatus. The scattering occurs directly in front of the thimble C and the diffraction pattern is recorded on the photographic plate. This type of arrangement is best suited for materials requiring high temperature because it is possible to raise the temperature of the material from 300°C to

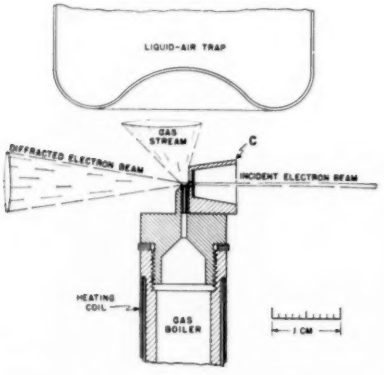

FIG. 4. Section of electron diffraction camera for high temperature work.

[10] R. Wierl, Ann. d. Physik **8**, 521 (1931).

[11] G. P. Thomson, Proc. Roy. Soc. **A117**, 600 (1928).

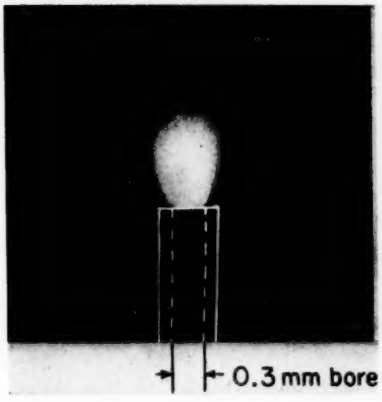

FIG. 5. Electron microscopic photograph of gas beam used for electron diffraction work. White lines showing contour of gas nozzle drawn in by the present author.

1200°C and take five exposures within 6 minutes. Other workers in this field have used slightly modified equipment including hot filaments for the electron source. De Broglie wave-lengths used range from 0.05A to 0.08A and the plate distances vary from 10 to 30 cm approximately, with exposure times from 30 seconds down to fractions of one second, depending on the amount of scattering required.

To illustrate the shape of the gas beam emerging from the nozzle, Fig. 5 shows an electron microscopic photograph of a gas stream under conditions similar to those used for electron diffraction obtained by Boersch[12] using the dark field method. The gas nozzle was 6 mm long and had a bore diameter of 0.3 mm. Carbon tetrachloride vapor was present in the boiler at a pressure of 30 mm Hg. In practice the electron beam penetrates the gas cloud, clearing the jet by about 0.5 mm. The gas density of the beam in the scattering volume is estimated at a few mm of Hg pressure.

Figure 6(a) shows a typical gas electron diffraction photograph of As_4.[9] A series of broad rings is seen whose intensity decreases uniformly

[12] H. Boersch, Zeits. f. Physik **107**, 493 (1937).

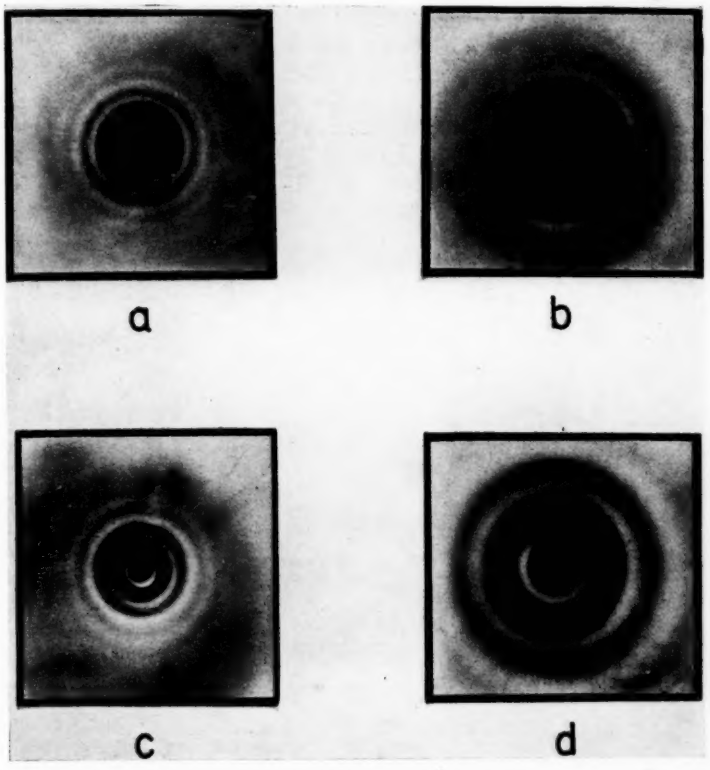

FIG. 6. Illustrative examples of electron diffraction photographs from gas molecules (a) As_4, (b) As_4O_6, (c) P_4, using short plate distance, and (d) P_4, for a long plate distance.

with angle in accordance with the structure of a regular tetrahedron, each ring affording an independent measurement of the As–As separation. Figures 6(b), 6(c) and 6(d) show one photograph of As_4O_6,[13] and two of P_4,[9] respectively. For exceptionally favorable cases it is possible to obtain densitometer records of the interference pattern out to the fourth maximum but beyond that point only visual methods can be used for locating the outer maxima and minima. In spite of the disappointing flatness of the theoretical curves, the eye is able to detect these changes in slope, or points of inflection, which appear as distinguishable maxima and minima. Utilizing this feature, much structural work has been done by the visual method simplifying the theoretical scattering formula by omitting the incoherent scattering and replacing the Bethe-Mott formula by the Rutherford scattering law after omitting the term $(\sin \frac{1}{2}\theta/\lambda)^4$. Thus the theoretical equations are reduced to a series of $\sin x_{ij}/x_{ij}$ terms with constant coefficients. This approximation is sufficiently good for large angles of scattering; however at small angles, scattering by the electrons should in some cases be included. A method for producing real maxima and minima for measurements was introduced by the writer[9] for studies of the P_4 molecule as shown in Fig. 7. We have on the right, at the top, a densitometer record taken of the first maximum; below is the relative

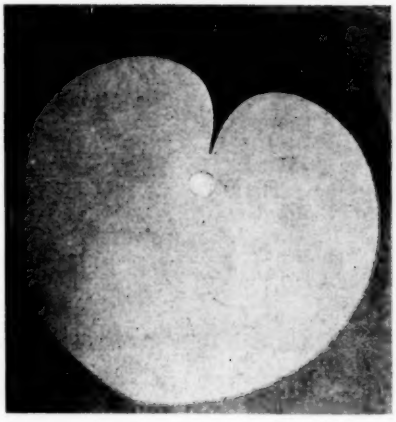

FIG. 8. Photograph of sector to be rotated within the electron diffraction camera for producing prominent electron diffraction maxima.

[13] L. R. Maxwell, S. B. Hendricks and Lola S. Deming, J. Chem. Phys. **5**, 626 (1937).

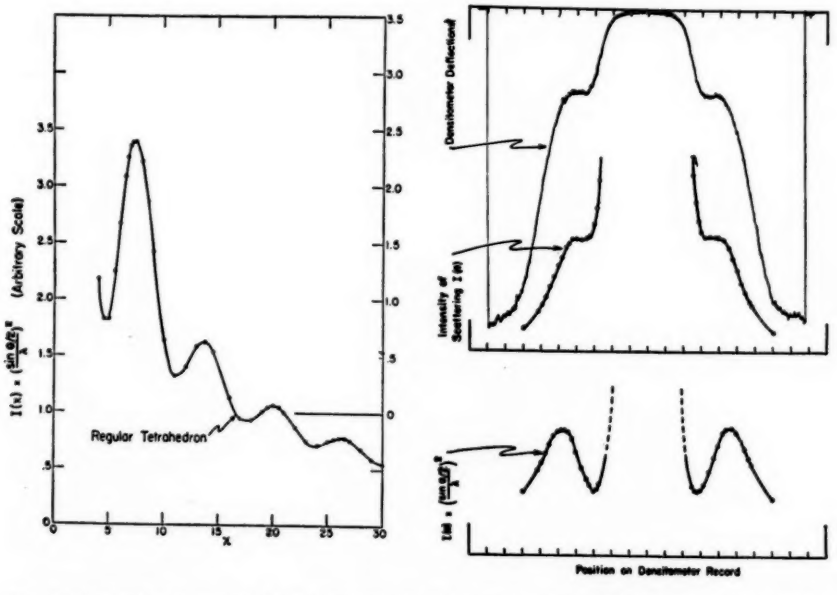

FIG. 7. Illustrating a method for the production of strong electron diffraction maxima for the P_4 molecule. Curve on the left theoretical, set of curves on the right experimental.

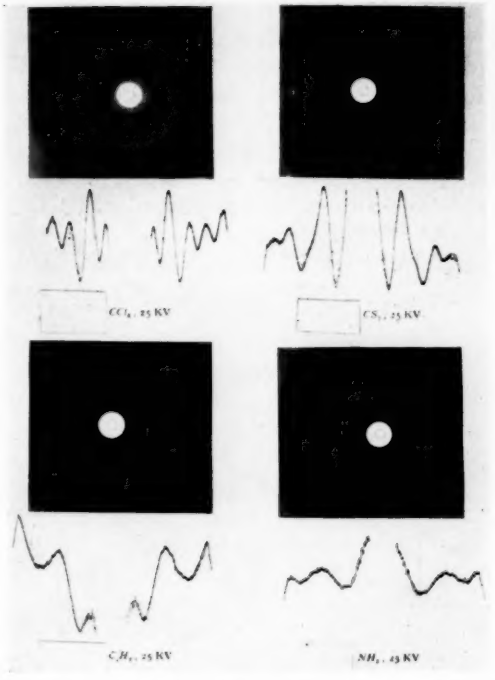

FIG. 9. Electron diffraction photographs obtained using the internal rotating sector.

intensity distribution following plate calibration and at the bottom the intensity curve multiplied by $(\sin \frac{1}{2}\theta/\lambda)^2$ which accentuates the first maximum to a well-defined peak. On the left is shown a theoretical curve of $I(x)\cdot(\sin \frac{1}{2}\theta/\lambda)^2$ which also gives a real maximum for comparison with the experimental one, hence an accurate determination of the P–P distance in the molecule. Another method for obtaining prominent experimental maxima utilizes a rotating sector placed in the diffraction camera to regulate the exposures so as to compensate for the rapidly decreasing background. Figure 8 shows a picture by P. P. Debye[14] of such a sector. Here carbon tetrachloride vapor was used for the diffracting material and the sector was stationary. The shape of the sector is shown by the light portion of the photograph since this region is shielded from the diffracted electrons. In Fig. 9 photographs made with such a rotating sector are reproduced for various materials, together with the corresponding densitometer traces which show true maxima.

[14] P. P. Debye, Physik. Zeits. **40**, 404 (1939).

A disadvantage of the above methods of analysis is the hit or miss character of treatment. After the experimental results have been obtained it is usually necessary to calculate many theoretical intensity curves before the best fit, and consequently the correct structure, can be obtained. It would be much better to go directly from the experimental intensity to the correct structure with one calculation. This has been accomplished by various x-ray investigators by

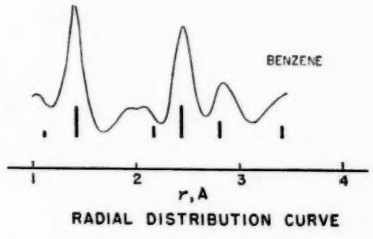

FIG. 10. Example of distribution function for the benzene molecule.

making use of the reciprocal Fourier integral theorem which permits direct determination of atomic electron distributions for monatomic gases, distance between nearest and next nearest neighbors, etc. for crystals and amorphous materials. Pauling and Brockway[15] have intro-

TABLE I. *Comparison between electron diffraction and band spectrum values for the nuclear separation of diatomic molecules.*

MOLECULE	NUCLEAR SEPARATION (A)		
	BAND SPECTRA	ELECTRON DIFFRACTION	REFERENCE
F_2	1.28	1.45±.05	1
S_2	1.88	1.92±.03	2
Cl_2	1.983	2.00±.02	3
Se_2	2.15	2.19±.02	4
Br_2	2.28	2.28±.02	5
ICl	2.315	2.30±.03	3
Te_2	2.61 (predicted)	2.59±.02	4
I_2	2.660	2.66±.01	6

[1] L. O. Brockway, J. Am. Chem. Soc. **60**, 1348 (1938).
[2] L. R. Maxwell, V. M. Mosley and S. B. Hendricks, Phys. Rev. **50**, 41 (1936).
[3] L. Pauling and L. O. Brockway, J. Chem. Phys. **2**, 867 (1934); see also reference 2.
[4] L. R. Maxwell and V. M. Mosley, Phys. Rev. **57**, 21 (1940).
[5] R. Wierl, Ann. d. Physik **8**, 521 (1931); see also Pauling and Brockway, reference 3.
[6] L. R. Maxwell, S. B. Hendricks and V. M. Mosley, Phys. Rev. **52**, 968 (1937).

[15] L. Pauling and L. O. Brockway, J. Am. Chem. Soc. **57**, 2684 (1935).

duced an analogous treatment for electron diffraction in a rather unusual manner in which only visual experimental measurements are used. Results of such methods are shown in Fig. 10 for the benzene molecule obtained recently by Schomaker and Pauling.[16] The curve represents a distribution function plotted against interatomic distances within the molecule while the vertical lines give expected positions and relative intensities. Three large peaks showing in the distribution function correspond to the three C–C distances in the benzene ring, i.e., 1.39, 2.43 and 2.83A, and quite good agreement is obtained. This distribution method often saves time by indicating the type of structure to be expected, however these predictions are confirmed by intensity calculations to guarantee correctness.

Results

Accuracy of the electron diffraction method can easily be determined from those diatomic molecules whose band spectrum separations in the ground state are accurately known. Tests of this nature have been made for diatomic chlorine, bromine, and iodine and in all cases the agreement was found within 1 percent. Other cases in which the band spectrum analyses were difficult to obtain, electron diffraction results proved particularly useful. Table I gives data for comparison of the two methods. The first column lists the molecules studied, the second column gives the internuclear separation (angstrom units) obtained from band spectra, and in the third column are the electron diffraction results. For fluorine the electron diffraction value of 1.45A is considerably greater than the spectroscopic value of 1.28A reported by Gale and Monk.[17] It has

Table III. *Summary of interatomic distances in the alkali halides.*

Molecule	Lattice Structure	Internuclear Distances (A)		
		Gas		
		Electron Diffraction	Theoretical	Lattice
NaCl	Sodium chloride type	2.51	—	2.814
Br	Sodium chloride type	2.64	—	2.981
I	Sodium chloride type	2.90	2.83	3.231
KCl	Sodium chloride type	2.79	—	3.139
Br	Sodium chloride type	2.94	2.96	3.293
I	Sodium chloride type	3.23	3.13	3.526
RbCl	Sodium chloride type	2.89	2.95	3.27
Br	Sodium chloride type	3.06	—	3.427
I	Sodium chloride type	3.26	3.36	3.663
CsCl	Caesium chloride type	3.06	3.07	3.560
Br	Caesium chloride type	3.14	3.18	3.713
I	Caesium chloride type	3.41	3.43	3.950

Table II. *Summary of electron diffraction data on boron hydrides.*

Molecule	Structure	Valence Angles	Bond Distances (A)	
			B–B	B–H
Diborane (B_2H_6)	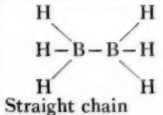	Boron tetrahedral	1.86±.04	1.27±.03
Tetraborane (B_4H_{10})	Straight chain butane-like	All tetrahedral internal rotation	1.84±.04	1.28±.03
Pentaborane (B_5H_{11})	Straight chain pentane-like	All tetrahedral internal rotation	1.81±.03	1.26±.03
Pentaborane (B_5H_9)	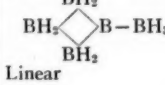	In square 90° HBH tetrahedral	1.76±.02	1.17±.04
Single hydride (BH)	Linear	—	—	1.226 (band spectra)
Sum of single bond radii (extrapolated)	—	—	1.78	1.21

[16] V. Schomaker and L. Pauling, J. Am. Chem. Soc. **61**, 1769 (1939).

[17] H. G. Gale and G. S. Monk, Astrophys. J. **69**, 77 (1929).

been suggested[18] that the spectroscopic value may not represent the separation for the ground state of this molecule. In the case of S_2 Olsson's[19] band spectrum value is given which is only slightly less than the electron diffraction value. Chlorine, bromine, iodine chloride, and iodine agree closely as shown in this table. For Te_2 the electron diffraction value agrees with the expected value computed by Huggins[20] using a semi-empirical method. Because of the complexities existing in their spectra differences are not unexpected for the sulfur group molecules.

Determination of the positions of the hydrogen atoms is possible by the electron diffraction method since electrons are scattered by protons, constituting an advantage over x-ray methods whereby only electronic distributions are detectable. In view of recent work using the rotating sector method, there appears to be a possibility of obtaining the N–H distance in ammonia. Bauer[21] has studied by electron diffraction boron hydride molecules which give the location of the hydrogen atoms. Arranged in columns of Table II are names of the molecules, structures obtained, valence angles, boron to boron separations, and boron to hydrogen separations. These molecules are of interest to chemists because of their electron deficiencies, i.e., the number of single bonds times 2 is greater than the total number of electrons available for linkage. Boron-boron and boron-hydrogen separations for the first three molecules are greater than would be expected from single bond radii data, showing the weaker character of these bonds. The B–B separation in B_5H_9 comes closest to the single bond value, probably involving normal electron pair bonds between the boron atoms. The hydrogen-boron distance obtained from band spectra is slightly lower than the electron diffraction value for B_2H_6, B_4H_{10}, and B_5H_{11}; and slightly greater than the distance found for B_5H_9. Boron hydrides are suitable molecules for locating the position of the hydrogen atoms because of the low scattering power of boron which gives an opportunity to obtain the scattering effects from the hydrogen nuclei.

[18] L. O. Brockway, J. Am. Chem. Soc. **60**, 1348 (1938).
[19] E. Olsson, Nature **137**, 745 (1936).
[20] M. L. Huggins, J. Chem. Phys. **4**, 308 (1936); J. Chem. Phys. **5**, 201 (1937).
[21] S. H. Bauer, J. Am. Chem. Soc. **60**, 805 (1938).

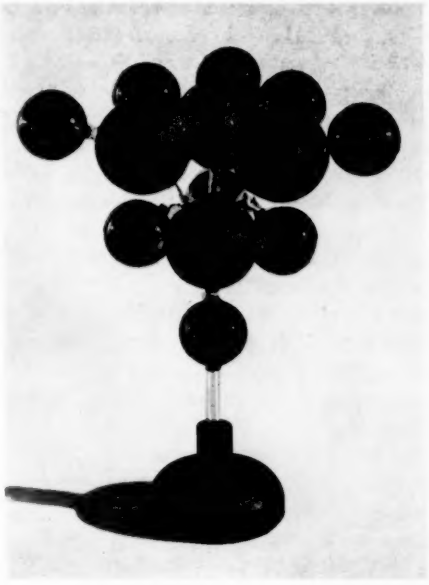

FIG. 11. Glass model showing structure of P_4O_{10}. Large dark spheres represent the positions of the phosphorus atoms, smaller lighter spheres represent the oxygens.

Since the alkali halides are diatomic molecules that lend themselves to theoretical treatment, I have prepared in Table III the internuclear distances of a large number of these halides as measured by electron diffraction.[22] Lattice values from x-ray analysis and theoretical values for gas molecules calculated by May[23] are shown for comparison. Gas distances determined by electron diffraction are consistently 10 to 15 percent lower than the corresponding separations existing in the solids, but are in approximate agreement with the theoretical values computed for the gas molecules, especially so for the caesium halides.

A large number of organic molecules, including various substitutions in acetylene, ethylene, ethane, methane, and benzene, has been studied by electron diffraction. Chief problems of interest are the constancy of bond distances and valence angles and the relationship between internuclear separations and type of chemical bond. Interesting dynamic problems have been studied in the series of disubstituted ethane molecules, ethylene

[22] L. R. Maxwell, S. B. Hendricks and V. M. Mosley, Phys. Rev. **52**, 968 (1937).
[23] A. May, Phys. Rev. **54**, 629 (1938).

chloride,[24] bromide,[25] and chlorobromide,[25] by Beach and others in regard to freedom of rotation about the carbon-carbon single bond. For all three cases it was found that the *trans*-configuration was most stable and that the potential barrier to internal rotation was at least 5 kcal./mole. However, for a trichloroethane[26] molecule, the most stable configuration was found to be about 50° from the *trans*-position. These workers have made certain potential barrier calculations, using electrostatic dipole and steric exchange repulsive interactions, which give fairly satisfactory agreement with the observed results.

Structure of the molecule tetranitromethane has been found by electron diffraction.[27] In this molecule each hydrogen atom of the methane molecule is replaced by an NO_2 group. It was found in this substituted molecule that the central carbon atom still maintains its tetrahedral valence angles; the O–N–O angle was found to be 127° while the NO_2 groups have a rotatory oscillation motion about the C–N bond. It was also necessary to include the temperature factor for the other modes of vibration before a satisfactory structure was obtained. The nitrogen valence angle of 127° is not far from a value recently obtained in some new structure determinations of NO_2[28] which indicate an angle of approximately 130°.

In conclusion I wish to give an example of a structure determination of a more complex molecule, phosphorus pentoxide, P_2O_5, which in the gas exists as a double molecule as shown both by vapor density measurements and electron diffraction investigations.[13] The phosphorus atoms are tetrahedral with 10 oxygens added to this arrangement. A model (P_4O_{10}) constructed to illustrate the complete structure[29] is shown in Fig. 11. The large dark spheres represent the position of the phosphorus atoms and there are 6 oxygen atoms (light spheres) on each edge of the regular tetrahedron held between the phosphorus atoms by a single-double bond resonance, with a separation somewhat less than the normal single bond distance. The remaining 4 oxygens, (light spheres) are located radially from the phosphorus atoms at a surprisingly short distance of about three-fourths of the single bond distance. This anomalous position may be due to the polar character of the bond. Also $P_4O_6S_4$ has a similar structure[30] where 4 sulphur atoms replace the outermost oxygens, resulting in an abnormally short P to S separation.

[24] J. Y. Beach and K. J. Palmer, J. Chem. Phys. **6**, 639 (1938).
[25] J. Y. Beach and A. Turkevich, J. Am. Chem. Soc. **61**, 303 (1939).
[26] A. Turkevich and J. Y. Beach, J. Am. Chem. Soc. **61**, 3127 (1939).
[27] A. J. Stosick, J. Am. Chem. Soc. **61**, 1127 (1939).
[28] L. R. Maxwell and V. M. Mosley, Phys. Rev. **57**, 1079A (1940).
[29] G. C. Hampson and A. J. Stosick, J. Am. Chem. Soc. **60**, 1814 (1938).
[30] A. J. Stosick, J. Am. Chem. Soc. **61**, 1130 (1939).

Table References

1. L. O. Brockway, J. Am. Chem. Soc. **60**, 1348 (1938).
2. L. R. Maxwell, V. M. Mosley and S. B. Hendricks, Phys. Rev. **50**, 41 (1936).
3. L. Pauling and L. O. Brockway, J. Chem. Phys. **2**, 867 (1934).
4. L. R. Maxwell and V. M.Mosley, P hys. Rev. **57**, 21 (1940).
5. R. Wierl, Ann. d. Physik **8**, 521 (1931).
6. L. R. Maxwell, S. B. Hendricks and V. M. Mosley, Phys. Rev. **52**, 968 (1937).
7. W. Grether, Ann. d. Physik **26**, 1 (1936).
8. L. R. Maxwell, V. M. Mosley and Lola S. Deming, J. Chem. Phys. **2**, 331 (1934).
9. H. Boersch, Acad. Wiss. Wien, IIb, **144**, 1 (1935).
10. H. Boersch, Monatsh. **65**, 311 (1935).
11. L. E. Sutton and L. O. Brockway, J. Am. Chem. Soc. **57**, 473 (1935).
12. L. Pauling and L. O. Brockway, J. Am. Chem. Soc. **57**, 2684 (1935).
13. L. R. Maxwell and V. M. Mosley, Phys. Rev. **57**, 1079A (1940).
14. P. C. Cross and L. O. Brockway, J. Chem. Phys. **3**, 821 (1935).
15. L. O. Brockway, Proc. Nat. Acad. Sci. **19**, 868 (1933).
16. K. J. Palmer and N. Elliott, J. Am. Chem. Soc. **60**, 1309 (1938).
17. K. J. Palmer, J. Am. Chem. Soc. **60**, 2360 (1938).
18. J. A. A. Ketelaar and K. J. Palmer, J. Am. Chem. Soc. **59**, 2629 (1937).
19. H. Braune and S. Knoke, Zeits. f. physik. Chemie **B23**, 163 (1933).
20. A. H. Gregg, G. C. Hampson, G. I. Jenkins, P. L. F. Jones and L. E. Sutton, Trans. Faraday Soc. **33**, 852 (1937).
21. R. W. Dornte, J. Am. Chem. Soc. **55**, 4126 (1933).
22. H. A. Lévy and L. O. Brockway, J. Am. Chem. Soc. **59**, 2085 (1937).
23. H. Braune and P. Pinnow, Zeits. f. physik. Chemie **B35**, 239 (1937).
24. S. H. Bauer, J. Am. Chem. Soc. **59**, 1096 (1937).
25. S. H. Bauer, J. Am. Chem. Soc. **60**, 805 (1938).
26. S. H. Bauer and L. Pauling, J. Am. Chem. Soc. **58**, 2403 (1936).
27. S. H. Bauer, J. Am. Chem. Soc. **60**, 524 (1938).
28. A. Stock and R. Wierl, Zeits. f. anorg. allgem. Chemie **203**, 228 (1931).

A Table of Molecular Structure by Electron Diffraction

The following table contains structure determinations of gas molecules by the electron diffraction method, obtained from publications up to the summer of 1940. Information presented covers the configurations, bond angles, and interatomic distances. Order of contents is as follows:

I. Diatomic molecules.
II. Triatomic molecules.
III. Boron, aluminum, gallium, and indium compounds.
IV. Silicon, titanium, germanium, tin, and lead compounds.
V. Nitrogen compounds.
VI. Phosphorus, vanadium, arsenic, niobium, antimony, tantalum and bismuth compounds.
VII. Sulphur, chromium, selenium, molybdenum, tellurium, tungsten, and uranium compounds.
VIII. Iron, cobalt, nickel, copper, osmium, and ruthenium compounds.
IX. Miscellaneous inorganic compounds.
X. Aliphatic compounds.
C_1 Group.
C_2 Group.
Ethane derivatives.
Ethylene derivatives.
Acetylene derivatives.
Miscellaneous.
C_3 Group.
C_4 Group.
C_5 Group.
C_6 Group.
XI. Aromatic compounds.
XII. C_{10} Group.
XIII. C_{12} Group.

Compound	Configuration	Distances (A)	References
		I. *Diatomic molecules.*	
N_2			142
F_2		1.45±0.05	1
S_2		1.92± .03	2
Cl_2		2.00± .02	3, 2, 12
Se_2		2.19± .02	4
Br_2		2.28± .02	5, 3, 12
Te_2		2.59± .02	4
I_2		2.66± .01	62, 6, 7
ICl		2.30± .03	3
HgCl		2.23± .03	4
TlCl		2.55± .03	7
TlBr		2.68± .03	7
TlI		2.87± .03	7
NaCl		2.51± .03	6
NaBr		2.64± .01	6
NaI		2.90± .02	6
KCl		2.79± .02	6
KBr		2.94± .03	6
KI		3.23± .04	6
RbCl		2.89± .01	6
RbBr		3.06± .02	6
RbI		3.26± .02	6
CsCl		3.06± .03	6
CsBr		3.14± .03	6
CsI		3.41± .03	6
Indium monohalides			134
		II. *Triatomic molecules.*	
N_2O	Linear	2.32±0.02 (between end atoms)	143. 5, 8, 147
F_2O	Angle F–O–F =100±3°	F–O =1.41±0.05	9, 10, 11
Cl_2O	" Cl–O–Cl=115±4°	Cl–O =1.68± .03	11, 12
NO_2	" O–N–O =130±2°	N–O =1.21± .02	8, 13
CO_2	Linear	C–O =1.13± .04	142, 143, 5
SO_2	Angle O–S–O =120± 5°	S–O =1.43± .01	143, 5, 14, 12 144
ClO_2	" O–Cl–O =137±15°	O–Cl =1.53± .02	95, 15, 12,
SeO_2	" O–Se–O = ?	O–Se =1.61± .03	16

Compound	Configuration	Distances (A)	References
	II. *Triatomic molecules.—(Continued).*		
CS_2	Linear	C–S = 1.54±0.03	143, 5, 14, 131
SCl_2	Angle Cl–S–Cl = 102±3°	S–Cl = 2.00± .02	17, 56
$TeCl_2$	" Cl–Te–Cl > 150°	Te–Cl = 2.36± .03	7
$TeBr_2$	" Br–Te–Br > 150°	Te–Br = 2.49± .03	7
COS	Linear	C–O = 1.16± .02	9, 10, 21, 14
		C–S = 1.56± .03	
NOCl	Angle Cl–N–O = 116±2°	N–Cl = 1.95± .02	69, 18, 135
		N–O = 1.14± .03	
NOBr	" Br–N–O = 117±3°	N–Br = 2.14± .02	69, 18, 135
		N–O = 1.15± .04	
$HgCl_2$	Linear	Hg–Cl = 2.28	86, 19, 20, 4
$HgBr_2$	"	Hg–Br = 2.38	86, 19, 20
ZnI_2	"	Zn–I = 2.42± .02	40
CdI_2	"	Cd–I = 2.60± .02	40
HgI_2	"	Hg–I = 2.55	86, 19, 20
ClCN	"	C–Cl = 1.67± .02	30
		C–N = 1.13± .03	
BrCN	"	C–Br = 1.79± .02	30
		C–N = 1.13± .04	
	III. *Boron, aluminum, gallium, and indium compounds.*		
BF_3	Planar	B–F = 1.30±0.02	22, 23
BCl_3	"	B–Cl = 1.73± .02	5, 20, 22
BBr_3	"	B–Br = 1.87± .02	22
$B(CH_3)_3$	"	B–C = 1.56± .02	22
B_2H_6	Ethane-like	B–B = 1.86± .04	24
	Boron tetrahedral	B–H = 1.27± .03	
B_4H_{10}	Butane-like	B–B = 1.84± .04	25
		B–H = 1.28± .03	
B_5H_{11}	Pentane-like	B–B = 1.81± .03	25
		B–H = 1.26± .03	
B_5H_9	Planar, four borons in a square	B–B = 1.76± .02	26
	Angles H–B–H tetrahedral	B–H = 1.17± .04	
B_2NH_7	Angle B–N–B tetrahedral	B–N = 1.56± .03	27
$B_3N_3H_6$	Benzene-like	B–N = 1.44± .02	28, 27
H_3BCO	B–C–O linear	B–C = 1.57± .03	29
	Boron angles tetrahedral	C–O = 1.13± .03	
		B–H = 1.20± .03	
$H_3BN(CH_3)_3$		B–N = 1.62± .15	29
		N–C = 1.53± .06	
AlB_2H_{12}	Aluminum and borons coplanar	Al–B = 2.14± .02	139
	Hydrogens attached to borons	B–H = 1.28± .05	
Al_2Cl_6	Two tetrahedra, sharing a common edge, each containing one metal atom.	Al–Al = 3.41± .20	31, 134
		Al–Cl = 2.06± .04	
		Al–Cl = 2.21± .04	
Al_2Br_6	"	Al–Al = 3.39± .10	31, 134
		Al–Br = 2.21± .04	
		Al–Br = 2.33± .04	
Al_2I_6	"	Al–Al = 3.24± .15	31, 134
		Al–I = 2.53± .04	
		Al–I = 2.58± .04	
$Ga_2(Halogen)_6$	"		134
$In_2(Halogen)_6$	"		134
GaI_3	Equilateral triangle		134
	IV. *Silicon, titanium, germanium, tin, and lead compounds.*		
SiF_4	Tetrahedral	Si–F = 1.54±0.02	32, 12, 23
$SiCl_4$	"	Si–Cl = 2.02± .02	5, 32, 12
$SiHCl_3$	Pyramid, angle 110±1°	Si–Cl = 2.01± .03	34, 35, 39, 137
$SiHBr_3$	Angle Br–Si–Br = 110±2.5°	Si–Br = 2.19± .05	36
		Br–Br = 3.63	
$SiBrCl_3$		Si–Cl = 2.05± .05	35
		Si–Br = 2.19± .05	
		Cl–Cl = 3.39± .01	
		Br–Cl = 3.41± .03	
$Si(CH_3)_4$	Tetrahedral	Si–C = 1.93± .03	37
SiH_2Cl_2	Angle Cl–Si–Cl = 110±1°	Si–Cl = 2.02± .03	38

Compound	Configuration	Distances (A)	References
	IV. *Silicon, titanium, germanium, tin, and lead compounds.—(Continued).*		
SiH_3Cl		Si–Cl = 2.06±0.05 Si–H = 1.46	38
Si_2H_6	Si–H bond angles = 109.5°	Si–Si = 2.32± .03 Si–H = 1.47± .03	39
Si_2Cl_6	Tetrahedral angles *trans*-position	Si–Si = 2.32± .06 Si–Cl = 2.00± .05	39
$TiCl_4$	Tetrahedral	Ti–Cl = 2.21± .04	5
$GeCl_4$	Tetrahedral	Ge–Cl = 2.08± .02	5, 12
$GeBr_4$	"	Ge–Br = 2.32	41
GeI_4	"	Ge–I = 2.48	42, 106
$Ge(CH_3)_4$	"	Ge–C = 1.98± .03	37
Ge_2H_6		Ge–Ge = 2.41± .02	43
Ge_3H_8		Ge–Ge = 2.41± .02	43
$SnCl_4$	Tetrahedral	Sn–Cl = 2.30± .02	5, 32, 12
SnI_4	"	Sn–I = 2.64	42, 106
$Sn(CH_3)_4$	"	Sn–C = 2.18± .03	37
$Pd(CH_3)_4$	"	Pd–C = 2.29± .05	37
	V. *Nitrogen compounds.*		
N_2O	See Section No. II		
NO_2	See Section No. II		
N_2O_4		N–N = 1.6 to 1.7	8
N_2O_5		N–O = 1.18 N–O′ = 1.3 to 1.4	8
NOCl	See Section No. II		
NOBr	See Section No. II		
NCCl	See Section No. II		
NCBr	See Section No. II		
NH_3			131
$N(CH_3)_3$	Pyramidal, angle = 108±4°	N–C = 1.47±0.02	37
N_2CH_3	Angle N–N′–N″ = 180° " C–N–N′ = 120±5°	N–C = 1.47± .02 N–N′ = 1.24± .02 N′–N″ = 1.10± .02	52, 53
HNO_3	Angle O–N–O = 130±5°	N–O = 1.22± .02 N–O′ = 1.41± .02	13
CH_3NO_3	Angle O–N–O = 125° 16′ " N–O′–C = 105±5°	N–O = 1.26 N–O′ = 1.36 C–O′ = 1.43± .05	53
FNO_3	Angle O–N–O = 125±5° " N–O′–F = 105±5°	N–O = 1.29± .05 N–O = 1.39± .05 F–O′ = 1.42± .05	53
$(CH_2)_6N_4$	Like P_4O_6 Angle C–N–C = 109.5° Angle N–C–N = 109.5°	N–N = 2.42 C–N = 1.47± .02	49
NH_7B_2	See Section No. III		
$N_3H_6B_3$	See Section No. III		

For other organic molecules containing nitrogen see Section No. X.

	VI. *Phosphorus, vanadium, arsenic, niobium, antimony, tantalum, and bismuth compounds.*		
P_4	Tetrahedral	P–P = 2.21±0.02	44
PF_3	Pyramidal, angle = 104±4°	P–F = 1.52± .04	32, 12
PCl_3	Pyramidal, angle = 101±2°	P–Cl = 2.00± .02	5, 32, 12
PBr_3	Pyramidal, angle = 100±2°	P–Br = 2.23± .01	20
PI_3	Pyramidal, angle = 100±5°	I–I = 3.79± .02	20, 106
$PFCl_2$	Pyramidal, angle = 102±3°	P–F = 1.55± .05 P–Cl = 2.02± .03	39
$P(CH_3)_3$	Pyramidal, angle = 100±4°	P–C = 1.87± .02	51
PF_5	Trigonal bipyramid	P–F = 1.57± .02	23, 39
PCl_5	Trigonal bipyramid	P–Cl = 2.10, 2.25 Cl–Cl = 3.08 min. dist.	47, 148
PF_3Cl_2	Trigonal bipyramid	P–F = 1.59± .03 P–Cl = 2.05± .03	39

Compound	Configuration	Distances (A)	References
VI. *Phosphorus, vanadium, arsenic, niobium, antimony, tantalum, and bismuth compounds.—(Continued).*			
POF_3	Angle F–P–F $=107\pm2°$	P–F $=1.52\pm0.02$ P–O $=1.56\pm .03$ F–F $=2.44\pm .02$	39
$POCl_3$	Angle Cl–P–Cl $=106\pm1°$	P–Cl $=2.02\pm .03$ P–O $=1.58$ Cl–Cl $=3.22\pm .03$	39
PSF_3	Symmetry C_{3v} Angle F–P–F $=99.5\pm2°$	P–F $=1.51\pm .02$ P–S $=1.85\pm .02$	45
$PSCl_3$	Symmetry C_{3v} Angle Cl–P–Cl $=107\pm3°$	P–Cl $=2.01\pm .02$ P–S $=1.94\pm .03$	46
POF_2Cl	Angle F–P–F $=106\pm3°$ Angle F–P–Cl $=106\pm3°$	P–F $=1.51\pm .03$ P–Cl $=2.01\pm .04$ P–O $=1.55\pm .03$	39
$POFCl_2$	Angle F–P–Cl $=106\pm3°$ Angle Cl–P–Cl $=106\pm3°$	P–F $=1.50\pm .03$ P–Cl $=1.99\pm .04$ P–O $=1.54\pm .03$	39
P_4O_6	Symmetry Td Angle P–O–P $=128\pm1.5°$	P–P $=3.00\pm .05$ P–O $=1.67\pm .03$	48, 49
P_4O_{10}	Symmetry Td Angle P–O–P $=123.5\pm1°$	P–P $=2.84\pm .03$ P–O $=1.62\pm .02$ P–O′ $=1.39\pm .02$	48, 49
$P_4O_6S_4$	Symmetry Td Angle P–O–P $=123.5\pm1°$	P–P $=2.85\pm .03$ P–O $=1.61\pm .02$ P–S $=1.85\pm .02$	50
$VOCl_3$	Angle Cl–V–Cl $=111°\ 17'\pm2°$ Angle Cl–V–O $=108°\ 12'\pm2°$	V–O $=1.56\pm .04$ V–Cl $=2.12\pm .03$ Cl–O $=3.00\pm .04$ Cl–Cl $=3.50\pm .03$	17
As_4	Tetrahedral	As–As $=2.44\pm .03$	44
AsF_3	Pyramidal	As–F $=1.72\pm .02$	32, 12
$AsCl_3$	Pyramidal, angle $=101\pm2°$	As–Cl $=2.16\pm .03$	32, 12
$AsBr_3$	Pyramidal, angle $=100\pm2°$	As–Br $=2.34\pm .03$	20, 106
AsI_3	Pyramidal, angle $=101\pm2°$	As–I $=2.54\pm .04$	20, 106
$As(CH_3)_3$	Pyramidal, angle $=96\pm5°$	As–C $=1.98\pm .02$	51
As_4O_6	Symmetry Td Angle As–O–As $=126\pm3°$	As–As $=3.20\pm .03$ As–O $=1.80\pm .02$	48, 49
$NbCl_5$	Trigonal bipyramid	Nb–Cl $=2.29\pm .03$	138
$NbBr_5$	Trigonal bipyramid	Nb–Br $=2.46\pm .03$	138
$SbCl_3$	Pyramidal, angle $=104°$	Sb–Cl $=2.37\pm .02$	20
$SbBr_3$	Pyramidal, angle $=97\pm2°$	Sb–Br $=2.49\pm .03$	20, 106
SbI_3	Pyramidal, angle $=98\pm2°$	Sb–I $=2.72\pm .03$	20, 106
$SbCl_5$			140
$TaCl_5$	Trigonal bipyramid	Ta–Cl $=2.30\pm .02$	138
$TaBr_5$	Trigonal bipyramid	Ta–Br $=2.45\pm .03$	138
$BiCl_3$	Pyramidal, angle Cl–Bi–Cl $=100\pm6°$	Bi–Cl $=2.48\pm .02$	146
$BiBr_3$	Pyramidal, angle Br–Bi–Br $=100\pm4°$	Bi–Br $=2.63\pm .02$	146
VII. *Sulphur, chromium, selenium, molybdenum, tellurium, tungsten, and uranium compounds.*			
S_2	See Section No. I		
S_{2+n}	Angle S–S–S $=ca.\ 100°$	S–S $=ca.\ 2.1$	2
S_8	Puckered ring	S–S $=2.08\pm0.02$	54, 55
SO_2	See Section No. II		
SOC	See Section No. II		
SCl_2	See Section No. II		
$S(CH_3)_2$	Angle C–S–C $=100$ to $110°$	S–C $=1.82\pm .03$	37
S_2H_2	Angle H–S–S $=95°$ (assumed)	S–S $=2.05\pm .02$ H–S $=1.33$ (assumed)	56
S_2Cl_2	Angle Cl–S–S $=103\pm2°$	S–S $=2.05\pm .03$ S–Cl $=1.99\pm .03$	57, 17
$S_2(CH_3)_2$	Angle C–S–S $=107\pm3°$	S–S $=2.04\pm .03$ C–S $=1.78\pm .03$	56
SO_3	Angle O–S–O $=120\pm2°$	S–O $=1.43\pm .02$ O–O $=2.48\pm .03$	17

Compound	Configuration	Distances (A)	References
VII. *Sulphur, chromium, selenium, molybdenum, tellurium, tungsten, and uranium compounds.—(Continued).*			
$SOCl_2$	Pyramidal Angle O–S–Cl $=106\pm1°$ Angle Cl–S–Cl $=114\pm2°$	S–O $=1.45\pm0.02$ S–Cl $=2.07\pm .03$ Cl–O $=2.84\pm .03$	17
$SCCl_2$	Angle Cl–C–Cl $=116\pm2°$	S–C $=1.63$ (assumed) C–Cl $=1.70\pm .02$ Cl–Cl $=2.88\pm .04$ S–Cl $=2.90\pm .04$	58
SO_2F_2	Angle F–S–O $=105\pm2°$ Angle F–S–F $=100\pm8°$	S–F $=1.56\pm .02$ S–O $=1.43\pm .02$	45
SO_2Cl_2	Angle O–S–O $=119°\ 48'\pm5°$ Angle Cl–S–Cl $=111°\ 12'\pm2°$ Angle Cl–S–O $=106°\ 28'\pm2°$	S–O $=1.43\pm .02$ S–Cl $=1.99\pm .02$ Cl–O $=2.76\pm .03$ Cl–Cl $=3.28\pm .10$ O–O $=2.48\pm .10$	17
$SO_2(CH_3)_2$ (dimethyl sulphone)	sulphur and carbon atoms have tetrahedral valence angles	C–S $=1.90\pm .03$ S–O $=1.44\pm .03$ C–H $=1.06$ (assumed)	130
SPF_3	See Section No. VI		
$SPCl_3$	See Section No. VI		
SC_4H_4 (thiophene)	See Section No. X. C_4 Group		
$S_4P_4O_6$	See Section No. VI		
SF_6	Regular octahedron	S–F $=1.58\pm .03$	59, 60
CrO_2Cl_2	Angle O–Cr–O $=105°\ 6'\pm4°$ " Cl–Cr–Cl $=113°\ 16'\pm3°$ Angle Cl–Cr–O $=109°\ 34'\pm3°$	Cr–O $=1.57\pm .03$ Cr–Cl $=2.12\pm .02$ Cl–O $=3.03\pm .03$ Cl–Cl $=3.54\pm .05$ O–O $=2.49\pm .10$	17
$Cr(CO)_6$	Regular octahedron Cr–C–O linear	Cr–C $=1.92\pm .04$ C–O $=1.16\pm .05$	87
Se_2	See Section No. I		
SeO_2	See Section No. II		
Se_6	Puckered ring	Se–Se $=2.32$	54, 55, 4
SeF_6	Regular octahedron	Se–F $=1.67$	59, 60
MoF_6	Rhombic bipyramid(?)	Closest Mo–F distance about 1.6	23
$MoCl_5$	Regular trigonal bipyramid	Mo–Cl $=2.27\pm .02$	88
$Mo(CO)_6$	Regular octahedron Mo–C–O linear	Mo–C $=2.08\pm .04$ C–O $=1.15\pm .05$	87
Te_2	See Section No. I		
TeF_6	Octahedral	Te–F $=1.82$	59, 60
$TeCl_4$		Te–Cl $=2.33\pm .02$ Cl–Cl $=3.37\pm .06$	145
WF_6	Rhombic bipyramid (?)	W–F $=1.64, 1.84, 2.00$	23
WCl_6	Regular octahedron	W–Cl $=2.26\pm .02$	88
$W(CO)_6$	Regular octahedron W–C–O linear	W–C $=2.06\pm .04$ C–O $=1.13\pm .05$	87
UF_6	Rhombic bipyramid (?)	U–F $=1.78, 1.99, 2.17$	23
VIII. *Iron, cobalt, nickel, copper, osmium, and ruthenium compounds.*			
$Fe(NO)_2(CO)_2$	Tetrahedral Fe–C–O linear Fe–N–O linear	Fe–N $=1.77\pm0.02$ Fe–C $=1.84\pm .02$ N–O $=1.12\pm .03$ C–O $=1.15\pm .03$	82
$Fe(CO)_5$	Trigonal bipyramid Fe–C–O linear	Fe–C $=1.84\pm .03$ C–O $=1.15\pm .04$	83
$Fe(CO)_4H_2$	CO groups tetrahedral about Fe atom Fe–C–O linear	Fe–C $=1.84\pm .03$ (in Fe–CO) Fe–C $=1.79\pm .04$ (in Fe–COH) C–O $=1.15\pm .05$	83

Compound	Configuration	Distances (A)	References
	VIII. *Iron, cobalt, nickel, copper, osmium, and ruthenium compounds.*—(*Continued*).		
$Co(NO)(CO)_3$	Tetrahedral Co–N–O linear Co–C–O linear	Co–C = 1.83±0.02 Co–N = 1.76± .02 C–O = 1.14± .03 N–O = 1.10± .04	82
$Co(CO)_4H$	CO groups tetrahedral about Co atom, hydrogen attached to one CO group	Co–C = 1.75± .08 (for COH group)	83
	Other	Co–C = 1.83± .02 C–O = 1.16± .05	
$Ni(CO)_4$	Tetrahedral Ni–C–O linear	Ni–C = 1.82± .03 C–O = 1.15± .02	84
Cu_2Cl_2		Cu–Cl = 2.13	85
Cu_2Br_2		Cu–Br = 2.25	85
Cu_2I_2		Cu–I = 2.40	85
OsO_4	Probably a rhomboid	Os–O = 1.79, 2.81	33, 133
OsF_8	Either a cube with..... or Archimedes antiprism with....	Os–F = 2.47 Os–F = 2.52	86
RuO_4	Probably a rhomboid	Ru–O = 1.66, 2.74	133
	IX. *Miscellaneous inorganic compounds.*		
$(HF)_n$	Zig-zag chain Angle F–F–F = 140±5°	F–H = 1.00±0.06 F–H′ = 1.55± .06 F–F = 2.55± .03	81
IF_5	Bipyramid (?)	I–F = 2.57	23
	X. *Aliphatic compounds.*		
C_1 Group			
CH_3F		C–F = 1.42±0.02	61
CH_2F_2	Angle F–C–F = 110±1°	C–F = 1.36± .02	61
CF_4	Tetrahedral	C–F = 1.36± .02	9, 10, 32, 12
CH_2FCl	Angle F–C–Cl = 110±2°	C–F = 1.40± .03 C–Cl = 1.76± .02	61
CHF_2Cl	Angle Cl–C–F = 110.5±1° Angle F–C–F = 110.5±1°	C–F = 1.36± .03 C–Cl = 1.73± .03	61
$CHFCl_2$	Angle Cl–C–Cl = 112 ±2° Angle F–C–Cl = 109 ±2°	C–F = 1.41± .03 C–Cl = 1.73± .04	61
CF_2Cl_2	Angle Cl–C–Cl = 113 ±2° Angle F–C–F = 109 ±2°	C–F = 1.35± .03 C–Cl = 1.74± .03	61
$CFCl_3$	Angle Cl–C–Cl = 111.5±1° Angle F–C–Cl = 107.5±1°	C–F = 1.40± .04 C–Cl = 1.76± .02	61, 101
$CFBr_3$		C–F = 1.44± .06 C–Br = 1.91± .04 Br–Br = 3.20± .03 Br–F = 2.70± .02	101
CH_3Cl		C–Cl = 1.77± .02	11
CH_2Cl_2	Angle Cl–C–Cl = 112±2°	C–Cl = 1.77± .02 Cl–Cl = 2.93± .02	5, 11, 12, 96
$CHCl_3$	Angle Cl–C–Cl = 112±2°	C–Cl = 1.77± .02 Cl–Cl = 2.93± .02	5, 11, 12 114, 124, 96
CCl_4	Tetrahedral	C–Cl = 1.76± .01	141, 5, 59, 60, 63, 62 32, 65, 66, 67, 68 3, 12, 57, 106 118, 64, 131
CH_3Br	Tetrahedral	C–Br = 1.91± .06	70, 71
CH_2Br_2	Angle Br–C–Br = 112±2°	C–Br = 1.91± .02	70, 71
$CHBr_3$	Angle Br–C–Br = 111±2°	Br–Br = 3.15± .03	72, 70, 71
$CBrCl_3$		C–Br = 2.01 C–Cl = 1.76	75
CBr_4	Tetrahedral	C–Br = 1.92± .02 Br–Br = 3.12± .03	5, 73, 71, 74, 106
CH_3I		C–I = 2.28± .05(?)	70
CH_2I_2	Angle I–C–I = 125±5°	C–I = 2.28± .05(?)	70
CHI_3		C–I = 2.12	73
CI_4	Tetrahedral	C–I = 2.12± .02	74

Compound	Configuration	Distances (A)	References
	X. Aliphatic compounds.—(Continued).		
C_1 Group (continued)			
CH_3NO_2	Angle O–N–O $=127\pm3°$ Angle N–C–N $=109°\ 28'$	C–N $=1.46\pm0.02$ N–O $=1.21\pm .02$	58, 77
$C(NO_2)_4$	Tetrahedral Angle O–N–O $=127°$	C–N $=1.47\pm .02$ N–O $=1.22\pm .02$	76
CH_3N_3	See Section No. V		
CH_3NO_3	See Section No. V		
CO_2	See Section No. II		
CS_2	See Section No. II		
COS	See Section No. II		
$COCl_2$	Angle Cl–C–Cl $=117\pm2°$ Angle Cl–C–O $=121°\ 30'\pm1°$	C–O $=1.28\pm .03$ C–Cl $=1.68\pm .02$	21, 58, 96
$COBr_2$	Angle Br–C–Br $=110\pm5°$	C–O $=1.13\pm .02$(?) C–Br $=2.05\pm .04$(?)	21
H_3BCO	See Section No. III		
CH_2O	Angle H–C–H $=120\pm1°$	C–O $=1.21\pm .01$ C–H $=1.09\pm .01$	78, 79
CH_3ONH_2 (α-methyl-hydroxylamine)	Angle C–O–N $=111\pm3°$	C–O $=1.44\pm .02$ N–O $=1.37\pm .02$ C–N $=2.31\pm .03$	58
CH_2N_2 (diazomethane)	Linear N–N–C	C–N $=1.34\pm .05$ N–N $=1.13\pm .04$	9, 10
C_2 Group			
	Ethane derivatives.		
C_2H_6		C–C $=1.55\pm .03$ C–H $=1.09\pm .03$	72, 80
C_2H_5Cl	Angle C–C–Cl $=111°\ 30'\pm2°$	C–C $=1.54$ (assumed) C–Cl $=1.76\pm .02$	89, 123
$C_2H_4Cl_2$(1,1)		Cl–Cl $=2.9\ \pm0.3$	92, 72
$C_2H_4Cl_2$(1,2)	Oscillation about the *trans*-position	C–C $=1.54$ (assumed) C–Cl $=1.76\pm .02$	92, 72, 104
$C_2H_3Cl_3$(1,1,1)	Angle Cl–C–Cl $=110\pm2°$	C–C $=1.54$ (assumed) C–Cl $=1.76\pm .02$ Cl–Cl $=2.89\pm .03$	123
$C_2H_3Cl_3$(1,1,2)	Oscillation about 50° from the *trans*-position Angle Cl–C–Cl $=111°\ 30'\pm2°$	C–C $=1.54$ (assumed) C–Cl $=1.75\pm .03$ C–H $=1.09$ (assumed)	91
C_2H_4ClBr	Oscillation about the *trans*-position	C–C $=1.54$ (assumed) C–Cl $=1.75\pm .02$ C–Br $=1.90\pm .02$	90
C_2H_5Br	Angle C–C–Br $=109\pm2°$	C–Br $=1.91\pm .02$	89, 123
$C_2H_4Br_2$(1,1)		Br–Br $=3.56\pm .15$	72
$C_2H_4Br_2$(1,2)	oscillation about the *trans*-position	C–C $=1.54$ (assumed) C–Br $=1.91\pm .02$	72, 90
C_2H_5I		C–I $=2.32\pm .04$	89
C_2H_4O (ethylene oxide)	three membered ring	C–C $=1.56\pm .05$ C–O $=1.45\pm .05$ C–H $=1.05\pm .07$	72, 57
C_2H_4O (acetaldehyde)	Angle C–C–O $=121\pm2°$	C–C $=1.50\pm .02$ C–O $=1.22\pm .02$ C–H $=1.09$ (assumed)	57, 122
C_2HOCl_3 (chloral)	CCl_3 group regular pyramid CHO group planar	C–C $=1.52\pm .02$ C–Cl $=1.76\pm .02$ C–O $=1.15\pm .02$ Cl–Cl $=2.95\pm .03$	136
C_2H_3OCl (acetyl chloride)	Angle C–C–Cl $=110\pm10°$ Angle O–C–Cl $=125\pm10°$	C–C $=1.54\pm .08$ C–O $=1.14\pm .05$ C–Cl $=1.82\pm .10$	21
C_2H_3OBr (acetyl bromide)	Angle C–C–Br $=110\pm10°$ Angle O–C–Br $=125\pm10°$	C–C $=1.54\pm .08$ C–O $=1.13\pm .05$ C–Br $=2.06\pm .10$	21
$C_2O_2Cl_2$ (oxalyl chloride)			92

Compound	Configuration	Distances (A)	References
		X. Aliphatic compounds.—(Continued).	
C_2 Group (*continued*)			
		Ethylene derivatives.	
C_2H_4	Angle H–C–H $=110\pm5°$	C–C $=1.34\pm0.02$ C–H $=1.06\pm .03$	72, 80
C_2H_3Cl	Angle C–C–Cl $=122\pm2°$	C–C $=1.38$ (assumed) C–Cl $=1.69\pm .02$	58
C_2H_3Br	Angle C–C–Br $=121\pm3°$	C–C $=1.34$ (assumed) C–Br $=1.86\pm .04$	65, 105
C_2H_3I	Angle C–C–I $=122\pm2°$	C–C $=1.34$ (assumed) C–I $=2.03\pm .04$	105
$C_2H_2Cl_2(1,1)$	Angle Cl–C–Cl $=116\pm2°$	C–C $=1.38$ (assumed) C–Cl $=1.69\pm .02$ Cl–Cl $=2.86\pm .02$	72, 58
$C_2H_2Cl_2$ (*cis*)	Angle Cl–C–C $=123.5\pm1°$	C–C $=1.38$ (assumed) C–Cl $=1.67\pm .03$ Cl–Cl $=3.22\pm .02$	72, 58
$C_2H_2Cl_2$ (*trans*)	Angle Cl–C–C $=122.5\pm1°$	C–C $=1.38$ (assumed) C–Cl $=1.69\pm .02$ Cl–Cl $=4.27\pm .02$	72, 58, 73
$C_2H_2Br_2$ (*cis*)		C–C $=1.32\pm .08$ C–Br $=2.05\pm .08$	65
$C_2H_2Br_2$ (*trans*)	Angle Br–C–C $=121\pm3°$	C–C $=1.34$ (assumed) C–Br $=1.85\pm .04$ Br–Br $=4.56\pm .02$	65, 73, 105
$C_2H_2I_2$ (*cis*)	Angle I–C–C $=125\pm2°$	C–C $=1.34$ (assumed) C–I $=2.03\pm .04$ I–I $=3.69\pm .02$	105
$C_2H_2I_2$ (*trans*)	Angle I–C–C $=122\pm2°$	C–C $=1.34$ (assumed) C–I $=2.03\pm .04$ I–I $=4.90\pm .02$	73, 105
C_2HCl_3	Angle Cl–C–C $=123\pm2°$	C–C $=1.38$ (assumed) C–Cl $=1.71\pm .03$	65, 58
C_2HBr_3		C–C $=1.32\pm .08$ C–Br $=2.05\pm .08$	65
C_2Cl_4	Angle Cl–C–C $=123°\ 45'\pm1°$	C–C $=1.38$ (assumed) C–Cl $=1.73\pm .02$	58, 65, 73
C_2Br_4		C–Br $=1.91$	73
C_2I_4		C–I $=2.10$	73
		Acetylene derivatives.	
C_2H_2		C–C $=1.22\pm0.08$	72, 131
C_2HCl		C–C $=1.21\pm .04$ C–Cl $=1.68\pm .04$	38
C_2HBr		C–C $=1.20\pm .04$ C–Br $=1.80\pm .03$	38
C_2Cl_2	Probably unsymmetrical model, Angle Cl–C–Cl $=112°$	C–C $=1.32$ C–Cl $=1.78$	127
C_2Br_2	Linear	C–C $=1.20\pm .03$ C–Br $=1.80\pm .03$	127, 73, 33
C_2I_2	Linear	C–C $=1.18$ C–I $=2.03$	127, 73
		Miscellaneous.	
C_2H_2O (ketene)	C–C–O linear	C–C $=1.35\pm0.02$ C–O $=1.17\pm .02$	46
$C_2H_2O_2$ (glyoxal)	Probably coplanar and in *trans*-position Angle C–C–O $=123\pm2°$	C–C $=1.47\pm .02$ C–O $=1.20\pm .01$ C–H $=1.09$ (assumed)	121
$(CH_2O_2)_2$ (formic acid dimer)	Planar Angle O–C–O $=125\pm5°$	O–O $=2.67\pm .04$ C–O $=1.29\pm .02$	63, 94
C_2N_2	Linear	C–C $=1.37\pm .02$ C–N $=1.16\pm .02$	72, 15, 119
CH_3CN (methyl cyanide)	C–C–N linear	C–C $=1.49\pm .03$ C–N $=1.16\pm .03$	93, 119
CH_3NC (methyl isocyanide)	C–N–C linear	C–N $=1.48\pm .03$ N–C $=1.17\pm .02$	93

Compound	Configuration	Distances (A)	References
	X. Aliphatic compounds.—(Continued).		
C_2 Group (continued)			
	Miscellaneous.—(continued)		
$(CH_3)_2O$	Angle C–O–C $=111\pm4°$	C–O $=1.42\pm .03$ C–C $=2.35\pm .05$	100, 11, 12
$(CH_3)_2S$	See Section No. VII		
$(CH_3)_2Hg$	Angle C–Hg–C linear (?)	Hg–C $=2.23\pm .04$	37, 20
$(CH_3)_2N_2$ (azomethane)	Angle C–N–N $=110\pm10°$	N–N $=1.24\pm .05$ C–N $=1.47\pm .06$	9, 10
$(CH_3)_2S_2$	See Section No. VII		
$(CH_3)_2SO_2$ (dimethyl sulphone)	See Section No. VII		
$(CO)_2(NO)_2Fe$	See Section No. VIII		
C_3 Group			
C_3H_4 (allene)	C–C–C linear Angle H–C–H $=109°\ 28'$	C–C $=1.34\pm0.02$ C–H $=1.06\pm .04$	72, 80
C_3H_4 (methyl acetylene)	Carbon atoms linear Angle H–C–C $=109°\ 28'$ in methyl group	C–C (triple bond) $=1.20\pm0.03$ C–CH_3 $=1.46\pm0.02$ C–H $=1.09$, 1.06	119
C_3H_6 (cyclopropane)	Angle C–C–C $=60°$ (assumed) Angle H–C–H $=109°\ 28'$	C–C $=1.53\pm0.03$ C–H $=1.09$ (assumed)	72, 80
C_3H_8 (propane)	Angle C–C–C $=111°\ 30'\pm3°$ Angle H–C–C $=109°\ 28'$	C–C $=1.54\pm0.02$ C–H $=1.09$	72, 96, 80
C_3H_7Cl (isopropyl chloride)	Angle C–C–Cl $=109\pm3°$ Angle C–C–C $=110\pm3°$	C–Cl $=1.75\pm0.02$ C–Cl (long distance) $=2.66\pm0.03$	123
C_3H_7Br (isopropyl bromide)	Angle C–C–Br $=109°\ 28'\pm3°$ Angle C–C–C $=109°\ 28'\pm3°$	C–Br $=1.91\pm0.03$ C–Br (long distance) $=2.81\pm0.03$	123
C_3O_2	Linear	C–C $=1.30\pm0.02$ C–O $=1.20\pm .02$	97, 9, 10, 52
$(CH_3)_2CO$ (acetone)	Angle C–C–C $=110°$ (assumed) Angle C–C–O $=125°$ (assumed)	C–C $=1.57\pm .04$	63
$(CH_3)_3B$	See Section No. III		
$(CH_3)_3N$	See Section No. V		
$(CH_3)_3P$	See Section No. VI		
$(CH_3)_3As$	See Section No. VI		
$(CH_3)_3NO$ (trimethylamine oxide)		C–N $=1.54\pm .02$ N–O $=1.36\pm .03$	130
$(CH_3)_3NBH_3$	See Section No. III		
$(CO)_3NOCo$	See Section No. VIII		
C_4 Group			
C_4H_2 (diacetylene)	Linear	C–C (triple bond) $=1.19\pm0.02$ C–C (single bond) $=1.36\pm .03$	72, 15, 119
C_4H_6 (1, 3-butadiene)	Planar, *trans* Angle C–C–C $=124\pm2°$	C–C (double bond) $=1.35\pm .02$ C–C (single bond) $=1.46\pm .03$ C–H $=1.06$ (assumed)	72, 111
C_4H_6 (dimethylacetylene)	Carbon atoms linear Angle H–C–C $=109°\ 28'$ (assumed)	C–C (triple bond) $=1.20$ (assumed) C–C (single bond) $=1.47\pm0.02$ C–H $=1.09$ (assumed)	119
$C_4H_6O_2$ (dimethylglyoxal)	Probably coplanar with *trans*-position Angle CO–C–O $=123\ \pm2°$ Angle CH_3–C–O $=122.5\pm1°$	C–C $=1.47\pm0.02$ C–CH_3 $=1.54\pm .02$ C–O $=1.20\pm .02$ C–H $=1.09$ (assumed)	121
C_4H_8 (*trans* 2-butene)	Carbon atoms coplanar Angle H_3C–C–C $=125°$	C–C (double bond) $=1.40\pm0.04$ C–C (single bond) $=1.56\pm .04$	116
C_4H_8 (*cis* 2-butene)	Carbon atoms coplanar Angle H_3C–C–C $=125°$	C–C (double bond) $=1.38\pm .03$ C–C (single bond) $=1.54\pm .03$	116
C_4H_8 (isobutene)	Angle C–C–C $=111°\ 30'$ (assumed)	C–C (double bond) $=1.34$ (assumed) C–C (single bond) $=1.54\pm0.02$ C–H $=1.09$ (assumed)	80
C_4H_{10} (butane)		C–C $=1.51\pm0.05$	72
C_4H_8O (*trans* 2,3-Epoxybutane)		C–C $=1.54\pm .03$ C–O $=1.43\pm .03$	116, 117
C_4H_8O (*cis* 2,3-Epoxybutane)		C–C $=1.54\pm .02$ C–O $=1.43\pm .03$	116, 117

Compound	Configuration	Distances (A)	References
	X. Aliphatic compounds.—(Continued).		
***C_4 Group** (continued)*			
$C_4H_8O_2$ (1,4-dioxane)	Angle C–O–C =110±5°	C–C =1.54 (assumed) C–O =1.46±0.04 C–H =1.06 (assumed)	11
$C_4H_8Br_2$ (*meso* and racemic 2,3-dibromobutane)	Angle C–C–Br =109.5±2° Angle C–C–C =110.5° (assumed)	C–C =1.54 (assumed) C–Br =1.91 (assumed) Br–Br =4.60±0.03 C–Br (non-bonded) =2.83±0.02	120
C_4H_7Cl (isocrotyl chloride)	Angle C–C–Cl =123±2° Angle C–C–C =111±3°	C–C =1.54 (assumed) C–Cl =1.72±0.02	123
$C_4H_4N_2$ (pyrazine)	Planar	C–C =1.39 C–N =1.35±0.02 C–H =1.09	111
C_4H_4O (furan)	Angle C–O–C =107±4° Angle O–C–C =109±3° Angle C–C–C =107±2°	C–C (double bond) =1.35 C–C (single bond) =1.46 C–O =1.41±0.02	111
C_4H_4S (thiophene)	Angle C–S–C = 91±4° Angle S–C–C =112±3° Angle C–C–C =113±3°	C–C (double bond) =1.35 (assumed) C–C (single bond) =1.44 (assumed) C–S =1.74±0.03 C–H =1.09 (assumed)	111
C_4H_5N (pyrrole)	Angle C–N–C =105±4° Angle N–C–C =110±3° Angle C–C–C =108±2°	C–C (double bond) =1.35 (assumed) C–C (single bond) =1.44 (assumed) C–N =1.42±0.02 C–H =1.09 (assumed)	111
$(CH_3)_6Si$	See Section No. IV		
$(CH_3)_4Ge$	See Section No. IV		
$(CH_3)_4Sn$	See Section No. IV		
$(CH_3)_4Pb$	See Section No. IV		
$(CH_3)_3CH$ (isobutane)	Angle C–C–C =111° 30′±2°	C–C =1.54±0.02	80, 98, 128
$(CH_3)_3CCl$ (*t*-butyl chloride)	Angle C–C–C =111° 30′±2°	C–C =1.54± .02 C–Cl =1.78±0.03	98
$(CH_3)_3CBr$ (*t*-butyl bromide)	Angle C–C–C =111° 30′±2°	C–C =1.54± .02 C–Br =1.92±0.03	70, 98
$(CH_2)_4I_2$ (1,4-diiodobutane)		No structure obtained	99
$(C_2H_5)_2O$	Angle C–O–C =100°	C–O =1.33±0.08	100
$(CO)_4Ni$	See Section No. VIII		
$(CO)_4CoH$	See Section No. VIII		
$(CO)_4FeH_2$	See Section No. VIII		
C_5 Group			
C_5H_6 (cyclopentadienne)	Single bond angle C–C–C=101±4° Single-double bond angles are 109±3° and 110±2°	C–C (double bond) =1.35 C–C (single bond) =1.53, 1.46 C–H =1.09	111
C_5H_8 (spiropentane)	Carbon atoms form two equilateral triangles	C–C =1.54 C–H =1.08	115
C_5H_{10} (cyclopentane)	Plane pentagon of carbon atoms	C–C =1.52±0.03 C–H =1.09 (assumed)	5, 72, 80
C_5H_{12} (pentane)		C–C =1.53± .05	5, 72
$(CH_3)_4C$ (neopentane)	Tetrahedral	C–C =1.54± .02 C–H =1.09	80, 115
$(CH_2Cl)_4C$		C–C =1.54 C–Cl =1.76	102
$(CH_2Br)_4C$		C–C =1.54 C–Br =1.93	103, 102
$(CH_2I)_4C$		C–C =1.54 C–I =2.10	103, 102
$(CH_2)_3Br_2$ (1,5-dibromopentane)		No structure obtained	99
C_5H_5N (pyridine)	Hexagon	C–C =1.39 C–N =1.37±0.03 C–H =1.09	111
$(CO)_5Fe$	See Section No. VIII		

Compound	Configuration	Distances (A)	References
	X. *Aliphatic compounds.—(Continued).*		
C_6 Group			
C_6H_{14} (hexane)		C–C =1.54±0.05	5, 72
C_6H_{12} (cyclohexane)	Angle C–C–C = 109° 28′ (assumed)	C–C =1.53±0.03 C–H =1.09 (assumed)	5, 80
C_6H_6 (dimethyldiacetylene)	Carbon atoms linear	C–C (triple bond) =1.20±0.02 C–C (single bond) =1.38±0.03 C–CH_3 =1.47±0.02	119
$C_6H_{10}Cl_2$ (1,4′-dichlorocyclohexane)	Puckered ring, carbon valence tetrahedral	C–Cl =1.76	108
$C_6H_{10}Br_2$ (1,4′-dibromocyclohexane)	Puckered ring, carbon valence tetrahedral	C–Br =1.93	108
$C_6H_{10}Br_2$ (1,3-dibromocyclohexane)	Puckered ring, carbon valence tetrahedral	C–Br =1.93	108
$C_6H_{10}Br_2$ (1,4-dibromocyclohexane)	Puckered ring, carbon valence tetrahedral	C–Br =1.93	108
$C_6H_{10}I_2$ (1,4′-diiodocyclohexane)	Puckered ring, carbon valence tetrahedral	C–I =2.12	109, 108
$C_6H_{10}I_2$ (1,3-diiodocyclohexane)	Puckered ring, carbon valence tetrahedral	C–I =2.12	108
$C_6H_8Br_4$ (1,2,4,5-tetrabromocyclohexane)	Carbon ring rigid symmetrical form. All valence angles tetrahedral	C–C =1.54 C–Br =1.93	129
$(CH_3–CHO)_3$ (paraldehyde)	Puckered ring, tetrahedral angle between bonds	C–C =1.54±0.02 C–O =1.43±0.02	57, 107
$(CH_3)_4C_2$ (tetramethylethylene)	Angle C–C–C = 111° 30′±2°	C–C =1.34 (double bond assumed) C–C =1.54±0.02 (single bond) C–H =1.09	80
$(CH_2)_6N_4$ (hexamethylenetetramine)	See Section No. V		
	XI. *Aromatic compounds.*		
C_6H_6	Planar	C–C =1.39±0.02 C–H =1.08± .04	92, 5, 3, 12, 110, 111
C_6H_5F	Planar	C–C =1.39 (assumed) C–F =1.34±0.04 C–H =1.06 (assumed)	132
1,2–$C_6H_4F_2$	Planar C–C–F angles undistorted	C–C =1.39 (assumed) C–F =1.35±0.03 C–H =1.06 (assumed)	132
C_6H_5Cl	Planar	C–C =1.39±0.02 C–Cl =1.69± .03	112
1,2–$C_6H_4Cl_2$	Planar C–C–Cl angles distorted	C–C =1.40 (assumed) C–Cl =1.71±0.03 Cl–Cl =3.15± .03	112
1,3–$C_6H_4Cl_2$	Planar	C–C =1.40 (assumed) C–Cl =1.69±0.03 Cl–Cl =5.35± .05	112
1,4–$C_6H_4Cl_2$	Planar	C–C =1.40 (assumed) C–Cl =1.69±0.03 Cl–Cl =6.18± .06	112
1,3,5–$C_6H_3Cl_3$	Planar	C–C =1.41 (assumed) C–Cl =1.69±0.03 Cl–Cl =5.38± .05 (meta)	112
1,2,4,5–$C_6H_2Cl_4$	Planar C–C–Cl angles distorted	C–C =1.40 (assumed) C–Cl =1.72±0.04 Cl–Cl =3.20± .04 (ortho) Cl–Cl =5.37± .06 (meta) Cl–Cl =6.25± .07 (para)	112
C_6Cl_6	Planar	C–C =1.41 (assumed) C–Cl =1.70±0.03 Cl–Cl =3.11 (ortho)	73, 113, 112
1,4–$C_6H_4Br_2$	Planar	C–C =1.41 C–Br =1.88±0.01	73, 113
1,3,5–$C_6H_3Br_3$	Planar	C–C =1.41 C–Br =1.88±0.01	73, 113

Compound	Configuration	Distances (A)	References
	XI. *Aromatic compounds.—(Continued).*		
C_6Br_6	Planar	C–C =1.41 C–Br =1.88±0.01	73, 113
1,2–$C_6H_4I_2$	Planar C–C–I angles distorted	C–C =1.42 (assumed) C–I =2.00±0.05 I–I =4.00±0.10	62, 125
1,3–$C_6H_4I_2$	Planar	C–C =1.42 (assumed) C–I =2.03± .05 I–I =5.97± .10	62
1,4–$C_6H_4I_2$	Planar	C–C =1.41 C–I =2.05± .01 I–I =6.92	62, 73, 113
1,3,5–$C_6H_4I_2$	Planar	C–C =1.41 C–I =2.05± .01	73, 113
1,4–$C_6H_4(CH_3)_2$	Planar	C_{ar}–C_{ar} =1.40± .01 C_{ar}–C_{al} =1.50± .01	110
1,3,5–$C_6H_3(CH_3)_3$	Planar	C_{ar}–C_{ar} =1.39 C_{ar}–C_{al} =1.54± .01	110, 80
$C_6(CH_3)_6$	Planar	C_{ar}–C_{ar} =1.39 C_{ar}–C_{al} =1.54± .01	110, 80
	XII. C_{10} *group.*		
$C_{10}H_{20}Br_2$ (1,10-dibromodecane)	No structure obtained		99
$C_{10}H_6I_2$ (1,8-diiodonaphthalene)	I–C–C angles deformed	I–I =3.7	125
$C_{10}H_6I_2$ (2,6-diiodonaphthalene)	Planar	I–I =9.1	125
	XIII. C_{12} *group.*		
$C_{12}H_8I_2O$ (4,4′-diiododiphenyl ether)	Angle C–O–C =118±3°	C–I =2.00 (assumed) C–C =1.42 (assumed) C–O =1.42 (assumed)	44
$C_{12}H_8I_2$ (4,4′-diiododiphenyl)		I–I =11.1	125
$C_{12}H_8Br_2Hg$ (4,4′-dibromodiphenyl mercury)	Angle Br–Hg–Br has a swing of 30° from linear position	C–Br =1.88 C–Hg =2.10	126
$C_6(CH_3)_6$	See Section No. XI		

Table References.—(*Continued*).

29. S. H. Bauer, J. Am. Chem. Soc. **59**, 1804 (1937).
30. J. Y. Beach and A. Turkevich, J. Am. Chem. Soc. **61**, 299 (1939).
31. K. J. Palmer and N. Elliott, J. Am. Chem. Soc. **60**, 1852 (1938).
32. L. O. Brockway and F. T. Wall, J. Am. Chem. Soc. **56**, 2373 (1934).
33. L. O. Brockway, Rev. Mod. Phys. **8**, 231 (1936).
34. M. de Hemptinne and J. Wouters, Nature **138**, 884 (1936).
35. M. de Hemptinne and J. Wouters, Nature **139**, 928 (1937).
36. J. Wouters, M. de Hemptinne and P. Capron, Sci. Abs. **40**, No. 2312, p. 545 (1937).
37. L. O. Brockway and H. O. Jenkins, J. Am. Chem. Soc. **58**, 2036 (1936).
38. L. O. Brockway and I. E. Coop, Trans. Faraday Soc. **34**, 1429 (1938).
39. L. O. Brockway and J. Y. Beach, J. Am. Chem. Soc. **60**, 1836 (1938).
40. O. Hassel and L. C. Strömme, Zeits. f. physik. Chemie **B38**, 466 (1937–38).
41. M. Rouault, Comptes rendus **206**, 51 (1938).
42. J. A. Hveding and L. C. Strömme, Chem. Abs. **32**, 4423[8] (1938).
43. L. Pauling, A. W. Laubengayer and J. L. Hoard, J. Am. Chem. Soc. **60**, 1605 (1938).
44. L. R. Maxwell, S. B. Hendricks and V. M. Mosley, J. Chem. Phys. **3**, 699 (1935).
45. D. P. Stevenson and H. Russell, Jr., J. Am. Chem. Soc. **61**, 3264 (1939).
46. J. Y. Beach and D. P. Stevenson, J. Chem. Phys. **6**, 75 (1938).
47. M. Rouault, Comptes rendus **207**, 620 (1938).
48. L. R. Maxwell, S. B. Hendricks and Lola S. Deming, J. Chem. Phys. **5**, 626 (1937).
49. G. C. Hampson and A. J. Stosick, J. Am. Chem. Soc. **60**, 1814 (1938).
50. A. J. Stosick, J. Am. Chem. Soc. **61**, 1130 (1939).
51. H. D. Springall and L. O. Brockway, J. Am. Chem. Soc. **60**, 996 (1938).
52. L. O. Brockway and L. Pauling, Proc. Nat. Acad. Sci. **19**, 860 (1933).
53. L. Pauling and L. O. Brockway, J. Am. Chem. Soc. **59**, 13 (1937).
54. J. D. Howe and K. Lark-Horovitz, Phys. Rev. **51**, 380A (1937).
55. J. Y. Beach, Pub. A. A. A. Sci. No. 7, 88 (1939).
56. D. P. Stevenson and J. Y. Beach, J. Am. Chem. Soc. **60**, 2872 (1938).

57. P. G. Ackermann and J. E. Mayer, J. Chem. Phys. **4**, 377 (1936).
58. L. O. Brockway, J. Y. Beach and L. Pauling, J. Am. Chem. Soc. **57**, 2693 (1935).
59. H. Braune and S. Knoke, Zeits. f. physik. Chemie **B21**, 297 (1933).
60. L. O. Brockway and L. Pauling, Proc. Nat. Acad. Sci. **19**, 68 (1933).
61. L. O. Brockway, J. Phys. Chem. **41**, 747 (1937).
62. S. B. Hendricks, L. R. Maxwell, V. M. Mosley and M. E. Jefferson, J. Chem. Phys. **1**, 549 (1933).
63. J. Hengstenberg and L. Brú, Anales soc. España. fis. quim. **30**, 341 (1932).
64. P. P. Debye, Physik. Zeits. **40**, 66 (1939).
65. R. W. Dornte, J. Chem. Phys. **1**, 566 (1933).
66. V. E. Cosslett and H. G. de Laszlo, Nature **134**, 63 (1934).
67. V. E. Cosslett, Trans. Faraday Soc. **30**, 981 (1934).
68. C. Degard, J. Piérard and W. van der Grinten, Nature **136**, 142 (1935).
69. J. A. A. Ketelaar, Chem. Weekblad **35**, 195 (1938).
70. R. W. Dornte, J. Chem. Phys. **1**, 630 (1933).
71. H. A. Lévy and L. O. Brockway, J. Am. Chem. Soc. **59**, 1662 (1937).
72. R. Wierl, Ann. d. Physik **13**, 453 (1932).
73. H. de Laszlo, Nature **135**, 474 (1935).
74. C. Finbak and O. Hassel, Zeits. f. physik. Chemie **B36**, 301 (1937).
75. P. Capron and M. de Hemptinne, Sci. Abs. **40**, 207 (1937).
76. A. J. Stosick, J. Am. Chem. Soc. **61**, 1127 (1939).
77. C. Degard, Comptes rendus **202**, 1278 (1936).
78. L. Brú, Anales soc. España fis. quim. **30**, 483 (1932).
79. D. P. Stevenson, J. E. Lu Valle and V. Schomaker, J. Am. Chem. Soc. **61**, 2508 (1939).
80. L. Pauling and L. O. Brockway, J. Am. Chem. Soc. **59**, 1223 (1937).
81. S. H. Bauer, J. Y. Beach and J. H. Simons, J. Am. Chem. Soc. **61**, 19 (1939).
82. L. O. Brockway and J. S. Anderson, Trans. Faraday Soc. **33**, 1233 (1937).
83. R. V. G. Ewens and M. W. Lister, Trans. Faraday Soc. **35**, 681 (1939).
84. L. O. Brockway and P. C. Cross, J. Chem. Phys. **3**, 828 (1935).
85. L. R. Maxwell and V. M. Mosley, Phys. Rev. **55**, 238A (1939).
86. H. Braune and S. Knoke, Naturwiss. **21**, 349 (1933).
87. L. O. Brockway, R. V. G. Ewens and M. W. Lister, Trans. Faraday Soc. **34**, 1350 (1938).
88. R. V. G. Ewens and M. W. Lister, Trans. Faraday Soc. **34**, 1358 (1938).
89. L. Brú, Anales soc. España fis. quim. **31**, 115 (1933).
90. J. Y. Beach and A. Turkevich, J. Am. Chem. Soc. **61**, 303 (1939).
91. A. Turkevich and J. Y. Beach, J. Am. Chem. Soc. **61**, 3127 (1939).
92. R. Wierl, Physik. Zeits. **31**, 366 (1930).
93. L. O. Brockway, J. Am. Chem. Soc. **58**, 2516 (1936).
94. L. Pauling and L. O. Brockway, Proc. Nat. Acad. Sci. **20**, 336 (1934).
95. L. O. Brockway, Proc. Nat. Acad. Sci. **19**, 303 (1933).
96. S. H. Bauer, J. Chem. Phys. **4**, 406 (1936).
97. H. Boersch, Naturwiss. **22**, 172 (1934).
98. J. Y. Beach and D. P. Stevenson, J. Am. Chem. Soc. **60**, 475 (1938).
99. J. A. A. Ketelaar and K. J. Palmer, J. Am. Chem. Soc. **59**, 2470 (1937).
100. L. Brú, Anales soc. España fis. quim. **30**, 486 (1932).
101. J. Wouters and M. de Hemptinne, Nature **141**, 412 (1938).
102. O. Hassel and L. C. Strömme, Zeits. f. physik. Chemie **B38**, 349 (1937–38).
103. H. de Laszlo, Comptes rendus **198**, 2235 (1934).
104. J. Y. Beach and K. J. Palmer, J. Chem. Phys. **6**, 639 (1938).
105. A. C. Hugill, I. E. Coop and L. E. Sutton, Trans. Faraday Soc. **34**, 1518 (1938).
106. O. Hassel and A. Sandbo, Zeits. f. physik. Chemie **B41**, 75 (1938).
107. D. C. Carpenter and L. O. Brockway, J. Am. Chem. Soc. **58**, 1270 (1936).
108. J. G. Gudmundsen and O. Hassel, Zeits. f. physik. Chemie **B40**, 326 (1938). For information on structure notation, see E. Halmöy and O. Hassel, Zeits. f. physik. Chemie **B16**, 234 (1932).
109. H. de Laszlo, Trans. Faraday Soc. **30**, 876 (1934).
110. P. L. F. Jones, Trans. Faraday Soc. **31**, 1036 (1935).
111. V. Schomaker and L. Pauling, J. Am. Chem. Soc. **61**, 1769 (1939).
112. L. O. Brockway and K. J. Palmer, J. Am. Chem. Soc. **59**, 2181 (1937).
113. H. de Laszlo, Proc. Roy. Soc. **A146**, 672 and 690 (1934).
114. C. Degard, Comptes rendus **201**, 951 (1935).
115. F. Rogowski, Ber. Deut. Chem. Ges. **72**, 2021 (1939).
116. L. O. Brockway and P. C. Cross, J. Am. Chem. Soc. **58**, 2407 (1936).
117. L. O. Brockway and P. C. Cross, J. Am. Chem. Soc. **59**, 1147 (1937).
118. C. Degard, Bull. Soc. Chim. Belg. **47**, 770 (1938).
119. L. Pauling, H. D. Springall and K. J. Palmer, J. Am. Chem. Soc. **61**, 927 (1939).
120. D. P. Stevenson and V. Schomaker, J. Am. Chem. Soc. **61**, 3173 (1939).
121. J. E. Lu Valle and V. Schomaker, J. Am. Chem. Soc. **61**, 3520 (1939).
122. D. P. Stevenson, H. D. Burnham and V. Schomaker, J. Am. Chem. Soc. **61**, 2922 (1939).
123. J. Y. Beach and D. P. Stevenson, J. Am. Chem. Soc. **61**, 2643 (1939).
124. C. Degard, Bull. Soc. Chem. Belg. **45**, 15 (1936).
125. H. de Laszlo, Trans. Faraday Soc. **30**, 892 (1934).
126. H. de Laszlo, Trans. Faraday Soc. **30**, 884 (1934).
127. H. de Laszlo, Trans. Faraday Soc. **30**, 825 (1934).
128. J. Y. Beach and J. Walter, J. Chem. Phys. **8**, 303 (1940).
129. E. Halmöy and O. Hassel, J. Am. Chem. Soc. **61**, 1601 (1939).
130. M. W. Lister and L. E. Sutton, Trans. Faraday Soc. **35**, 495 (1939).
131. P. P. Debye, Physik. Zeits. **40**, 404 (1939).
132. H. Oosaka, Bull. Chem. Soc. Japan **15**, 31 (1940).
133. H. Braune and K. W. Stute, Angew. Chemie **51**, 528 (1938).
134. H. Brode, Verh. Deutsch. Phys. Ges. **20**, 14 (1939).
135. J. A. A. Ketelaar, Chem. Abs. **33**, 7635^3 (1939).
136. C. Degard, Chem. Abs. **33**, 467^8 (1939).
137. M. H. Pirenne, J. Chem. Phys. **7**, 144 (1939).
138. H. A. Skinner and L. E. Sutton, Trans. Faraday Soc. **36**, 668 (1940).
139. J. Y. Beach and S. H. Bauer, private communication, to be published in the J. Am. Chem. Soc., October, 1940.
140. M. Rouault, Comptes rendus **208**, 1290 (1939).
141. H. Mark and R. Wierl, Naturwiss. **18**, 205 (1930).
142. F. Kirchner, Physik. Zeits. **31**, 1025 (1930).
143. R. Wierl, Physik. Zeits. **31**, 1028 (1930).
144. V. Schomaker and D. P. Stevenson, J. Am. Chem. Soc. **62**, 1270 (1940).
145. D. P. Stevenson and V. Schomaker, J. Am. Chem. Soc. **62**, 1267 (1940).
146. H. A. Skinner and L. E. Sutton, Trans. Faraday Soc. **36**, 681 (1940).
147. R. A. Spurr and V. Schomaker, private communication, to be published in the J. Am. Chem. Soc.
148. L. Pauling, *The Nature of the Chemical Bond* (Cornell University Press, New York, 1939), p. 103.

For tables of atomic radii see references 80, 37, 61, 106 and 20.

III. The Raman Spectra Method*

GEORGE M. MURPHY
Sterling Chemistry Laboratory, Yale University, New Haven, Connecticut
(Received March 26, 1940)

THE Raman effect is a phenomenon which depends on the scattering of light, a subject which has been studied by many investigators. As long ago as the fifteenth century, for example, Leonardo da Vinci[1] believed that the blue of the sky was caused by light scattered by suspended particles of ice or dust in the atmosphere. But it was not until 1899, that Lord Rayleigh[2] showed that the color of the sky is indeed due to scattered light but the scattering particles are the molecules of air themselves. This light is commonly called Rayleigh radiation and is found to have the same frequency as that of the incident light. Like reflected light, it is generally of no interest to the spectroscopist since he would be happier if there were none of it.

Careful examination shows that in addition to the Rayleigh radiation, there is a small amount of scattered light which has a frequency different from that of the incident light. These altered frequencies were first studied experimentally by Raman[3] in 1928 and independently at about the same time by Landsberg and Mandelstam.[4] Some theoretical predictions had been made by Smekal[5] in 1923 and by Kramers and Heisenberg[6] in 1925.

Since the effect results from the interaction of light with matter, a rather complicated theory[7] is needed to account for it. The following simple classical considerations, however, show that it should exist. Assume that the scattering particle is a diatomic gas molecule and let the two identical nuclei be held fixed at their equilibrium distance, r_e. Because of the symmetrical arrangement of the electric charge and the mass of the molecule, it has no permanent dipole moment. But if it is now irradiated with monochromatic light of frequency, ν, the electrons are periodically displaced in the rhythm of the incident light and a dipole moment is induced in the molecule. Let the electric vector of the incident light be:

$$\mathbf{E}=\mathbf{E}_0 \cos 2\pi\nu t, \tag{1}$$

then the induced moment,

$$\mathbf{M}_i=\alpha_e\mathbf{E}=\alpha_e\mathbf{E}_0 \cos 2\pi\nu t, \tag{2}$$

where α_e is the polarizability and is a measure of the ease with which the negative charge distribution of the molecule may be deformed. The secondary waves which are emitted by the molecule are of the same frequency as that of the incident light and these constitute the Rayleigh radiation.

Now let the molecule vibrate along the line joining the nuclei. The polarizability will vary with the internuclear distance and for small displacements, x

$$\alpha_v=\alpha_e+\alpha_1\mathbf{x} \tag{3}$$

and if the vibration is simple harmonic

$$\mathbf{x}=\mathbf{x}_0 \cos 2\pi\nu t. \tag{4}$$

The induced moment for the vibrating molecule now becomes

$$\begin{aligned}\mathbf{M}_i&=\alpha_v\mathbf{E}\\&=\alpha_e\mathbf{E}_0 \cos 2\pi\nu t+\tfrac{1}{2}\alpha_1\mathbf{x}_0\mathbf{E}_0\\&\quad\times\{\cos 2\pi(\nu+\omega)t+\cos 2\pi(\nu-\omega)t\}.\end{aligned} \tag{5}$$

The scattered light now consists of the Rayleigh radiation and two new frequencies, $\nu\pm\omega$ where ω

---

* Invited paper presented at the joint Symposium on Optical Methods for the Study of Molecular Structure, at the New York Meeting of the Optical Society of America and the American Physical Society, February 23, 1940.

[1] *The Note Books of Leonardo da Vinci*, edited by Edward MacCurdy (Reynal & Hitchcock, New York, 1938).

[2] Lord Rayleigh, Phil. Mag. **47**, 375 (1899).

[3] Sir C. V. Raman, Ind. J. Phys. **2**, 387 (1928).

[4] G. Landsberg and L. Mandelstam, Naturwiss. **16**, 57, 772 (1928).

[5] A. Smekal, Naturwiss. **11**, 873 (1923).

[6] H. A. Kramers and W. Heisenberg, Zeits. f. Physik **31**, 681 (1925).

[7] For a complete account of the theory as well as applications to problems of molecular structure see G. Placzek, "Rayleigh-Streuung und Raman-Effekt" in Marx, *Handbuch der Radiologie, Quantenmechanik der Materie und Strahlung* (Akademische Verlagsgesellschaft m. b. H., Leipzig, 1934), Part 2, pp. 205–374.

is a natural vibrational frequency of the molecule. Similar simple considerations show that if the molecule is rotating and not vibrating, two altered frequencies will again appear, the shift now depending on the moment of inertia of the molecule. An actual molecule is simultaneously rotating and vibrating, hence both types of Raman spectra will occur.

The simple diagram shown in Fig. 1 explains the situation with the aid of energy levels. Let a photon of energy, $h\nu$ fall upon a molecule in its normal state. The molecule may re-emit the same light quantum without change of state or it may emit light of frequency, $h\nu' = h\nu - E_2 + E_1$, by transition to the state 2. The scattered light is called Stokes radiation and is of shorter frequency than the incident light. If the molecule is initially in the state 2, it may revert to the normal state with emission of light, $\mathbf{h\nu' = h\nu + E_2 - E_1}$ which is of higher frequency than the incident light. This is called anti-Stokes radiation. Since the intensity of the scattered light is proportional to the number of molecules which are causing the scattering, it is obvious that Stokes lines are considerably more intense than anti-Stokes lines at the ordinary conditions of experiment.

Since the discovery of the Raman effect, a very large number of papers have appeared concerning it. It is thus impossible to discuss but a small part of the available data and its application to chemical and physical problems.[8] At the risk of giving a false picture of the great usefulness of the Raman effect, this report is limited to some results on a few simple gases.

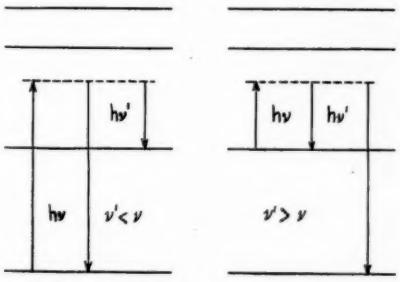

FIG. 1. Mechanism of Stokes radiation ($\nu' < \nu$) and of anti-Stokes radiation ($\nu' > \nu$).

EXPERIMENTAL METHOD

The experimental method[9] is well known and little need be said of it here. The gas is contained in a suitably shaped vessel and is at a pressure as high as convenient since the scattering is proportional to the number of molecules irradiated.

FIG. 2. Complete Raman spectrum of a diatomic gas molecule. The pure rotation and rotation-vibration absorption spectra in the infra-red are shown below for comparison.

A light source is focused on the gas and the light which is scattered at right angles to the source is focused on the slit of a spectrograph. The principle requirement of the light source is that it be of high intrinsic brilliance. It should either be monochromatic or else have a spectrum containing only a few widely separated lines. These requirements are well fulfilled by the mercury arc. If necessary, filters may be used to obtain monochromatic light. Since the intensity of the scattered light is proportional to the fourth power of the frequency, the bright mercury line, 2536A is often used. Since light must be conserved in as many ways as possible, the spectrograph should have a wide aperture. Knowledge concerning the state of polarization of the Raman lines is of considerable value but due to the low intensity this is a matter of some experimental difficulty.[10]

RAMAN SPECTRA OF A DIATOMIC GAS

A highly idealized picture of the complete Raman spectra of a diatomic gas is shown in Fig. 2. The broad Rayleigh line is in the center of

[8] Applications of Raman spectra to chemical and physical problems are discussed in considerable detail by K. W. F. Kohlrausch, *Der Smekal-Raman-Effekt* (J. Springer, Berlin, 1931), supplementary volume, 1938; and by J. H. Hibben, *The Raman Effect and Its Chemical Applications* (Reinhold Publishing Co., New York, 1939).

[9] For further details, consult the books cited in reference 8. Particularly convenient light sources have been described by Geo. Glockler and C. E. Morrell, J. Chem. Phys. **4**, 15 (1936) and by J. S. Kirby-Smith and L. G. Bonner, J. Chem. Phys. **7**, 880 (1939).

[10] A simple method, using a Polaroid disk has been described by F. F. Cleveland and M. J. Murray, J. Chem. Phys. **7**, 396 (1939).

a group of pure rotational Raman lines which are approximately evenly spaced. The Stokes and anti-Stokes lines here are of about equal intensity but since they are very close to the broad exciting line, they are difficult to obtain experimentally. The spacing between these lines is inversely proportional to the moment of inertia of the molecule and hence gives a measurement of the internuclear distance. The most prominent feature of the spectrum is the broad, unresolved line which is the Q branch of the rotation-vibration spectrum. In general, this is the only part of the Raman spectrum that is observed and its companion anti-Stokes line is usually too faint to obtain. Its distance from the Rayleigh line is approximately equal to the vibrational frequency of the molecule. The Q branch is surrounded symmetrically by O and S branches (corresponding to changes in the rotational quantum number, J of ± 2) and as in the pure rotation spectrum, the spacing between the lines is a measure of the internuclear distance.

If both nuclei in the molecule are identical, the alternate lines in the spectrum show alternation of intensities, as indicated in Fig. 2, this phenomenon giving a measure of the nuclear spin. If the two nuclei are not identical, no such alternation occurs.

As described above, the Raman effect depends upon a nonvanishing polarizability. Absorption by a molecule in the infra-red, however, depends upon a nonvanishing component of electric moment. If both nuclei in a molecule are identical, the molecule will therefore not absorb in the infra-red but if the two nuclei are different, such absorption occurs. The resulting pure rotation and rotation-vibration spectra are shown in Fig. 2 for comparison with the Raman effect. The spacing between lines is approximately one-half that in the Raman effect but it also may be used to determine the molecular constants. The difficulty of working in the far infra-red where this absorption occurs is not present with the Raman effect since the latter is in the visible or ultraviolet regions where the photographic technique is easy. However this advantage is perhaps overweighed by the fact that the Raman spectrum is considerably less intense than the infra-red absorption.

The pure rotation Raman spectrum of nitrogen gas is shown in Fig. 3. This beautiful spectrogram was obtained by Mr. Charles E. Miller[11] of Columbia University and is strikingly like the predicted spectrum shown in Fig. 2. The alternation of intensities is 2 to 1, showing that the nuclear spin of nitrogen is unity.

Raman Spectra of Polyatomic Molecules

The mechanical motions of a molecule containing more than two atoms are somewhat more

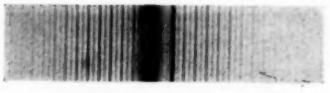

Fig. 3. Rotational Raman spectrum of nitrogen gas.

complicated than that of a diatomic molecule and hence the resulting spectrum is quite complex. If the molecule contains n atoms, $3n$ coordinates are required to describe its motion. Of these $3n$, three are needed to fix its position with regard to fixed axes and hence correspond with translation of the molecule as a whole. These are of little interest to the spectroscopist. Three more coordinates are needed to describe the orientation around an axis fixed in the rigid molecule, two fixing the latitude and longitude and the third giving the amount of rotation around the axis. These account for the rotational structure of the Raman and infra-red bands. The remaining $3n-6$ coordinates determine the vibrational motion of the molecule, unless the molecule is linear, when there are only $3n-5$ vibrations.

Classical mechanics may be used to a large extent in discussing the motion and as a first approximation, all of the nuclei are fixed so that the molecule cannot rotate. The kinetic and potential energies of the molecule are now expressed in terms of some appropriate coordinates, q_i and the corresponding velocities, $\dot{q}_i$. The kinetic energy, T becomes:

$$2T=\Sigma a_{ij}\dot{q}_i\dot{q}_j, \quad (3n^2 \text{ terms}; 3n \text{ velocities}) \quad (6)$$

where the a_{ij} are some function of the masses of

[11] C. E. Miller, J. Chem. Phys. **6**, 902 (1938). I should like to thank Mr. Miller for permission to reproduce this photograph here.

the nuclei and if the motion is simple harmonic, the potential energy, V is:

$$2V=\Sigma b_{ij}q_iq_j, \quad (3n^2 \text{ terms}; 3n \text{ coordinates}) \quad (7)$$

where the b_{ij} are force constants. The equations of motion should then be solved by the well-known methods but unfortunately the occurrence of cross-product terms in T or V or both make this procedure impossible in general. Also we do not know the shape of a specific molecule and therefore cannot write down explicit equations for T and V. But we may always make judicious guesses concerning the shape and may then solve the individual cases and compare the results with experiment to determine the geometry of the molecule. The appearance of cross-product terms in T and V may be overcome by a linear transformation to new coordinates

$$q_k=\Sigma B_{kl}Q_l, \quad (8)$$

after which T and V become

$$2T=\Sigma\dot{Q}_i^2, \quad (9)$$

$$2V=\Sigma\lambda_iQ_i^2 \quad (10)$$

and then the equations of motion are easily solvable. The new coordinates, Q_k are called normal coordinates[12] and the solution of the equations of motion shows that each nucleus executes a simple harmonic oscillation about its equilibrium position with the frequency,

$$2\pi\nu_k=(\lambda_k)^{\frac{1}{2}}. \quad (11)$$

All of the nuclei move with the same frequency and the same phase; that is, they all pass through their equilibrium positions and reach their positions of maximum amplitude at the same time. The complete motion of the molecule is thus complex but it may be considered as a superposition of $3n-6$ normal vibrations, each with its own frequency.

The ideal situation would be to know the force constants, b_{ij} since the λ and hence the observed frequencies are the $3n-6$ roots of the secular determinant

$$|a_{ik}\lambda-b_{ik}|=0. \quad i,k=1,2,\cdots 3n. \quad (12)$$

Having obtained the λ from Eq. (12), one could immediately calculate the appearance of the spectrum. But since we do not know the force constants, the calculation is reversed and the force constants are calculated from the observed spectrum.

The solution of the secular equation may prove very difficult, especially for complicated molecules. However, in principle it is always solvable and in practice it is not necessary to solve it since considerable information concerning the normal vibrations may be obtained from a study of the symmetry of the molecule. By the methods of group theory[13] and with an assumed symmetry for the molecule, one can obtain with relative ease the following results: the total number of vibrational frequencies which will appear in the infra-red in absorption or in the Raman effect; the selection rules for overtone and combination bands and diagrams for the motion involved in each normal vibration.[14]

The symmetry of the molecule and the methods of group theory may also be used to obtain information concerning the state of polarization of the Raman lines. The polarizability of a molecule may be written

$$\alpha=\alpha'+\alpha'', \quad (13)$$

where α' is called the average polarizability and α'' is a factor of anisotropy. These two parts are independent and additive for the polarizability

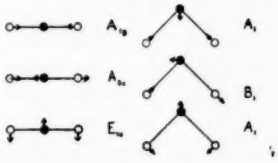

FIG. 4. Normal vibrations of molecules belonging to the symmetry groups $D_{\infty h}$ and C_{2v}.

of the molecule and the latter may be considered as a mixture of two kinds of molecules, part of them having the polarizability, α' and the rest having α''. If the incident light is polarized,

[12] For further details concerning normal coordinates and the method of small vibrations in polyatomic molecules, see D. M. Dennison, Rev. Mod. Phys. 3, 280 (1931) or L. Pauling and E. B. Wilson, Jr., *Introduction to Quantum Mechanics* (McGraw-Hill Book Co., New York, 1935).

[13] The application of group theory to the vibrations of polyatomic molecules is discussed by J. E. Rosenthal and G. M. Murphy, Rev. Mod. Phys. 8, 317 (1936).

[14] A useful summary of the selection rules and other properties of the normal vibrations for a large number of molecules has been given by E. B. Wilson, Jr., J. Chem. Phys. 2, 432 (1934).

molecules of the first kind will produce completely polarized scattered light but the molecules of the second kind will result in scattered light polarized perpendicular to the direction of the original beam. If the scattered light is then investigated with a Nicol prism (or Polaroid), parallel and perpendicular to the polarization of the incident light, the two parts of the polarizability may be distinguished. The ratio of the intensity of the two kinds of scattering is called the degree of depolarization and is given by

$$\rho = 3\alpha''^2/(5\alpha'^2+4\alpha''^2) \qquad (14)$$

for linearly polarized light and for unpolarized light

$$\rho_n = 2\rho/(1+\rho). \qquad (15)$$

From (14) it is seen that ρ varies between 0, where $\alpha''=0$ and $\frac{3}{4}$ where $\alpha'=0$. The quantity α' will be different from zero only for a totally symmetric vibration (group representation, A_1). For all other vibrations, $\rho=\frac{3}{4}$ and $\rho_n=6/7$. The anisotropic factor, α'' is of more complicated symmetry and little can be said about it from symmetry considerations alone. In the case of cubic symmetry and for totally symmetric vibrations, $\alpha''=0$, hence $\rho=\rho_n=0$. For other cases of totally symmetric function $0\leqq\rho\leqq\frac{3}{4}$.

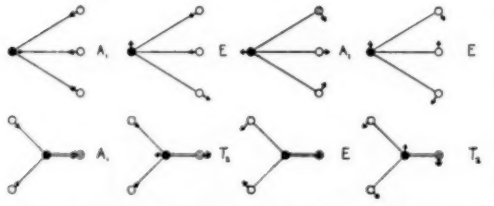

FIG. 5. Normal vibrations of molecules belonging to the symmetry groups C_{3v} and T_d.

FORCE CONSTANTS

A complete knowledge of both the Raman and infra-red absorption spectra of a polyatomic molecule will thus result in the determination of bond angles, distances and force constants. The latter are of particular interest to the chemist since they furnish information concerning the strength of a bond and thus the ease with which a given molecule will take part in a chemical reaction.[15]

The remainder of this report is concerned with a few selected molecules. The order of discussion is not that of increasing complexity of the spectrum but in order of increasing number of atoms in the molecule. The Raman spectrum will be similar to that shown in Fig. 2 but for more complete details, the books given in reference (16) should be consulted.[16]

LINEAR TRIATOMIC MOLECULES

The molecule, carbon dioxide, is known to be linear since it has no permanent dipole moment. Chemical evidence shows that the two oxygen atoms are equivalent and therefore they must be symmetrically arranged in the molecule. There are three normal vibrations, one being doubly-degenerate, that is two of the roots of the secular determinant, Eq. (12) are equal. This means that there are two equivalent vibrations in different directions in space but both having the same frequency. The normal vibrations are shown in Fig. 4. Simple considerations show that only in the vibrational mode,[17] A_{1g} is there a nonvanishing polarizability and hence only this frequency will appear in the Raman effect. The other two frequencies, A_{2u} and E_{1u} are unsymmetrical and hence have a nonvanishing component of electric moment and will occur in absorption in the infra-red. Experimental evidence supports these conclusions. Other triatomic linear molecules are carbon disulfide, nitrous oxide and hydrogen cyanide but the two latter are unsymmetrical and in these cases all three frequencies are permitted in both the Raman effect and in the infra-red.

SYMMETRICAL BENT TRIATOMIC MOLECULES

The most notable example of this type of molecule is water. Other examples are hydrogen sulfide and sulfur dioxide. The rotational fine

[15] Force constants and their determination and significance are discussed by R. deL. Kronig, *Optical Basis of the Theory of Valency* (Cambridge University Press, 1935) and in Eucken-Wolf, *Hand- und Jahrbuch der chemischen Physik*, Vol. 9, Section II, "Molekül- und Kristallgitterspektren," (Akademische Verlagsgesellschaft m. b. H., Leipzig, 1934). See also J. W. Linnett, J. Chem. Phys. 8, 91 (1940).

[16] Considerable information concerning the Raman spectra of gases is given by G. B. B. M. Sutherland, *Infrared and Raman Spectra* (Methuen and Co., London, 1935).

[17] The meaning of the group theory symbols to describe the symmetry of the molecules shown in Figs. 4 and 5 and the symbols used for the modes of vibration are explained in references 7 or 13.

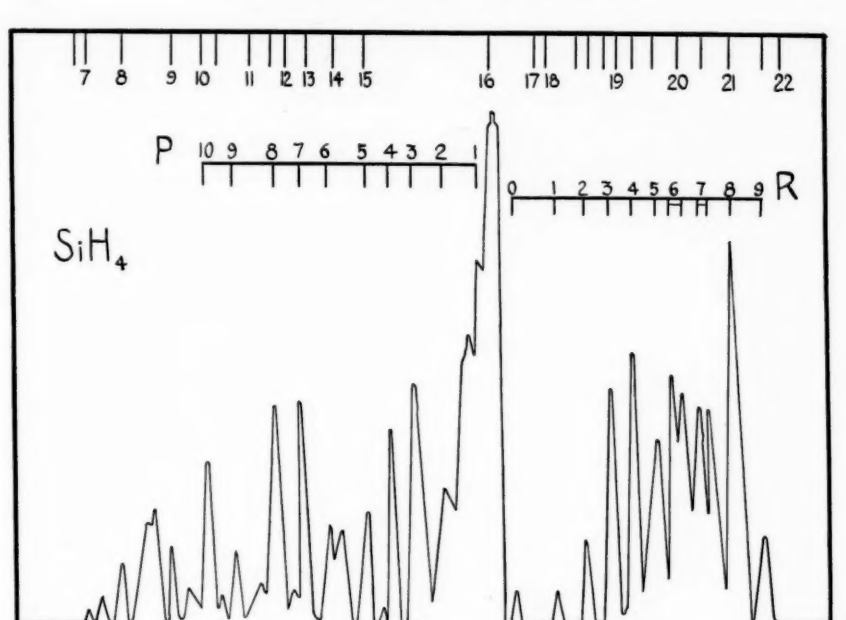

FIG. 6. Theoretical envelope of the 910 cm^{-1} fundamental vibrational band of silane showing fine structure caused by the Coriolis perturbation arising from the Raman frequency. The experimentally observed lines are from Steward and Nielsen (Phys. Rev. **47**, 828 (1935)).

structure of both the Raman bands and the infra-red bands of these molecules is very complex indicating that they are not linear. This is due to the fact that the molecules are asymmetric tops, having three unequal moments of inertia. The normal vibrations are shown in Fig. 4, all three frequencies being permitted in both the Raman effect and in the infra-red. One interesting feature of the spectrum of water is the fact that one of the frequencies observed in the Raman effect appeared to be about 50 cm^{-1} greater than the same vibration observed in the infra-red. This disturbing conclusion has been recently shown by Darling and Dennison[18] to be untrue. The earlier calculations had been based upon a mechanical picture for the molecule which was much too simple. The molecule is actually an anharmonic oscillator and a nonrigid rotator and there are interaction terms between rotation and vibration. The valence angle[18] in water is 104° 31′ and the O–H distance is 0.958A.

PYRAMIDAL TETRATOMIC MOLECULES

The most important type of tetratomic molecule is the regular pyramid having two equal moments of inertia but the third one is unequal to the other two. Important examples are ammonia, phosphine and arsine. The normal vibrations are shown in Fig. 5 of which two are doubly degenerate. All appear both in the Raman effect and in the infra-red. An important feature of molecules of this type is the fact that the nitrogen atom in ammonia, for example, oscillates back and forth through the plane of the three hydrogen atoms. This results in a doubling of the energy levels. The effect could not be detected in the Raman spectrum but has been observed in the rotational spectrum and in rotation-vibration spectra. The symmetry properties of the pairs of closely spaced levels are such that transitions are

[18] B. T. Darling and D. M. Dennison, Phys. Rev. **57**, 128 (1940).

allowed between them. In ammonia this corresponds to about 0.67 cm^{-1} or 15 mm wave-length. The molecule should thus absorb in this region of ultra-short radio waves, a conclusion which has been verified experimentally by Cleeton and Williams.[19] In the case of phosphine and arsine, the pyramid is much taller than in ammonia,[20] the heights in ammonia, phosphine and arsine being 0.30, 0.67 and 0.75A, respectively. And since an increase in the height of the pyramid results in a decrease in the doublet separation, the doubling of levels in phosphine corresponds to absorption of radiation of 60 m wave-length. It should thus be possible to detect this experimentally using radio waves but unfortunately the coefficient of absorption is less than that of ammonia by a factor of about 10^8 which would make this experiment very difficult.

Pentatomic Molecules

The most important molecule of this type is the tetrahedron with three equal moments of inertia, the spherical top. Examples are found in methane, silane, germane and carbon tetrachloride. There are nine normal vibrations but only four different frequencies, one being doubly degenerate and two triply degenerate. These are shown in Fig. 5 and all appear in the Raman effect but only the two triply degenerate ones (T_2) in the infra-red. In the doubly-degenerate vibration, E of tetrahedrally symmetrical molecules, the pair of superimposed atoms shown in Fig. 4 move in opposite directions, the black one, for example moving into the plane of the paper and its companion moving out of this plane. The rotational structure of the two infra-red bands should consist of simple P, Q and R branches similar to that of the rotation-vibration Raman band shown in Fig. 2. The centers of these two regions of absorption[21] in methane occur at approximately 3014 and 1306 cm^{-1}, respectively, and while the former band is essentially of the theoretical appearance, the latter is considerably more complex than was expected. This is due to two kinds of Coriolis interactions between vibration and rotation. The first type has been discussed by Teller and by Johnston and Dennison[22] while the second type which is of more interest to us here has been treated by Wilson[23] and

[19] C. E. Cleeton and N. H. Williams, Phys. Rev. **45**, 234 (1933).

[20] G. B. B. M. Sutherland, E. Lee and Cheng-Kai Wu, Trans. Faraday Soc. **35**, 1373 (1939).

[21] A. H. Nielsen and H. H. Nielsen, Phys. Rev. **48**, 864 (1935).

[22] E. Teller, *Hand- und Jahrbuch d. chem. Physik* (1934), Vol. 9, p. 125; M. Johnston and D. M. Dennison, Phys. Rev. **48**, 868 (1935).

[23] E. B. Wilson, J. Chem. Phys. **4**, 313 (1936).

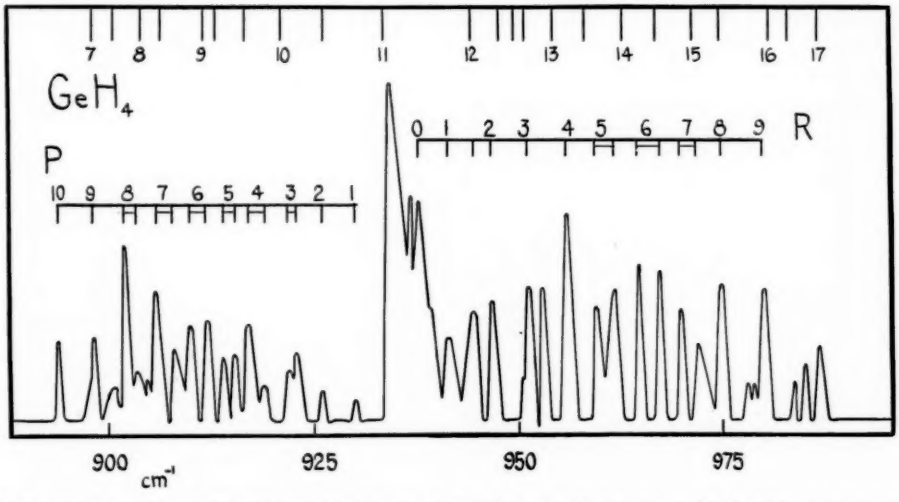

Fig. 7. Theoretical envelope of the 934 cm^{-1} fundamental vibrational band of germane showing fine structure caused by the Coriolis perturbation arising from the Raman frequency. The experimentally observed lines are from Steward and Nielsen (Phys. Rev. **48**, 861 (1935)).

applied to the spectrum of methane by Childs and Jahn.[24] The infra-red levels are perturbed by a nearby vibrational state, which in this case is the doubly degenerate frequency, E, which is optically inactive in the infra-red but which occurs in the Raman effect. The theoretical spectra[25] of silane and germane are shown in Figs. 6 and 7. In each case, the Q branch which is the most intense region of absorption is expected to consist of a single line. In silane, the Raman frequency is at 978 cm^{-1} while the infra-red frequency is at 910 cm^{-1}. The presence of the Raman frequency has shifted the Q branch towards lower frequencies. In the case of germane, the Raman frequency is at about 820 cm^{-1} while the infra-red frequency is at 934 cm^{-1} and since the Raman frequency is now lower than the infra-red frequency, the Q branch has been shifted in the opposite direction.

Ethane, C_2H_6

The molecule, ethane, is of considerable interest at the present time because of the fact that the two methyl groups may rotate around the line joining the two carbon atoms. Present experimental evidence is not sufficient to distinguish between the two possible forms shown in Fig. 8. If the hydrogen atoms are eclipsed, both ends of the molecule are as D_{3h} in the figure while if the atoms are staggered, the ends are like D_{3d}. For either model, there are 12 distinct frequencies of which eleven are shown by Bartholomé and Karweil.[26] The twelfth is the free rotation around the carbon-carbon bond. The latter is optically inactive and does not occur as a fundamental frequency either in the Raman effect or in the infra-red. If the molecule is D_{3d}, six of the remaining frequencies will appear in the Raman effect and five in the infra-red. For the eclipsed model, nine Raman frequencies will occur. All of the Raman spectra on this molecule have been observed in liquid ethane and since the selection principles may not hold there, it is not possible to determine the symmetry of the molecule but the staggered model seems to be preferred. Careful Raman measurements on gaseous ethane would help to settle this question. The inactive frequency may be determined from certain allowed combination bands but the most reliable method is from measurements of the heat capacity[27] of the gas. These show that rotation around the carbon-carbon bond is not free but is restricted by a barrier of about 2750 cal. per mole.

FIG. 8. Model of the ethane molecule, C_2H_6. If the hydrogen atoms are eclipsed both ends are like D_{3h}. If they are staggered, both ends are D_{3d}.

Benzene, C_6H_6

As an example of a still more complicated molecule, benzene may be considered. Possible symmetries are the plane, regular hexagon, D_{6h}; the Kekule model, D_{3h} and the trigonally puckered model, D_{3d}. Considerable dissension once existed concerning this molecule since a simple symmetry rule states that if a molecule possesses a center of symmetry no frequency may occur both in the Raman effect and in the infra-red. This situation existed in benzene and therefore the model, D_{6h} was excluded in favor of the puckered ring although chemical evidence favored the former. This discrepancy is now understood since much of the Raman data was obtained with liquid benzene and the selection rules may break down there. The present interpretation[28] is D_{6h}. There are 30 vibrational frequencies but only 20 different ones of which 10 are nondegenerate and 10 are doubly degenerate. Only 4 fundamental frequencies are permitted in the infra-red and 7 in the Raman effect, the remainder being optically inactive.

The great need in Raman spectra at the present time is not for work on more and more complicated molecules but more careful work on the

[24] W. H. J. Childs and H. A. Jahn, Proc. Roy. Soc. **A169**, 451 (1939).
[25] G. M. Murphy, J. Chem. Phys. **8**, 71 (1940).
[26] E. Bartholomé and J. Karweil, Zeits. f. physik. Chemie B39, 1 (1938).
[27] G. B. Kistiakowsky, J. R. Lacher and F. Stitt, J. Chem. Phys. **7**, 289 (1939).
[28] W. Angus, C. R. Bailey, J. B. Hale, C. K. Ingold, A. H. Leckie, C. G. Raisin, J. W. Thompson and C. L. Wilson, J. Chem. Soc. 971 (1936). The normal vibrations are shown here.

simpler ones. Many of the simplest gases have never been studied. The state of polarization should be carefully measured and the rotational fine structure of rotational-vibrational bands should be resolved and relative intensities determined. An even simpler experiment would consist in the pure rotation spectrum which can be detected with spectrographs of not too great resolving power. The experimental requirements are more easily met than the corresponding ones in the far infra-red. The principle difficulty is in the intensity of the light source. More careful attention to focusing and conservation of light would help along these lines. Raman tubes should be so designed that gases may be studied under high pressures and spectrographs of large light-gathering power should be used. With this information on simpler molecules some of the more difficult problems of rotational-vibrational interaction and anharmonicity could be solved.

The Transmission of Infra-Red Light by Fog

J. A. SANDERSON
Naval Research Laboratory, Anacostia Station, Washington, D. C.

(Received July 12, 1940)

The transmission by 0.244 km of foggy atmosphere has been measured in the infra-red spectrum from 1 to 12μ with a residual ray apparatus employing quartz plates, and with an infra-red spectrometer. The transmission curves when corrected for the transmission of the clear atmosphere were found to be nonselective with wave-length.

EARLIER data on the transmission of long wave-length infra-red light by natural fog obtained by Granath and Hulburt[1] and Hulburt[2] showed that fog becomes only slightly more transparent with increasing wave-length, and that infra-red light offers no practical advantage over visible light in penetrating it. The wave-lengths employed in their experiments were 0.4 to 7μ. The measurements did not extend through the 9 to 11μ region of high transmission by water vapor, and, although the distinction between absorption by water vapor and scattering by particles of water is clear cut, it seemed desirable that experimental measurements be extended to cover this region.

The experiments were begun with the intention of adding a point at 9μ to the earlier curve by Hulburt, and a simple residual ray apparatus using two quartz plates was set up. Subsequently, an infra-red spectrometer became available and made possible the determination of the transmission coefficients of several fogs of fairly uniform density through the infra-red spectrum from 1 to 12μ.

Measurements with both instruments led to the same result: that the attenuation of light by fog is fairly uniform across the spectrum and, particularly, that no advantage is to be derived by using light of wave-length 9–11μ in penetrating fog.

The experiments were made on the bank of the Potomac River; the fogs were clean and apparently free from smoke and probably were typical of fogs encountered at sea. The source of light consisted of two 600-watt Globar heaters at the focus of a 65-cm metal mirror, 0.244 kilometer from the point of observation. The temperature of the source was about 1200°K.

In the measurements with the residual ray apparatus, the light was focused by a 10-cm aluminized mirror of 20 cm focal length on a vacuum thermocouple after two reflections from quartz plates, giving rise to the well-known 9μ reflection band, or two aluminized glass plates reflecting the whole energy of the source. The thermocouple was constructed by the method of Pfund[3] and was evacuated only with a mechanical oil pump. The receiving area was 1 mm in diameter and coated with zinc black.[4]

Further purification of the 9μ spectrum obtained with the quartz plates was effected by the use of a differential mica filter 0.1 mm thick which became opaque at 7.5μ, where quartz reflection begins, while transmitting some 60 percent of the light at shorter wave-lengths. The procedure was to take as 9μ galvanometer deflections the quantities obtained by subtracting from the total deflection with quartz plates the deflection obtained with the mica filter in place. Using a galvanometer of good sensitivity (0.1 μv/mm) and a scale distance of 2.5 meters, the clear weather deflection was about 400 mm, of which 100 mm represented light transmitted by the mica filter, i.e., of wave-length less than 7.5μ.

With the aluminum reflectors in place, the thermocouple was connected to a Rubicon galvanometer (1.25 μv/mm) the sensitivity of which was further reduced by a 2-ohm shunt to 8 μv/mm. Under this condition, the deflection obtained for the entire energy of the source was about 100 mm in clear weather. Needless to say, the shunt was not used during the most dense fogs.

[1] L. P. Granath and E. O. Hulburt, Phys. Rev. **34**, 140 (1929).
[2] E. O. Hulburt, Physics **5**, 101 (1934).
[3] A. H. Pfund, Rev. Sci. Inst. **8**, 417 (1937).
[4] A. H. Pfund, J. Opt. Soc. Am. **23**, 375 (1933).

By interposing the mica filter, galvanometer deflections arising entirely from light of wave-length less than 7.5μ could be determined. Three different spectral distributions of energy were thus available for comparison: the complete energy of the source, the part of this energy below 7.5μ, and the relatively sharp reflection band of quartz at 9μ. The data were obtained by observing the galvanometer deflections with quartz and aluminum reflectors, with and without the mica filter interposed, and taking the ratio of these or the proper difference to corresponding deflections observed when the fog had lifted sufficiently (as it generally did) so that no further increase in energy could be measured.

It was soon apparent that a satisfactory measure of visibility was the total energy received from the source, and all the transmission factors were plotted with total energy (galvanometer reading with aluminum reflectors) as abscissae. The results of measurements on three separate days of fog are given in Fig. 1 in which the transmission for 9μ light and light from the source of wave-length less than 7.5μ are given. Each curve obviously is the locus of points representing transmission of the total energy of the source, so that the deviation of points representing other wave-length bands from these curves is a measure of the behavior of fog toward those wave-lengths. The variation in total energy for clear weather conditions meant only that the thermocouple sensitivity was not exactly reproduced for the three separate sets of

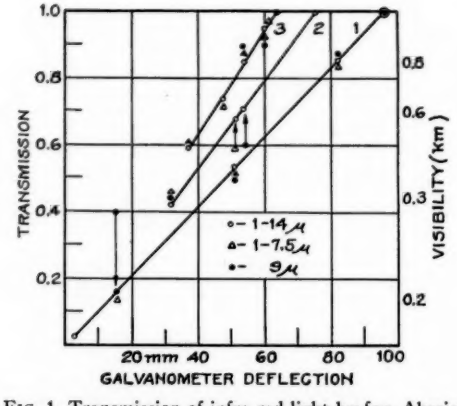

FIG. 1. Transmission of infra-red light by fog. Abscissae are galvanometer deflections produced by the total energy of the source (1–14μ).

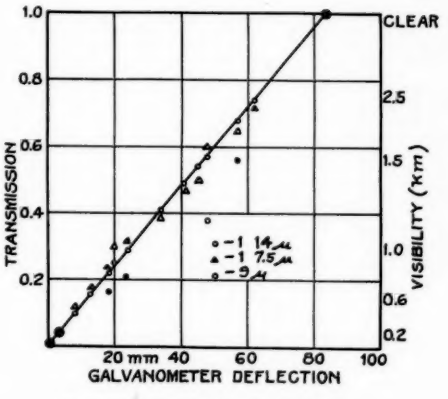

FIG. 2. Transmission by falling snow.

measurements which in turn resulted from the practice of pumping the thermocouple only at intervals of two or three weeks.

Since galvanometer deflections with aluminum reflectors in place were used as abscissae, these were determined immediately before and after observations with quartz plates, so that a great many more measurements resulted for the broad bands 1–7.5μ and 1–14μ than for the narrower 9μ band. The difficulty of making consistent 9μ measurements was increased by the necessity of allowing time for temperature equilibrium to be established between the thermocouple and the quartz plates when they were put in position, with the obvious result that often the scene changed sufficiently between determination of an abscissa with aluminum reflectors and a 9μ measurement that difficulty was experienced in properly locating 9μ points on the curves. This necessitated that some 9μ measurements be discarded, because it was not possible to record them except by interpolating by guess between two abscissae. Of course, all the data could have been plotted with visibility as abscissae, but the difficulty of determining this quantity visually is great, and better consistency of results was found to obtain when total energy values were used.

The three curves of Fig. 1 show that while transmission values for the individual wave-length bands may deviate from the curve to which they belong by as much as 10 percent, the deviation is irregular and not at all indicative that any spectral region is better transmitted

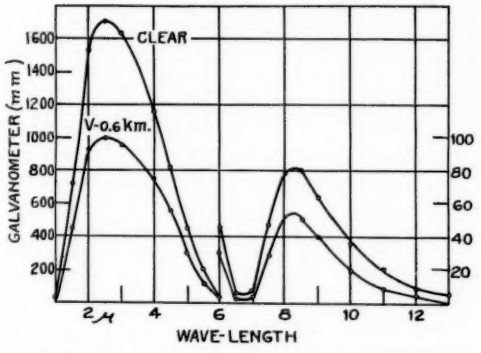

FIG. 3. Spectral energy distribution curves for clear and foggy weather.

than another. The single event of apparent high transmission for 9μ light occurred for the most dense fog ($V=0.2$ km, curve 1) and the abscissa could not be checked at this point because of a sudden clearing. Undoubtedly this point is out of place.

With the same apparatus, two sets of measurements were made through thickly falling snow, and they have been incorporated in one curve given in Fig. 2. The points for 1 and 4 percent transmission contain measurements for all the wave-length bands employed. It is worthy of remark that through snow so dense as completely to obscure the scene, no galvanometer deflections could be measured. The 9μ points lie consistently below the transmission curve for other wave-lengths, but under the difficult conditions of observing through snow in the presence of blustery winds the effect is probably only experimental error. It was not confirmed by later measurements with the spectrometer.

The measurements with a crude residual ray apparatus were made under spectral resolution comparable with that of all earlier experiments on the infra-red transmission of fog. The data are considered to be consistent in view of the difficulty of observing through a continually changing medium.

More complete data were subsequently obtained by using an infra-red spectrometer with a 4-cm potassium chloride prism in place of the residual ray apparatus. An image of the source was formed on the first slit by a concave mirror of 40 cm focal length, and the slit was opened to 1.25 mm so that it received the entire image. The second slit was also 1.25 mm wide. The spectrum formed on the second slit was focused on a Pfund type thermocouple with a short rectangular receiving area so that only light from the part of the slit illuminated by the source was intercepted.

It will be recognized that the effective slit widths were great, being about 2μ in the 3 to 5μ region and about 0.75μ at 9 or 10μ. The atmospheric absorption bands at 2.7 and 4.4μ could not be recognized at all, but the strong 6μ water band appeared in the spectra, as energy curves for clear and foggy weather show (Fig. 3). Regardless of the wide slits, the spectrometer enabled transmission measurements to be made under higher resolving power than has been applied to the problem heretofore and in addition, the mechanical advantage of the spectrometer was great, since measurements for wave-lengths 1 to 12μ could be made with such rapidity and freedom from extraneous disturbances that complete energy curves for fog of nearly constant density could be obtained.

The observations were made at intervals of 0.5μ and irregularly through the spectrum so that a progressive change in fog density might

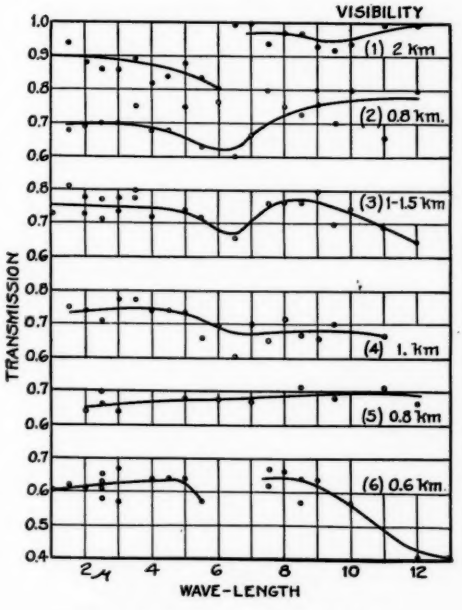

FIG. 4. Spectral transmission of fog.

not give rise to an apparent change in transmission with wave-length. In addition, frequent recursions to some arbitrary wave-length, usually 2.5μ, were made and constancy of energy at that wave-length was taken to mean constant fog density. There resulted several curves for fogs each of fairly constant density.

The clear weather energy curves were obtained as soon after the fog lifted as possible, and, therefore, before the humidity had greatly changed. Accordingly, the transmission curves given in Fig. 4 represent approximately the true transmission of the fog without undue influence of water vapor. The curves 1 to 6 are essentially flat, and show nonselective attenuation by fog. Curve 1, for least dense fog, shows the greatest relative transparency in the 9μ region, but it will also be observed that three separate measurements in the 9–10μ region are nearly as low as those at shorter wave-lengths. This curve was determined under conditions of clearing and shows no greater discrepancies than are allowable. The points of curve 2 for visibility 0.8 kilometer also are erratic. The behavior of points in the 9–11μ region, not determined consecutively, shows that the scene was changing in an irregular manner. The remaining transmission spectra 3 to 6 were made under conditions of more constant fog density. No selective region of high transmission appears in any of them.

All the curves show increased absorption at 6μ, indicating that the humidity actually was less during the clear weather measurements than during fog, but not much less, because such a curve obtained by dividing galvanometer deflections for a foggy day by clear weather deflections of a subsequent less humid day always showed intense absorption at 6.5μ.

It is concluded from the results in Fig. 4 that the attenuation by fog particles is uniform across the spectrum, and that no single region of optimum transmission exists.

Figure 5 represents measurements through falling snow which also lead to the conclusion that no significant variation in the attenuation by scattering occurs with change in wave-length. The curves were not drawn through the 6μ water band because no reliable galvanometer deflections could be obtained there, even though it had been possible to measure the light transmitted by fog at this wave-length. However, the sharp downward trend of each curve near the water band points to lower humidity after the cessation of snowfall than during heavy snow.

It will be seen upon comparing Fig. 1 with Fig. 2 and Fig. 4 with Fig. 5 that, for a given visibility range, higher transmission of infra-red light by fog than by falling snow was observed. This phenomenon is probably caused by the increased brightness of the scene during snowfall and with snow-covered ground which may have been great enough to lower the threshold brightness difference necessary for visual discrimination between object and background.

In the theory of Stratton and Houghton[5] the attenuation coefficient is

$$\sigma = \pi r^2 n k$$

where r is the radius of the water droplet, n the number of drops per cm^3, and k is a function of λ/r given in Fig. 6, after Breckenridge.[6] K passes through a minimum value at $\lambda/r = 0.56$, which is in agreement with the experimental observations of Houghton[7] on the transmission of visible light by artificial fogs of fairly uniform particle size. It is not to be expected, however, that a natural fog consisting of a wide array of particle sizes would show such a region of greater transmission, because a summation of terms $\pi r^2 n K$

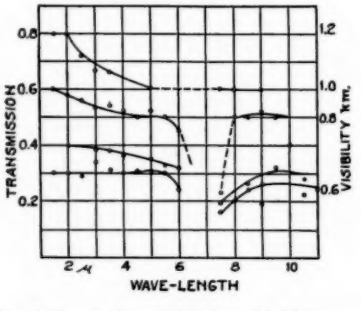

FIG. 5. Spectral transmission of falling snow.

[5] J. A. Stratton and H. G. Houghton, Phys. Rev. **38**, 159 (1931). In their paper the equation was written $2\pi r^2 nk$. It is believed that the 2 is an error since their $K \doteq 1$ for $\lambda/r \doteq 0$.

[6] F. C. Breckenridge, *International Illumination* (Great Britain, September, 1931).

[7] H. G. Houghton, Phys. Rev. **38**, 152 (1931).

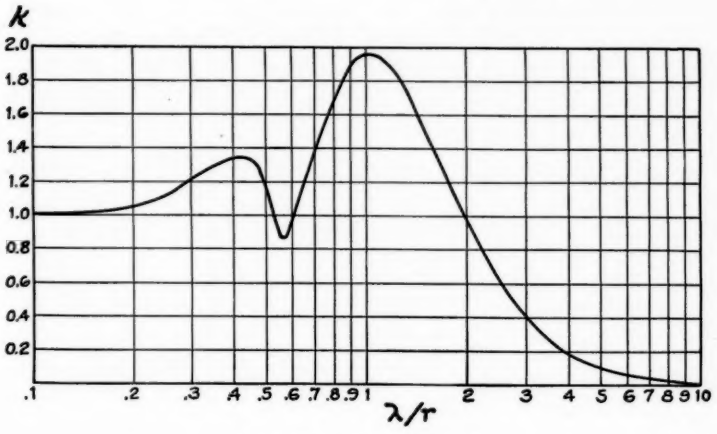

FIG. 6. K as a function of λ/r.

over the fog would flatten out such peaks of transmission.

Houghton[8,9] and Houghton and Radford[10] have measured the particle size distribution in many natural fogs and have found that a fog contains 1 to 10 drops per cm³ of diameters ranging from about 5 to 100μ, with an average diameter of about 50μ, while a cloud may contain 50 to 500 drops per cm³ with an average diameter of 20μ. When attenuation coefficient as a function of wave-length is calculated, using Fig. 6, for any of the actual fogs described by them, it is found that a curve essentially flat results. The magnitude of the attenuation coefficient calculated in this way for a fog consisting of 1 particle per cm³ is about 10^{-5} cm² which is comparable, for example, with the experimental value,

$$\sigma = 2 \times 10^{-5}$$

derived from curve 6, Fig. 4.

The increasing opacity of the atmosphere at wave-lengths above 13μ, arising from the carbon dioxide band at 15μ and the rotation spectrum of water beginning at 18μ, together with the paucity of energy at those wave-lengths produces difficulty in making measurements in this region. No attempt was made in this investigation to go beyond the spectral region of relatively high atmospheric transmission.

Another experiment was carried out to determine whether the infra-red radiation from the sun is attenuated less by clouds than the visible light. The reflecting telescope and thermocouple that were used need not be described in detail except to say that the sensitivity was such that one-millionth part of the total solar energy would have produced a measurable deflection. The result was that no galvanometer deflection was observed when the sun was hidden from view by clouds. Additional observations were made through a selenium powder filter,[4] opaque up to 2.5μ but 70 percent transparent at wave-lengths greater than 8μ, which served to eliminate much of the intense scattered light of short wave-length. No galvanometer deflections were obtainable when the sun was not visible to the eye.

It may be well to point out that smoky fogs, consisting of small particles through which the sun's disk appears red instead of pearly white when viewed at high altitudes would be expected to show higher transmission in the infra-red than in the visible spectrum.

[8] H. G. Houghton, Physics **2**, 467 (1932).
[9] H. G. Houghton, J. Ae. Sci. **6**, 408 (1939).
[10] H. G. Houghton and W. H. Radford, Papers in Oceanography and Meteorology, M. I. T. and Woods Hole Oceanographic Institution, Vol. VI, No. 4 (November, 1938).

The Refractive Index of Matter in Cylindrical Form

A. H. PFUND
Johns Hopkins University, Baltimore, Maryland
(Received June 26, 1940)

THE procedure to be described was developed some time ago and has been shown annually to students in optics as a demonstration experiment. Recently there has been renewed interest in the work, and hence it seemed worth while to present a brief note.

The arrangement of the apparatus is shown (elevation) in Fig. 1 where A is a test tube (15 mm in diameter) containing an axial glass rod *R* (6 mm in diameter). About 7 mm back of the test tube, a straight wire *W* (1 mm diameter) is mounted at an angle of about 53° with the vertical; several inches back of this are mounted, in succession, a sheet of ground glass G and a 100-watt incandescent lamp. Upon pouring acetone into the test tube, the virtual image of the wire, due to the action of the two cylindrical lenses, will take on the appearance shown in Fig. 1. Actual photographs showing the wire images are presented in Fig. 2, where 2A applies to acetone ($n=1.36$) in the test tube, 2B, to carbon bisulphide ($n=1.62$) and 2C, to a mixture of benzene and carbon bisulphide having nearly the same refractive index ($n=1.51$) as the glass rod.

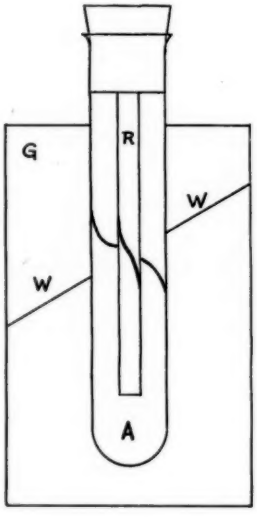

FIG. 1. General disposition of apparatus: ground glass *G* bearing diagonal wire *W* whose image is modified, as shown, by the cylindrical mass of liquid in the test tube *A* and the glass rod *R*.

It is evident that this procedure lends itself to refractive index measurements. Obviously there are at least two modes of attack: (1) the same axial glass rod and test tube are to be used for all liquids studied, or (2) liquids are to be poured into an initially empty test tube which, in turn, is to be immersed in a larger glass vessel containing the same liquid throughout. This

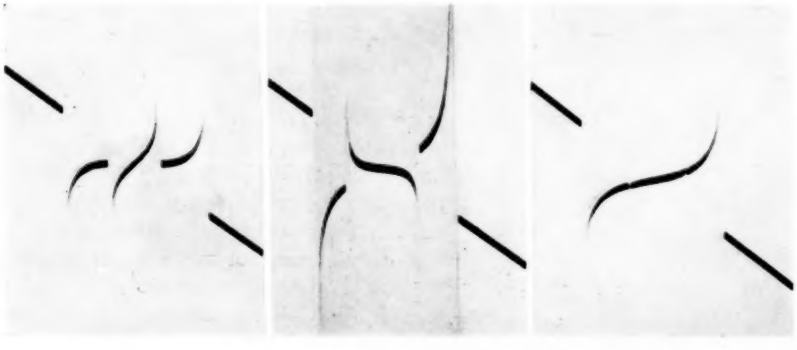

A B C

FIG. 2. Appearance of wire image when test tube is filled with the following liquids: *A*, acetone ($n=1.36$), *B*, carbon bisulphide ($n=1.62$), *C*, mixture having nearly the same refractive index as the glass rod ($n=1.51$).

simply means that the filled test tube now assumes the role previously taken by the glass rod.

As for the quantities actually to be measured, there are again at least two: (1) the vertical distance between the ends of the wire image seen in the glass rod, or (2) the slope of the central portion of the wire image. The first criterion was abandoned because of indefiniteness of the ends of the wire image. The procedure according to the second method involves the use of a telescope mounted at a distance of a meter from the test tube. A protractor was attached to the fixed barrel of the telescope while a radial pointer moving across the face of the protractor was attached to the rotatable eyepiece tube. The procedure then is to adjust the centrally mounted cross hair parallel to the center of the wire image and to record the position of the pointer on the protractor. While the total change of the slope, in the range $n=1.33$ to 1.62, is between 80° and 90°, the accuracy of setting is only moderate. This difficulty was met in part, by mounting a diaphragm 5 mm in diameter over the telescope objective so as to increase the sharpness of the wire image. Furthermore, a color screen transmitting only yellow light was attached to the eyepiece. The greatest improvement, however, was achieved by setting the cross hair tangent to the concave portions of the wire image, as at xx' in Fig. 3. Numerous tests showed that settings could be repeated to within 0.3°—resulting in refractive index uncertainties of one or two units in the third decimal place.

To correlate refractive indices and protractor readings, measurements were carried out on a series of liquids whose refractive indices were determined with an Abbe refractometer. The resultant calibration curve is presented in Fig. 4, from which it is evident that the greatest sensitivity is found in the region where the refractive index of glass rod and liquid are approximately the same.

It was realized that this procedure was susceptible of yielding even more accurate results when applied to the evaluation of the refractive index of the axial glass rod. For such determinations monochromatic light is essential. Using as criterion the continuity of the wire image, it was found that variations of refractive index by a few units in the fourth decimal place brought about changes of the type somewhat exaggerated in Fig. 5. Calling the refractive indices of the glass rod and liquid n_g and n_l, respectively, Fig. 5A applies to the condition that $n_g > n_l$, while in 5B, $n_g < n_l$.

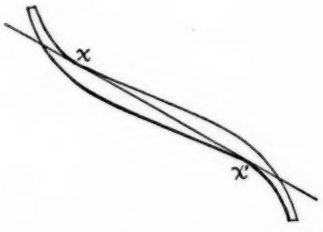

FIG. 3. Accuracy of setting improved by adjusting cross-hair to tangency to wire image at xx'.

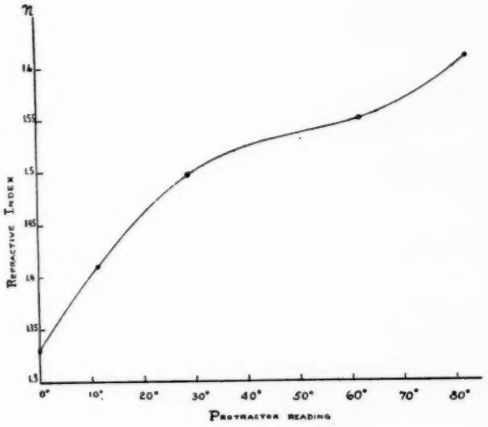

FIG. 4. Calibration curve.

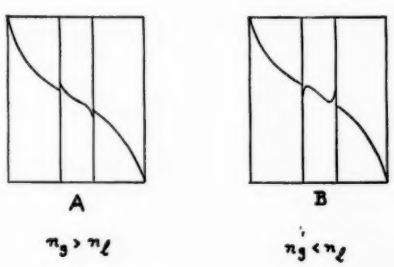

FIG. 5. Appearance of wire image when: *A*—refractive index of glass rod (n_g) >that of fluid (n_l); *B*—refractive index of glass rod (n_g) <that of fluid (n_l).

On the basis of the preceding discussion it is evident that but little ingenuity is required to design a compact and self-contained refractometer.* This has not been done, since better refractometers are already in existence. It did seem worth while, however, to present an experimental procedure which will yield moderately accurate results under conditions which preclude the use of a conventional refractometer.

* In comparison with refractometers such as the Abbe, Pulfrich, etc. the procedure here described has a distinct advantage in that it has no upper limit, i.e. conventional refractometers involve the use of "critical angles"—as a result of which no measurements are possible in cases where the refractive index of the liquid is greater than that of the refractometer prism.

The Use of Step Weakeners in Photographic Photometry*

GEORGE E. MOORE AND HAROLD W. WEBB
Columbia University, New York, New York

(Received June 26, 1940)

This paper describes the calibration and use of a five-step weakener in determining the intensities of spectral lines. The employment of a very constant source of radiation consisting of a quartz mercury arc, the voltage of which was held to ±0.2 volt by an air jet controlled by a relay in the arm of a Wheatstone bridge, made the calibration and use of the weakener comparatively simple and rapid. The results of actual measurements are given to illustrate the precision to be expected when using such a weakener.

FEW details have been published[1] in regard to the use of step weakeners in photographic photometry. Such a step weakener has recently been constructed and used in this laboratory with very satisfactory results and as some new procedures were developed, its calibration and use are here briefly described.

The weakener consists of a polished plate of crystalline quartz, cut as a 5° wedge with average thickness 0.8 mm, and divided into 5 parallel steps by sputtered platinum film. Each step was 0.7 mm wide. The film was protected by a similar clear plate placed over the first in the reversed position. The step weakener was mounted so that the sputtered film was less than 1 mm from the face of the spectrograph slit. Since the entire weakener covered only 3.5 mm of the slit, uniform illumination was not difficult.

Since the spectral selectivity of the platinum films was dependent upon the film thickness and conditions of sputtering, complete calibration of each step was necessary. This was made comparatively simple by the use of a quartz mercury arc of unusually constant intensity.† The arc was operated at 47.0 volts and 2.5 amperes with a series resistance on a 120-volt storage battery. The arc drop was held constant to better than ±0.2 volt by controlling the mercury vapor pressure by means of eight radial air jets, directed against the quartz a few millimeters above the mercury pool and controlled by a magnetically operated valve in the compressed air supply line. This valve was controlled by a relay, controlled in turn by a D'Arsonval type relay (sensitivity 20 microamperes) in the bridge arm of a balanced Wheatstone bridge, of which the arc and its series resistance formed one path and two adjustable resistors of approximately 3500 and 5000 ohms, the other path. The D'Arsonval relay was protected from overload by an auxiliary relay.

After equilibrium was attained the radiation from this arc in the spectral region 15,000 to 2480A was very steady. The spectral distribution was constant to within one percent over periods of several hours, while the absolute intensities of the intense lines of the arc, with the exception of 2537, were constant to within 3 percent and changed very slowly, so that suitable corrections could be readily applied.

The relative transmissions of the five steps of the weakener were determined photographically. The radiation entering the spectrograph was reflected from a large plane block of magnesium carbonate placed in a vertical position close to the slit at a 45° angle with the collimator axis. The intensity of the radiation entering the slit was varied by changing the source to block distance, which always exceeded 100 cm, so that

TABLE I. *Ratio of transmission of step n to transmission of step 1 for λ5461.*

EXPOSURE	*D* (CM)	STEP 2	STEP 3	STEP 4	STEP 5
a	171.6	0.575	0.400	0.268	0.199
b	190.1	.556	.412	.264	.198
c	215.9	.557	.435	.273	.205
d	240.6		.403	.274	.206
e	267.7				.198
f	299.8				
Average		.563	.412	.270	.201
Ave. deviation from mean		.010	.010	.004	.003

* Publication assisted by the Ernest Kempton Adams Fund for Physical Research of Columbia University.

[1] G. R. Harrison, J. Opt. Soc. Am. **24**, 59 (1934) gives bibliography.

† This method of stabilizing an arc was suggested by Dr. L. B. Johnson of the General Electric Company.

errors in determining the effective distances were unimportant. Stray reflections from the walls, etc., were eliminated.

The procedure used is illustrated by the following typical measurement made with λ5461. A wide spectrograph slit was used (0.5 mm). With the step weakener in place, six exposures, referred to as *a*, *b*, *c*, *d*, *e* and *f*, all with identical exposure times, were made on a single plate. In these exposures, the distances, *D*, from the carbonate block to the source were as given in column 2, Table I. Due to the step weakener, the exposure for each line was divided into five different spectra of different densities referred to as 1, 2, 3, 4 and 5, respectively, number 1 being through the first step, the transmission of which was arbitrarily taken as 1.00. A single microphotometer record was made giving the densities for λ5461 in these thirty spectra, by moving the plate in the recording microphotometer parallel to the spectral lines.

In Fig. 1 microphotometer galvanometer deflections are plotted against relative intensities (proportional to $1/D^2$). The galvanometer deflections due to step number 1 gave the points $a1 \cdots f1$, the intensity for $a1$ being taken as 1.00. The galvanometer deflections for step 2, located on the curve drawn through these six points, determined the points $a2$, $b2$ and $c2$. The ratio of the intensities corresponding to the points $a1$ and $a2$, together with similar ratios for $b1$, $b2$ and $c1$, $c2$ gave three independent values of the relative transmissions of step 2 and 1. In this case, the values obtained were 0.575, 0.556 and 0.557, respectively. Using the average value, the abscissae for the points $d2$, $e2$ and $f2$ were computed and plotted against measured galvanometer deflections. The transmission ratio of steps 3 and 1 were calculated from the curve thus extended and the curve was then carried to $f3$. The process was then repeated for steps 4 and 5. The results for a single plate are given in Table I.

TABLE II. *Ratio of intensities of lines in sources I and II.*

STEP/λ=	3340	2967	2926	2893	2753	2700	2652	2600	2482	2309	2378
1	0.525	0.528			0.540			1.15			
2	.524	.524	1.32	0.583	.557	1.98		1.15		2.14	1.95
3	.494	.517	1.28	.577	.525	2.04	1.38	1.07	2.16	2.06	2.01
4	.501	.507	1.25	.570	.540	2.08	1.35	1.08	2.18	2.03	2.02
5	.516	.477	1.30	.571	.553	2.00	1.35	1.07	2.17	2.00	1.98
Average	.513	.511	1.29	.575	.543	2.03	1.36	1.10	2.17	2.06	1.99
ad in %	2.1	2.9	1.7	.9	1.8	1.7	1.0	4.7	0.3	1.9	1.6

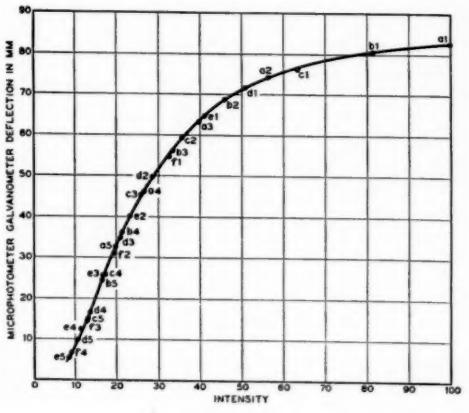

FIG. 1.

The average deviation from the mean was reduced to less than 0.004 for all steps by averaging results from several plates.

No measurable change in the films has yet been observed during a period of more than 2½ years.

The precision which may be expected when using these step weakeners for determining the ratio of the intensities of a given line in two sources is illustrated in Table II. The data for this table were obtained from a single plate consisting of five exposures of the constant voltage arc at five measured values of *D* and one of the second source. All exposures had the same duration and the carbonate block and the step weakener were used as before. For each spectral line, a curve similar to Fig. 1 was plotted directly using the twenty-five spectra from the controlled arc and the calibration data previously obtained for the weakener. From this curve and the five spectra of the afterglow (see column 1), three to five independent determinations of the ratio of the intensities of the line in the two sources were obtained, the number of determinations depending on the overlap of densities.

It may be noted that if somewhat less precision were permissible (average deviation about twice as great), the data available from the single plate just described could have been used for determining the ratios of the intensities of the lines in the two sources without previous calibration of the weakener, by combining the processes leading to Tables I and II.

Properties of the Witch of Agnesi—Application to Fitting the Shapes of Spectral Lines

ROY C. SPENCER
Brace Laboratory of Physics, University of Nebraska, Lincoln, Nebraska
(Received June 27, 1940)

The witch of Agnesi, $y=ha^2/(a^2+x^2)$ is of importance to physicists because it approximates the spectral energy distribution of spectral lines, particularly x-ray lines. This paper reviews the known properties of the witch such as graphical construction, parametric form of the equation and nth derivatives. New series for these derivatives are developed which are better adapted for use in correcting experimental curves by the method derived by the author. The points on the curve whose ordinates are $\frac{1}{4}$, $\frac{1}{2}$ and $\frac{3}{4}$ of the maximum have special properties which are described.

THE plane curve known as the "witch of Agnesi"

$$y=h/[1+(x/a)^2]=ha^2/(a^2+x^2) \qquad (1)$$

is of importance to physicists because it approximates the spectral energy distribution of x-ray lines and optical lines, as well as the power dissipated in sharply tuned resonant circuits. The maximum height is h while the half-width at half-maximum is a. Henceforth, we shall designate a as the "half-width."

Hoyt[1] was the first to show that the witch gave a good fit in the case of x-ray lines. Richtmyer[2] and others[3] have continued to compare x-ray line shapes with that of the witch.

H. E. White[4] has reviewed the factors affecting the shape of spectral lines. The following effects each cause a distribution of energy which has the shape of a witch: the classical electromagnetic theory of line widths, the quantum-mechanical theory of line widths, collision damping and the Stark effect broadening. The one exception is the Doppler broadening due to the random heat motion of the radiating atoms, which gives a Gauss error distribution of intensity.

Weisskopf[5] has pointed out that if each ordinate of a witch is spread out into a second witch, the result is also a witch whose width is the sum of the two widths. Thus, the widths of all the above effects, excepting that of the Doppler effect, are additive, and the resultant line shape is a witch. The witch is, therefore, the prototype of the energy distribution of spectral lines, just as the Gauss error curve[6] is the prototype of distribution curves used in statistics.[7]

HISTORICAL SKETCH

The witch of Agnesi is named after Maria Agnesi, who discussed in 1748 the case when $h=a$ under the name of "Versiera." This curve had been treated by Fermat[8] before 1666 and by Grandi in 1703. If $h=2a$, the curve is termed the "Pseudo versiera." This was considered by Gregory in 1658 and by Leibnitz in 1674. The "versiera" may usually be found in any collection of plane cubic curves.[8,9]

[1] A. Hoyt, Phys. Rev. **40**, 477 (1932).
[2] F. K. Richtmyer and S. W. Barnes, Phys. Rev. **46**, 352 (1934). F. K. Richtmyer, S. W. Barnes and E. Ramberg, Phys. Rev. **46**, 843 (1934).
[3] L. G. Parratt, Phys. Rev. **46**, 749 (1934); L. G. Parratt, Rev. Sci. Inst. **5**, 395 (1934); R. C. Spencer, Phys. Rev. **46**, 1108L (1934).
[4] H. E. White, *Introduction to Atomic Spectra* (McGraw-Hill Book Co. Inc., 1934), Chap. 21.
[5] V. Weisskopf, Physik. Zeits. **34**, 1 (1933). See also discussion preceding Eq. (8) in either paper of reference 2.
[6] Known also as the normal error curve or probability curve. H. L. Rietz, *Handbook of Mathematical Statistics* (Houghton Mifflin Co., 1924), p. 11; D. Brunt, *The Combination of Observations* (Cambridge University Press, 1917), Chapter 2.
[7] Most statistical distributions may be approximated by the Gram-Charlier Series consisting of the Gauss error function $y=e^{-x^2/2}$ and its derivatives. See T. C. Fry, *Probability and its Engineering Uses* (D. Van Nostrand Co., New York, 1928), p. 251. Also Rietz reference 6 pp. 114–115, and Brunt, reference 6 pp. 145–146.
[8] Gino Lorio, *Specielle Algebraische und Transsendente Ebene Kurven* (B. G. Teubner, 1902), pp. 75–80; or the Italian edition, *Curve Plane Special* (Ulrico Hoepli, Milan, 1930), Vol. I, pp. 93–99.
[9] Published articles on the curve of Agnesi have in the past been concerned mostly with the geometry. For instance, Mister, *Mathesis*, Vol. 7, 1887 compared the properties of the witch, the circle and the cissoid as regards construction of the curves and areas etc. M. J. Neuberg, *Mathesis*, Vol. 9 (1909–10), pp. 93–96 reviewed the known properties of the witch and added some new material on tangents, parametric equations and point of inflection. M. R. Goormaghtigh, *Mathesis*, Vol. 36 (1922), pp. 314–317, treated the tangents, normals and centers of curvature. See Gino Lorio, reference 8, the Italian edition for a more complete bibliography.

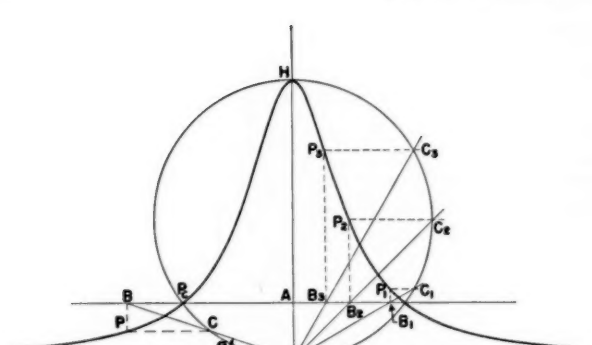

FIG. 1. Graphical construction of witch. First, construct a circle such that its diameter is the maximum ordinate, h. Second, draw a horizontal line through a point A on the vertical axis such that $OA=a$, the half-width at half-maximum of the witch. Any straight line OBC through the origin will cut the horizontal line at B and the circle at C. The right triangle BCP then determines the point P on the curve.

GRAPHICAL CONSTRUCTION

Figure 1 shows how the witch may be constructed with a circle and straight lines. The method is adapted from one described by Wieleitner.[10] The diameter of the circle OH is h. A horizontal line is drawn at a height a, above the x axis equal to OA. Let OC_1 be a straight line drawn from the origin, which intersects the horizontal line at point B_1 and the circle at point C_1. Then P_1, the point on the witch, is at the intersection of a vertical line through B_1 and a horizontal line through C_1. Other points on the witch such as P_2 and P_3 may be located in a like manner. The intersection of the circle and horizontal line at P_c is also a point on the curve.

PARAMETRIC FORM

The witch may be expressed in terms of the parameter θ, the angle that the straight line OC makes with the x axis.

$$x=a\cot\theta, \tag{2}$$

$$y=h\sin^2\theta=h(1-\cos 2\theta)/2. \tag{3}$$

For example, in Fig. 1, the lines OC_1, OC_2, and OC_3 are drawn at angles of 30°, 45° and 60°, respectively, resulting in ordinates of $\frac{1}{4}$, $\frac{1}{2}$ and $\frac{3}{4}$ of the maximum ordinate h. The corresponding values of x are $\sqrt{(3)}\,a$, a and $a/\sqrt{3}$.

A useful dependent variable in addition to y is

$$y'=h-y=hx^2/(a^2+x^2) \tag{4}$$

or in terms of θ

$$y'=h\cos^2\theta=h(1+\cos 2\theta)/2. \tag{5}$$

[10] Heinrich Wieleitner, *Spezielle Ebene Kurven* (G. J. Goschensche, Leipzig, 1908).

RECIPROCAL RELATIONSHIPS

There is an interesting relationship between the ordinate at x and that at $x'=a^2/x$. If θ' denotes the complement of θ, then (1)–(4) again hold providing the primed and unprimed quantities are interchanged. The relationships of the variables are summarized as follows:

$$\begin{aligned} xx'&=a^2,\\ y+y'&=h,\\ \theta+\theta'&=90°. \end{aligned} \tag{6}$$

Thus (1) becomes

$$y'=ha^2/(a^2+x'^2). \tag{7}$$

The point P_1 with an ordinate of $h/4$ and an abscissa $x=\sqrt{(3)}\,a$ transforms to the point P_3 which is lower than the peak by the amount $h/4$ and has an abscissa of $x=a/\sqrt{3}$. Their respective angles of 30° and 60° are complements.

Again, (3) may be transformed to

$$y'=h\sin^2\theta'=h(1-\cos 2\theta')/2. \tag{8}$$

AREA OF WITCH

Since

$$adx/(a^2+x^2)=-d\theta=d\theta' \tag{9}$$

the integral of (1) from $-\infty$ to $+\infty$ is πah, the same as that of an ellipse with semi-axes a and h.

DERIVATIVES OF THE WITCH

The author has developed series[11] for predicting the effect of the apparatus upon the shape of a smooth function such as the energy distribution of a spectral line. The experimental curve is

[11] R. C. Spencer, Phys. Rev. **38**, 618 (1931), Eq. (21).

given by

$$G(x)=\phi(x)-\mu_1'\phi'(x)+(\mu_2'/2!)\phi''(x)\cdots +(-1)^n(\mu_n'/n!)\phi^n(x), \quad (10)$$

where μ_n' is the nth moment of the apparatus function and $\phi^n(x)$ is the nth derivative of the original function.

Since the shape of spectral lines may frequently be approximated by a witch, it will be of advantage to study its derivatives in order to make use of (10).

Successive differentiation[12,13] of (3) results in

$$\frac{d^ny}{dx^n}=(-1)^n\frac{n!ah}{(a^2+x^2)^{(n+1)/2}}\sin(n+1)\theta. \quad (11)$$

This may be expressed in terms of θ

$$\frac{d^ny}{dx^n}=(-1)^n\frac{n!h}{a^n}\sin^{n+1}\theta\sin(n+1)\theta. \quad (12)$$

The factor $\sin(n+1)\theta$ determines the roots of the derivatives, which occur at values of θ given by

$$\theta=\pi k/(n+1) \quad (13)$$

in which k takes on values of the integers from 0 to $n+1$. The two extremes correspond to $x=\pm\infty$. Table I lists the values of θ given by (13). The roots are shown graphically in Fig. 2 where each dot represents a direction of θ for which the corresponding derivative is zero. Note that all odd derivatives are zero for $\theta=90°$. The angle 60° is a root of both the second derivative (point of inflection) and the fifth derivative.

Polynomial form for derivative

The derivatives of the witch may be expressed in the form of a power of y times a polynomial in either x or y. First, $\sin(n+1)$ in (12) is expanded[14] in powers of $\sin\theta$, which is in turn expressed terms in of y by use of (3)

$$\sin^2\theta=y/h. \quad (14)$$

Henceforth, we shall assume that h and a are each unity.

$$d^ny/dx^n=(-1)^n n!Y_n(y), \quad (15)$$

where $Y_n(y)$ is a polynomial of the $(n+1)$th degree in y, except that the odd derivatives include an added factor of x

$$dY_n/dx=(n+1)Y_{n+1}. \quad (16)$$

The polynomials may be built up directly from the following expressions which are adapted to the calculation of the odd and even polynomials, respectively.

$$Y_n=xy(2Y_{n-1}-Y_{n-2}/x), \quad (17)$$

$$Y_n=(2-2y)\frac{Y_{n-1}}{x}-yY_{n-2}. \quad (18)$$

The first few polynomials are

$$\begin{aligned} Y_0&=y, & Y_3&=4xy^3(1-2y),\\ Y_1&=2xy^2, & Y_4&=y^3(5-20y+16y^2),\\ Y_2&=y^2(3-4y), & Y_5&=xy^4(6-32y+32y^2),\\ & & Y_6&=y^4(7-56y+112y^2-64y^3). \end{aligned} \quad (19)$$

The numerical coefficients within the paren-

TABLE I. *Roots of* $\sin(n+1)\theta$.

n	θ
0	0°, 180°
1	0°, 90°, 180°
2	0°, 60°, 120°, 180°
3	0°, 45°, 90°, 135°, 180°
4	0°, 36°, 72°, 108°, 144°, 180°
5	0°, 30°, 60°, 90°, 120°, 150°, 180°

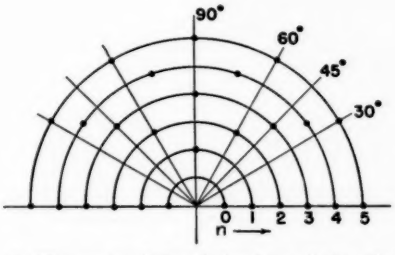

FIG. 2. The roots of the derivatives of the witch are indicated by black dots placed at positions such that $\theta=\pi k/(n+1)$ where $k=0, 1, 2\cdots(n+1)$. For example, the point of inflection or root of the second derivative $(n=2)$ occurs at $\theta=60°$. The three radial lines on the right-hand sides of Figs. 1 and 2 are the same.

[12] Isaac Todhunter, *Differential Calculus* (Macmillan, seventh edition, 1875), p. 64–66.

[13] W. Laska, *Sammlung von Formeln der Mathematik* (Friedrich Vieweg und Sohn, 1894), p. 110, Eq. (7).

[14] W. Laska, reference 13, p. 409 gives a series for $\sin(n+1)\theta$. A 5 has been omitted from the denominator of y^5 in Eq. (13).

theses may be somewhat reduced if y is changed to $(1-y')$. The expressions for Y_0 and Y_1 are unchanged. The remaining ones are

$$\begin{aligned} Y_2&=y^2(-1+4y'),\\ Y_3&=4xy^3(-1+2y'),\\ Y_4&=y^3(1-12y'+16y'^2),\\ Y_5&=2xy^4(-1-8y'+16y'^2),\\ Y_6&=y^4(-1+8y'-48y'^2+64y'^3). \end{aligned} \tag{20}$$

Polynomial in x

If, in the parenthesis of Y_n, the highest power of y is factored out, there will remain within the parenthesis a series of powers of $1/y$, or powers of $(1+x^2)$. Expansion by the binomial theorem results in a new form for the derivative.

$$d^ny/dx^n=(-1)^n n!y^{n+1}X_n(x), \tag{21}$$

where X_n is a polynomial of the nth degree in x. The equation analogous to (16) is

$$dX_n/dx=(n+1)X_{n-1}. \tag{22}$$

The polynomials may be built up from lower polynomials by use of

$$X_n=2xX_{n-1}-(x^2+1)X_{n-2}. \tag{23}$$

The first few polynomials are

$$\begin{aligned} X_0&=1, & X_3&=4x^3-4x,\\ X_1&=2x, & X_4&=5x^4-10x^2+1,\\ X_2&=3x^2-1, & X_5&=6x^5-20x^3+6x,\\ & & X_6&=7x^6-35x^4+21x^2-1. \end{aligned} \tag{24}$$

TABLE II. *Derivatives of the witch divided by n! at intervals of ¼ of the maximum ordinate.*

y	1	¾	½	¼
$\frac{dy}{dx}$	0	$\frac{-3\sqrt{3}}{8}$	$\frac{-1}{2}$	$\frac{-\sqrt{3}}{8}$
$\frac{d^2y}{dx^2}$	−1	0	$\frac{1}{4}$	$\frac{1}{8}$
$\frac{d^3y}{dx^3}$	0	$\frac{9\sqrt{3}}{32}$	0	$\frac{-\sqrt{3}}{32}$
$\frac{d^4y}{dx^4}$	1	$\frac{-27}{64}$	$\frac{-1}{8}$	$\frac{1}{64}$
$\frac{d^5y}{dx^5}$	0	0	$\frac{1}{8}$	0

Simplification of (10)

A substitution of either (15) or (21) in (10) simplifies the expression for the experimental curve. The corresponding equations are

$$G(x)=\sum \mu_n Y_n(y), \tag{25}$$

$$G(x)=\sum \mu_n y^{n+1}X_n(x). \tag{26}$$

The application of the above series is further simplified if applied to the points whose ordinates are ¼, ½ or ¾ of the maximum ordinate, since many of the derivatives are zero. Table II lists the first five derivatives divided by n! at these points. Directly above each zero entree occurs the maximum value for the next smaller derivative. For example, at $y=\frac{3}{4}$, the second and fifth derivatives are zero while the first and fourth derivatives are a maximum, and are, therefore, insensitive to slight errors in the x coordinate.

CURVE FITTING

There are two methods for fitting a witch to a set of experimental data. The first is the graphical construction shown in Fig. 1. The second method, shown in Fig. 3, is a quick means of measuring the half-width of the witch as well as checking its goodness of fit at several points without actually drawing the curve.

The first step of the latter method is to draw the lines HM and HN from the vertex H so that they are tangent to the set of data. The points of tangency P_2' and P_2 will have ordinates equal to half the maximum ordinate if the curve is a witch.[15] For other curves such as the Gauss error curve, this is not true. Next draw a horizontal line at half the maximum ordinate which cuts HM and HN in points P_2' and P_2. The half-maximum width, a, of the witch is equal to half of $P_2'P_2$ or equal to one-fourth of the base MN.

Other tangent lines may be used to check the goodness of fit as follows. The equation of the tangent to a curve is

$$(Y-y)=(X-x)dy/dx. \tag{27}$$

On substituting the first derivative of the witch, $-2xy^2$ and setting $X=0$, the y intercept of the tangent is found to be

$$Y=y(3-2y)=y(1+2y'). \tag{28}$$

[15] R. C. Spencer, Phys. Rev. **49**, 422A (1936).

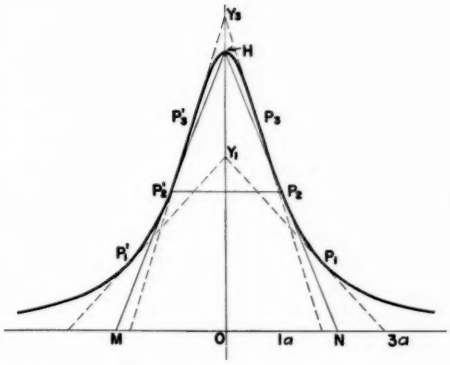

FIG. 3. Construction of tangents to witch. Tangents to the $\frac{1}{4}$, $\frac{1}{2}$ and $\frac{3}{4}$ maximum points have y intercepts of 5/8, 1 and 9/8 maximum, indicated by points Y_1, H, Y_3. These tangents aid in measuring the width, checking for goodness of fit and drawing the curve. See Table III for construction of other tangents.

Table III gives the values of y, y', x, dy/dx, and the y intercept for a number of points for which these values are simple fractions or decimals. For instance, a tangent drawn through the $\frac{3}{4}$ maximum point, will have a y intercept of $Y_3=9/8$, just $\frac{1}{8}$ above the peak. The tangent lines for the $\frac{3}{4}$ and $\frac{1}{4}$ points are shown by dashed lines in Fig. 3.

Spectral energy distributions are more apt to differ from the witch in the wings than elsewhere. The closeness of fit in this region may be easily checked by noting that the ordinate at M or $N(x=2a)$ should be $\frac{1}{5}$ and the ordinate at $x=3a$ should be $\frac{1}{10}$ of the maximum ordinate.

CONCLUSION

The witch, $y=ha^2/(a^2+x^2)$ is of importance to physicists because the shape of spectral lines both theoretically and experimentally may frequently be approximated by it. (One exception is the effect of the Doppler broadening which is represented by the Gauss error curve.) Certain useful known properties are reviewed such as the method of graphical construction, the parametric form of the equation and the nth derivative expressed in the parametric form. The derivatives have been expanded in a polynomial form better suited for use in the author's method of correcting experimental curves for the effect of the apparatus. Tables and graphs give the properties of the witch at a number of selected points. The points whose ordinates are $\frac{1}{4}$, $\frac{1}{2}$ and $\frac{3}{4}$ of the maximum ordinate are of particular importance, first, because they are the natural points at which to measure the widths of the curve, and second, because most of the earlier derivatives are either zero or a maximum at these points, thus facilitating the correction of the experimental curve.

TABLE III. *Slopes and y intercepts.*

y	y'	x	dy/dx	$y(1+2y')$
1	0	0	0	1
0.9	0.1	1/3	−0.54	1.08
0.8	0.2	1/2	−0.64	1.12
3/4	1/4			9/8
1/2	1/2	1	−1/2	1
1/4	3/4			5/8
0.2	0.8	2	−0.16	0.52
0.1	0.9	3	−0.06	0.28

The Density of Silicate Glasses as a Function of Composition*

MAURICE L. HUGGINS
Kodak Research Laboratories, Rochester, New York
(Received July 6, 1939)

The volume per gram atom of oxygen in a well-annealed silicate glass is given quite accurately by the equation $V_O = k + b_{Si} + c_{Si}N_{Si} + \Sigma c_M N_M$, where k is a very small constant characteristic of the annealing technique, N_{Si} and N_M are the numbers of Si or other "metal" atoms per atom of oxygen, b_{Si} and c_{Si} are constants which are different for different ranges of N_{Si} values, and c_M are constants valid (insofar as can be determined from present data) for all values of N_M. For boron-containing glasses separate terms are required for tetrahedrally surrounded and for triangularly surrounded atoms, the relative numbers of which depend on the relative amounts of Si, B and O. With the aid of the above equation, one can calculate densities from compositions simply and quite accurately. The empirical results obtained are interpreted theoretically.

INTRODUCTION

MUCH is now known of the structures of crystalline silicates,[1] and rapid progress is being made, especially by Warren and coworkers[2] toward a knowledge of the atomic distribution in silicate glasses.

The strongest interatomic forces in most silicate crystals and glasses are doubtless those between adjacent silicon and oxygen atoms. These atoms are believed to be held together by shared electron-pair bonds, which are quite polar. For many purposes it is satisfactory and convenient to treat the substances as assemblages of negatively charged oxide (O^{--}) ions and positively charged ions (Si^{++++}, Al^{+++}, Ca^{++}, Na^{+}, etc.) of the more metallic elements.

In all crystalline silicates of known structure each silicon atom is surrounded tetrahedrally by four oxygen atoms. In orthosilicates each oxygen has but one silicon neighbor; in silica itself each oxygen bridges between two silicons; other silicates contain both bridging and nonbridging oxygens, in relative proportions depending on the ratio, N_{Si}, of the number of Si atoms to the number of O atoms. (In a few crystals containing Al, B or other atoms whose attractions for oxygen are comparable to that of Si, some of the oxygens have no silicon neighbors. Except for such cases, the fraction of oxygen atoms which are bonded to two silicon atoms equals $4N_{Si}-1$.) The ratio of bridging to nonbridging oxygens in turn largely determines the nature of the silicon-oxygen structure—small ions, chains or rings, sheets, network—and hence the closeness of packing. When not prevented by these requirements, the oxygen atoms tend to form a close-packed array, each with 12 other oxygens equidistant from it, as already noted. The positive ions tend to be surrounded by oxygens, at distances depending on their ionic sizes. They also tend to be as far from other like-charged ions as possible, especially if the magnitudes of the charges are large.

The same tendencies must exist in silicate glasses. X-ray data on the latter[2] bear out this statement. This suggests a study of the variation of the volume per gram atom of oxygen (V_O) with the ratios (N_{Si}, N_{Na}, etc.) of the numbers of atoms of other elements to the number of oxygen atoms. The results of such a study are reported here. Besides the silicate glasses, a few sodium borate glasses, for which data are available, are also considered.

The data used have been obtained from Morey's very useful book, *The Properties of Glass*,[3] except for the $Na_2O-K_2O-SiO_2$ system,

* Communication No. 769 from the Kodak Research Laboratories.

[1] Cf., for example, W. L. Bragg, *The Structure of Silicates* (Akademische Verlagsgesellschaft, Leipzig, second edition, 1932); W. L. Bragg, *Atomic Structure of Minerals* (Cornell University Press, 1937).

[2] B. E. Warren, Zeits. f. Krist. **86**, 349 (1933); J. Am. Ceramic Soc. **17**, 249 (1934); Phys. Rev. **45**, 657 (1934); J. App. Phys. **8**, 645 (1937); B. E. Warren and A. D. Loring, J. Am. Ceramic Soc. **18**, 269 (1935); B. E. Warren and J. Biscoe, J. Am. Ceramic Soc. **21**, 49, 259 (1938).

[3] G. W. Morey, *The Properties of Glass* (Reinhold Publishing Corporation, New York, 1938).

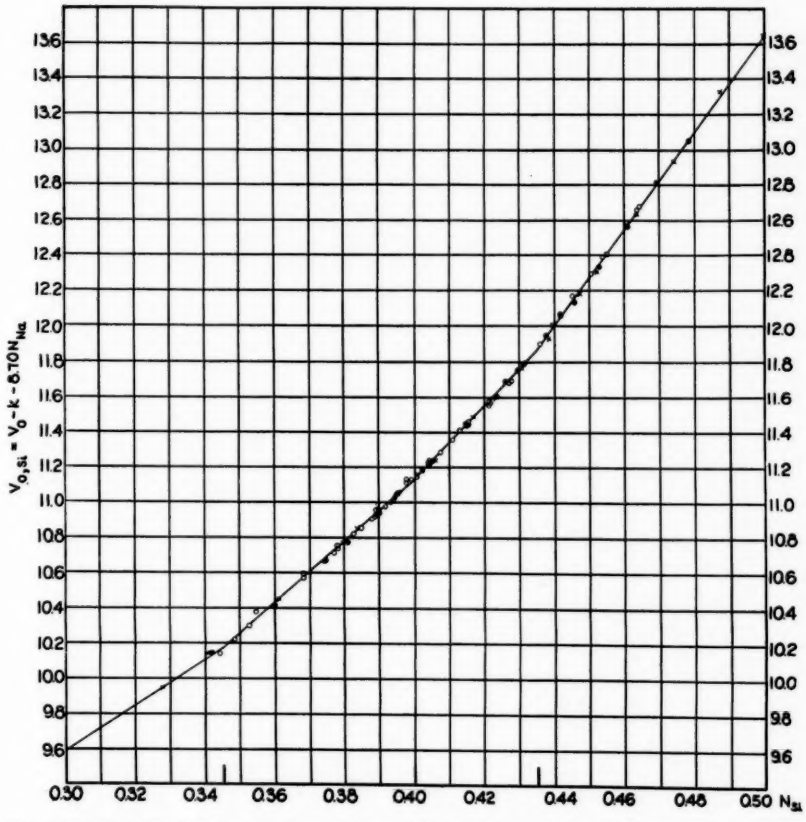

FIG. 1. Na_2O-SiO_2. × Morey and co-workers; ○ Finn and co-workers; ● Turner and co-workers.

the data for which are taken from a recent publication by Young, Glaze, Faick and Finn.[4]

GENERAL METHOD

Determination of the constants

From the density ρ of a glass, the weight fractions f_M, and the molecular weights W_M of the component oxides M_mO_n, the volume per gram atom of oxygen can be computed by means of the equation

$$V_O = \frac{1}{\rho \sum n_M f_M / W_M}. \qquad (1)$$

The number of atoms (or gram atoms) of the element M per atom (or gram atom) of oxygen is given by the equation

$$N_M = \frac{m_M f_M / W_M}{\sum n_M f_M / W_M}. \qquad (2)$$

For electrical neutrality the sum of the positive valences must equal the sum of the negative valences.

$$\sum \nu_M N_M = 2. \qquad (3)$$

Hence, since

$$\nu_M = 2n_M / m_M, \qquad (4)$$

TABLE I.

RANGE OF N_{Si}	b_{Si}	c_{Si}
0.27(?) to 0.345	5.69	13.00
0.345 to 0.40	4.21	17.27
0.40 to 0.435	2.66	21.14
0.435 to 0.50	0.00	27.26

[4] J. C. Young, F. W. Glaze, C. A. Faick and A. N. Finn, J. Research Nat. Bur. Stand. **22**, 453 (1939).

the relation

$$\sum \frac{n_M}{m_M} N_M = 1 \qquad (5)$$

holds. This relation can also be derived, obviously, from Eq. (2).

By far the most data are available for the Na_2O-SiO_2 system. Three extensive sets of density-composition values on well-annealed glasses have been published, from experimental work done at the Geophysical Laboratory, at the National Bureau of Standards, and at the University of Sheffield in England. The three sets do not quite agree with each other, probably a result of differences in annealing technique. As an approximate correction for these differences, a small constant ($k=0.01$ for the National Bureau of Standards data, $k=0.05$ for the Sheffield data) has been subtracted from each of the V_O values from two of these laboratories. The same corrections have also been applied to the V_O values for all other glasses from these laboratories.

TABLE II.

M	c_M	$\frac{m}{n}c_M$ +5.7	V_O Crystal	Co. No. Crystal	M	c_M	$\frac{m}{n}c_M$ +5.7	V_O Crystal	Co. No. Crystal
Li	3.9	13.5	14.8	4	B′	12	13.7	9.6	
Na	8.7	23.1	27.3	4	B″	19	18.3		
K	15.5	36.7	40.6	4	Al	15	15.7	8.5	6
Rb	22	49.7	50.3		Fe	~14	~15	10.4	6
Be	3	8.7	8.3	4				17.5	
Mg	10.3	16.0	11.1	6	Bi	16	16.3	18.3	
Ca	10.3	16.0	16.5	6				18.9	
Sr	~15	~21	22.1	6				9.4	6
Ba	16	21.7	26.8	6	Ti	14	12.7	9.6	6
Zn	11	16.7	14.5	4				10.4	6
Pb	18	23.7	23.4		Zr	16	13.7	11.2	8
			27.9						

Plotting V_O-k against N_{Si} for the Na_2O-SiO_2 glasses, fairly sharp changes in slope are apparent. (See Fig. 1, which is similar to this plot except for a change in the vertical scale.) As Glaze, Young and Finn[5] found, when plotting specific volumes against percentage compositions, the data agree quite well with a series of straight lines. This does not mean that the glasses are mixtures of definite compounds. Breaks would

[5] F. W. Glaze, J. C. Young and A. N. Finn, J. Research Nat. Bur. Stand. 9, 799 (1932).

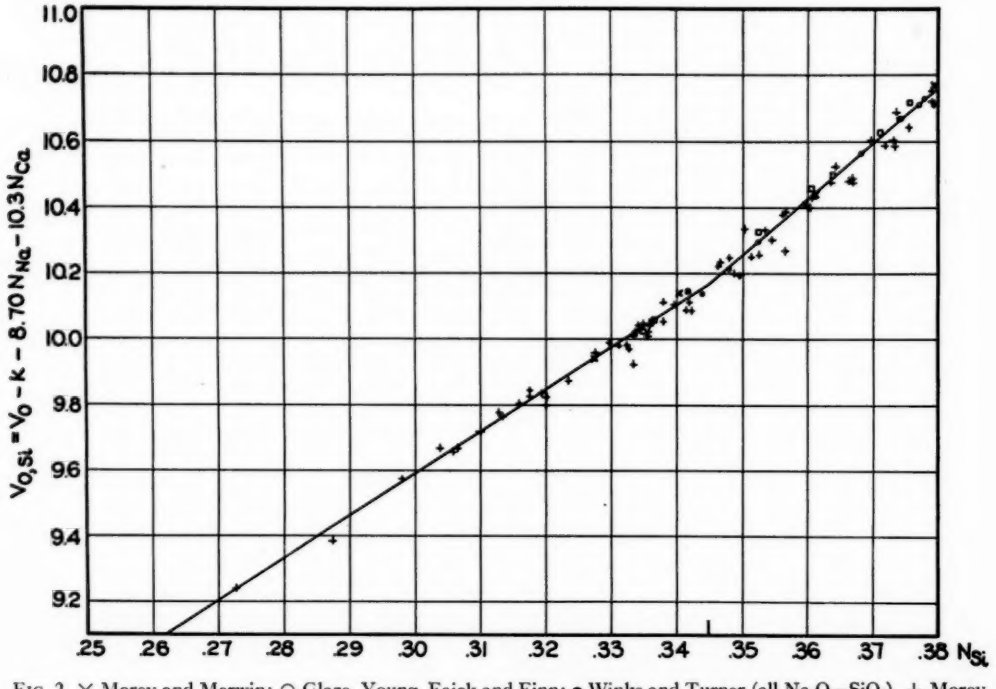

FIG. 2. × Morey and Merwin; ○ Glaze, Young, Faick and Finn; ● Winks and Turner (all Na_2O-SiO_2). + Morey and Merwin; □ Glaze, Young and Finn (all $Na_2O-CaO-SiO_2$).

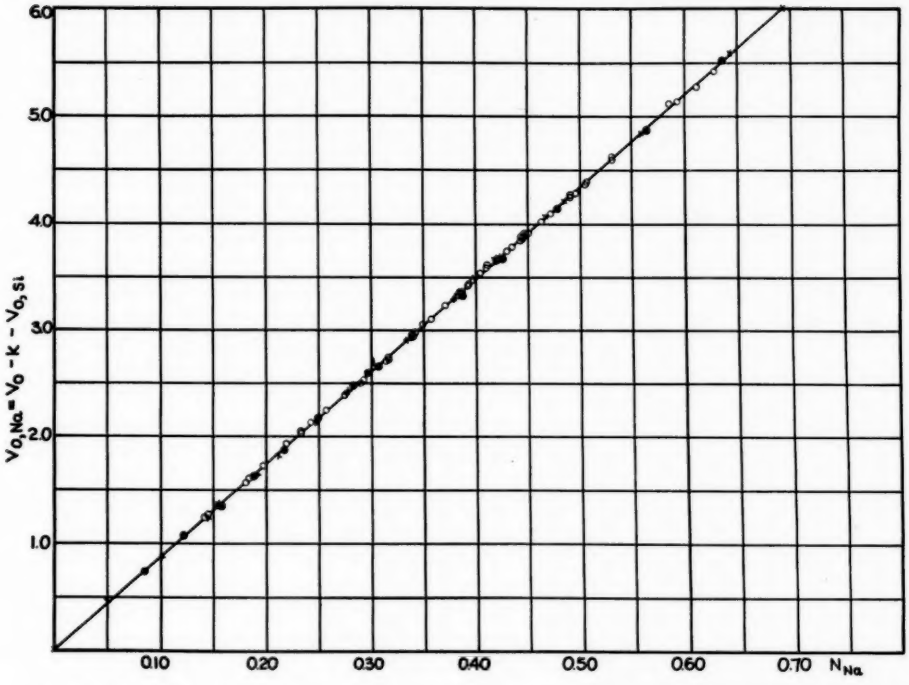

FIG. 3. Na_2O-SiO_2. × Morey and co-workers; ○ Finn and co-workers; ● Turner and co-workers.

be expected as a result of changes in the type of silicon-oxygen structure as the N_{Si} ratio changes. There is doubtless some rounding at the breaks, but it is apparently slight for well-annealed glasses. For simplicity it will here be neglected.

Similar breaks are found in making comparable graphs for other silicates, the breaks occurring at the same values of N_{Si}. The assumption has therefore been made and tested that V_O is, in general, additive, obeying a relation of the form

$$V_O = k + \sum V_{O,M}, \tag{6}$$

where

$$V_{O,Si} = b_{Si} + c_{Si} N_{Si} \tag{7}$$

and, for all the component elements other than Si and O,

$$V_{O,M} = c_M N_M. \tag{8}$$

The values deduced for the constants are listed in Tables I and II. As shown in Figs. 1–23, this additive relation agrees reasonably well with the published data on a large number of glasses, considering differences in heat treatment, inaccurate knowledge of the composition in many instances, etc.

The dependence of $V_{O,Si}$ on N_{Si}, for N_{Si} between 0.27 and 0.345, was deduced from data by Morey and Merwin on glasses in the $Na_2O-CaO-SiO_2$ system. (See Fig. 2 in which are plotted points for glasses having $N_{Si}<0.38$ only.) The exact position of the break, given in Table I as $N_{Si}=0.345$, is somewhat uncertain. The substitution of a curve with two or more breaks (say, at 0.333 and 0.364) in this region or with a continuously changing slope would fit the data as well or better. Treating the problem purely empirically, however, the fewer the breaks in the curve (and hence the fewer the required constants), the better.

It should be noted that the constants given for strontium and iron may be quite inaccurate —the former because it is deduced from data, by Eskola, on two glasses only (Fig. 12), and the latter because it is deduced from data, by Turner and co-workers, on glasses containing both ferric

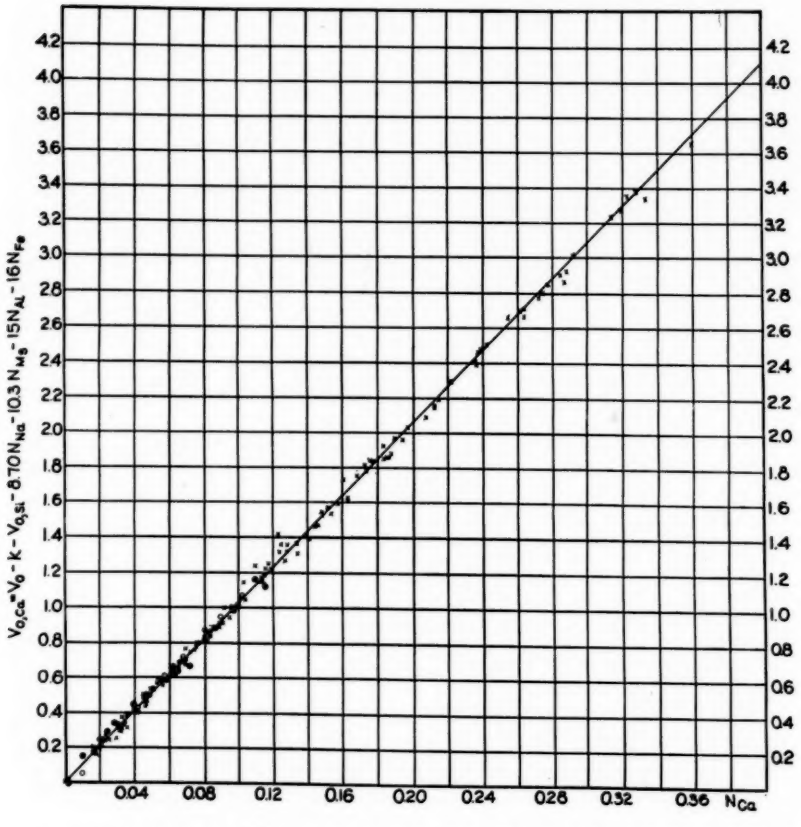

FIG. 4. $Na_2O-CaO-SiO_2$. × $Na_2O-CaO-SiO_2$ Morey and co-workers; ○ $Na_2O-CaO-SiO_2$ Finn and co-workers; ● $Na_2O-CaO-SiO_2$ ($-MgO-Al_2O_3-Fe_2O_3$) Turner and co-workers.

and ferrous iron, in unknown ratio and in relatively small amounts, with several other oxides also present. The best straight line through the observed points (Fig. 17) would intersect the axis of ordinates below the origin, suggesting that the true c_{Fe} value is somewhat larger than the value (14) in Table II.

The simple treatment described above proves inadequate for boron-containing glasses. Subtraction of the contributions of all the other atoms from V_O leaves a residuum which is not a function of N_B alone, but which depends also on the kinds and amounts of other elements present, especially silicon. This is doubtless due primarily to the fact that the boron atoms in the structure are in part surrounded tetrahedrally by four oxygens and in part surrounded triangularly by but three. The relative amounts of the two types seem to depend chiefly on the value of $N_{Si}+N_B$. They doubtless vary also with the thermal history of the sample.

After various unsuccessful attempts, a procedure was found which seems to be fairly satisfactory for well-annealed glasses. It is based on the following assumptions:

(1) If $(N_{Si}+N_B)$ is less than one-half, all of the boron atoms are tetrahedrally surrounded:

$$N_B=N_{B'}, \quad \text{if} \quad (N_{Si}+N_B)<0.50. \qquad (9)$$

(2) If $(N_{Si}+N_B)$ is greater than one-half, each oxygen atom has two silicon or boron neighbors (either 2Si, 2B, or 1Si and 1B). This requirement may be expressed mathematically by the

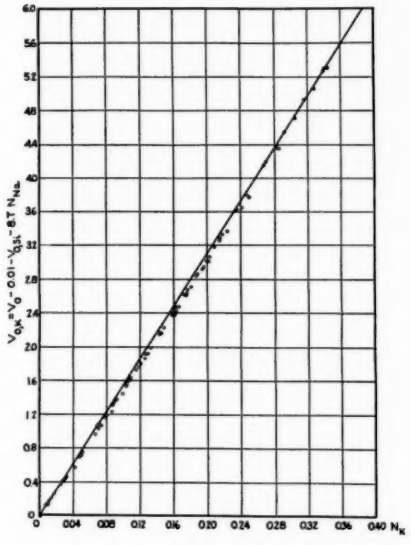

FIG. 5. ● K_2O-SiO_2; ○ $Na_2O-K_2O-SiO_2$. Data by Finn and co-workers.

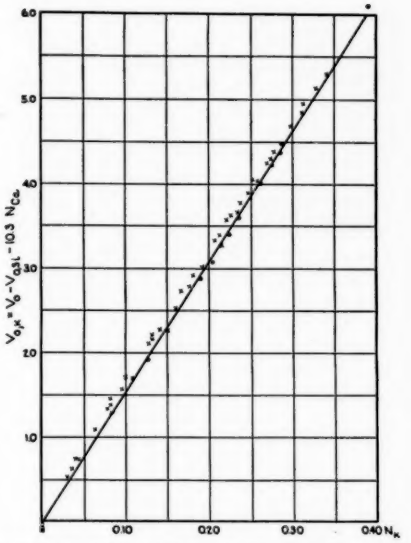

FIG. 6. ○ K_2O-SiO_2; × $K_2O-CaO-SiO_2$. Data by Morey and co-workers.

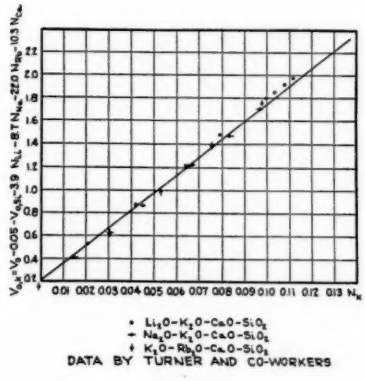

FIG. 7.

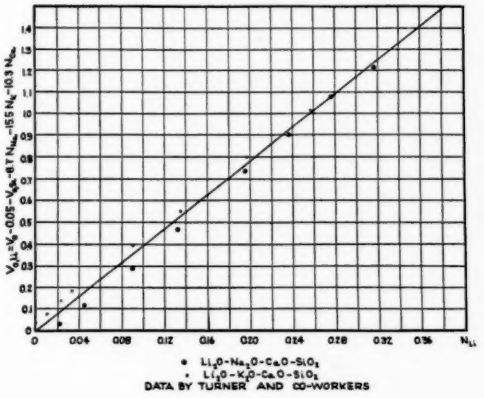

FIG. 8.

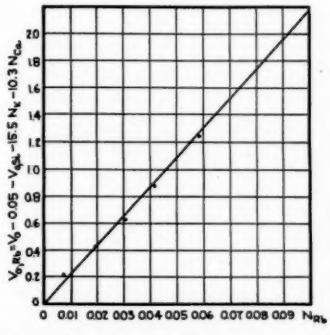

FIG. 9. $K_2O-Rb_2O-CaO-SiO_2$. Data by Turner and co-worker.

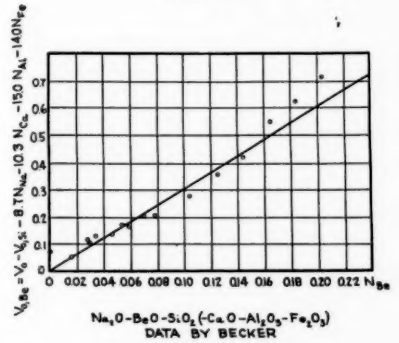

FIG. 10.

following equation:

$$2N_{Si}+2N_{B'}+\tfrac{3}{2}N_{B''}=1. \quad (10)$$

Combining this with

$$N_B=N_{B'}+N_{B''}, \quad (11)$$

we obtain

$$N_{B'}=2-4N_{Si}-3N_B, \quad \text{if } (N_{Si}+N_B)>0.50 \quad (12)$$

and

$$N_{B''}=4N_{Si}+4N_B-2, \quad \text{if } (N_{Si}+N_B)>0.50. \quad (13)$$

(3) For all values of $(N_{Si}+N_B)$ greater than 0.435,

$$V_{O,Si}=27.26N_{Si}, \quad (14)$$

as for values of N_{Si} greater than 0.435 in glasses containing no boron.

For smaller values of $(N_{Si}+N_B)$, one would presumably use Eq. (7), with the constants of Table I, the range of validity of each pair of constants (b_{Si} and c_{Si}) being now a range of $(N_{Si}+N_B)$ rather than of N_{Si} alone. Whether or not the $c_{B'}$ constant which is applicable for

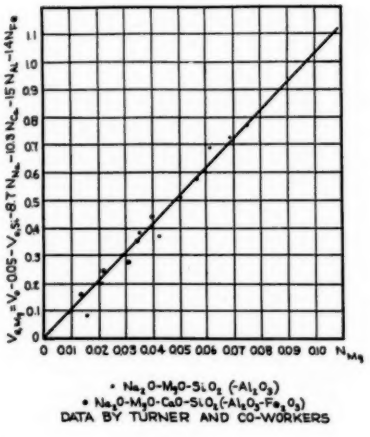

FIG. 11.

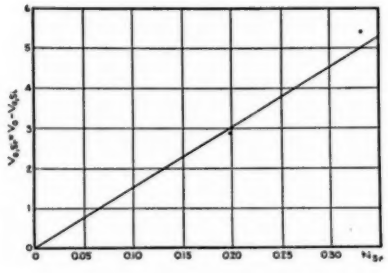

FIG. 12. $SrO-SiO_2$. Data by Eskola.

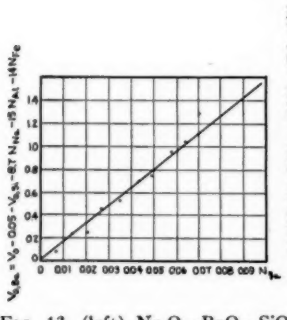

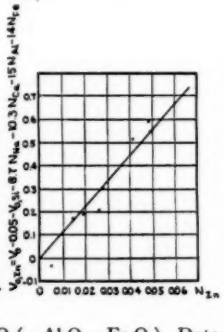

FIG. 13. (left) $Na_2O-BaO-SiO_2(-Al_2O_3-Fe_2O_3)$. Data by Turner and co-workers.

FIG. 14. (right) $Na_2O-ZnO-SiO_2$ $(-CaO-Al_2O_3-Fe_2O_3)$. Data by Turner and co-workers.

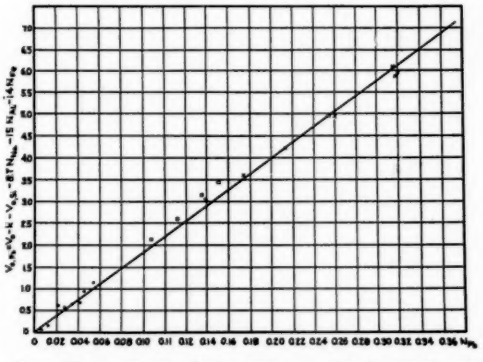

FIG. 15. × $Na_2O-PbO-SiO_2$; □ $Na_2O-K_2O-PbO-SiO_2$ (Merwin and Andersen ($k=0$)); ● $Na_2O-PbO-SiO_2$ $(-Al_2O_3-Fe_2O_3)$ (English, Turner and Winks ($k=0.05$)).

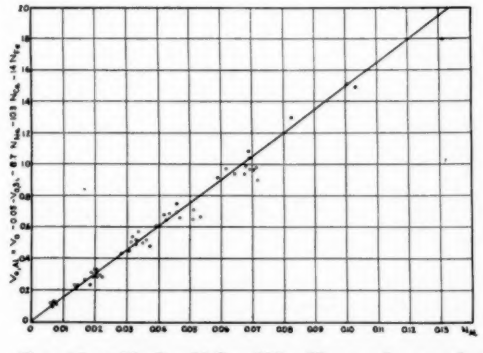

FIG. 16. ○$Na_2O-Al_2O_3-SiO_2$, Finn and co-workers; ● $Na_2O-Al_2O_3-SiO_2$ $(-CaO-Fe_2O_3)$, Turner and co-workers.

$(N_{Si}+N_B)>0.435$ would also be applicable for the lower ranges is problematical. Unfortunately, data are available for only two glasses in this lower range. These are obviously not sufficient to test this point.

Using Eqs. (9), (12), and (13) for calculating $N_{B'}$ and $N_{B''}$, reasonably good agreement was found with the relation

$$V_{O,B}=V_{O,B'}+V_{O,B''}=c_{B'}N_{B'}+c_{B''}N_{B''}, \quad (15)$$

as shown in Figs. 21 to 23, inclusive. The deviations of the experimental points from the straight lines are perhaps due, in large measure, to an excess of triangularly surrounded boron atoms over the number calculated—a result of inadequate annealing. As would be expected, this excess seems to occur most frequently for $(N_{Si}+N_B)$ near 0.50, with N_B relatively large as compared with N_{Si}.

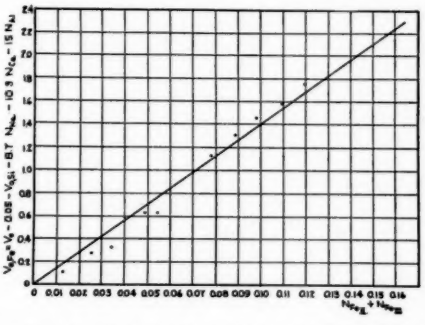

FIG. 17. $Na_2O-FeO-Fe_2O_3-SiO_2$ $(-CaO-Al_2O_3)$. Data by Turner and co-workers.

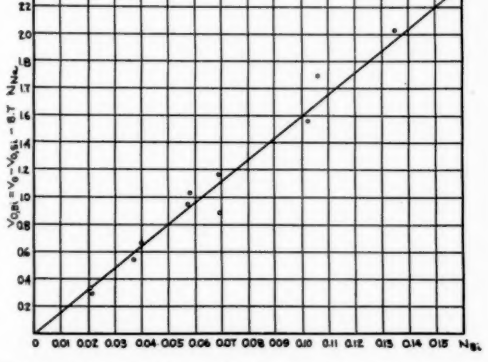

FIG. 18. $Na_2O-Bi_2O_3-SiO_2$. Data by Riegel and Sharp.

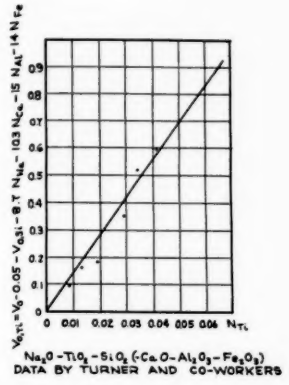

FIG. 19. $Na_2O-TiO_2-SiO_2$ $(-CaO-Al_2O_3-Fe_2O_3)$ DATA BY TURNER AND CO-WORKERS

Glasses in the $Na_2O-B_2O_3$ system fall into line with the sodium borosilicate glasses (Fig. 23).

Calculation of densities

From the agreement shown in the figures, one can conclude that the assumed additivity relations hold quite accurately throughout the composition ranges for which data are now available. The density can therefore be calculated from the composition by means of the equation

$$\rho=\frac{1}{(k+b_{Si}+c_{Si}N_{Si}+\sum' c_M N_M)n_M f_M/W_M}, \quad (16)$$

where $\sum'$ indicates a summation over all the atoms other than oxygen and silicon, the N_M values are computed with the aid of Eq. (2), and the b and c constants are obtained from Tables I and II.

The fractional difference between the observed density and that calculated in this way, for any of the glasses considered in this paper, is about one-fifteenth the deviation from the straight line of the point representing that glass on one of the figures, since the density is inversely proportional to V_O, which has a magnitude of about 15 cc. For the sodium silicate glasses the average difference between calculated and observed densities is about one-tenth of one percent of the actual value, that is, roughly 0.002. In other cases it is somewhat greater.

DISCUSSION

The close proportionality between $V_{O,M}$ and N_M, except for silicon, means that the addition

to a glass of an ion of the element M (with enough O^{--} to neutralize it) has the same effect on the average volume per oxygen, regardless of the composition of the glass—at least, within the ranges considered here.

The changes of slope in the $V_{O,Si}$ *vs.* N_{Si} curve, on the other hand, show that the addition of a silicon atom (plus two oxygens) produces a change of the average volume per oxygen which depends on the relative amounts of silicon and oxygen already present. The fact that $V_{O,Si}$ shows practically the same dependence on N_{Si} in different glass systems indicates that the amounts of components other than silicon and oxygen have little effect on this curve.

Some speculation as to the reasons for the breaks in the $V_{O,Si}$ *vs.* N_{Si} curve being where they are is perhaps in order. For N_{Si} at or near 0.50, the arrangement of oxygens is far from a close-packed one.[2] For N_{Si} values much smaller, on the other hand, analogy with known crystal structures suggests that the oxygen distribution probably approximates close packing. The break at 0.435 (corresponding to $3Na_2O \cdot 10SiO_2$) may well mark the division between glasses in which all of the oxygen atoms are close packed and those in which some are in a more open arrangement.

It is probably significant that the break in the curve at 0.400 (corresponding to $Na_2O \cdot 2SiO_2$) is at the composition for which, on the average, three of the four oxygens around each silicon atom are shared with other silicons, as in the sheet-like silicate structures. For larger N_{Si} values, some silicons are bonded to four shared oxygens and some to three; for smaller N_{Si} values, some are bonded to three and some to two.

As already noted, the change in slope at $N_{Si}=0.345$ may be replaced by two or more

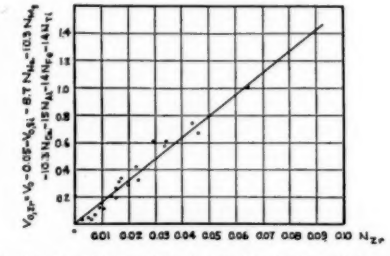

FIG. 20. $Na_2O-ZrO_2-SiO_2$ ($-MgO-CaO-Al_2O_3-Fe_2O_3-TiO_2$). Data by Turner and co-workers.

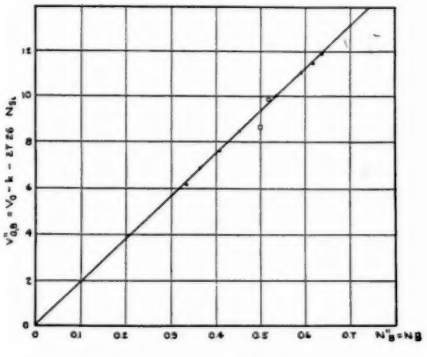

FIG. 22. $B_2O_3-SiO_2$. □ Data by Morey and co-workers; ● data by Turner and co-workers.

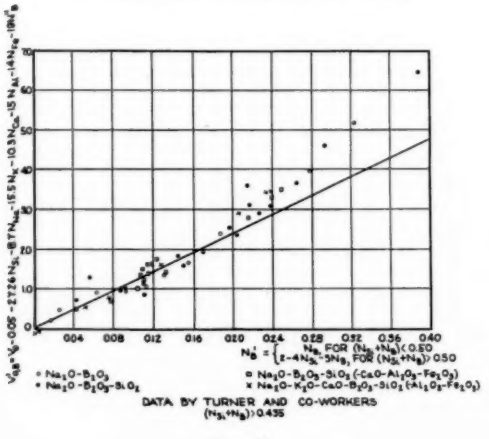

FIG. 21.

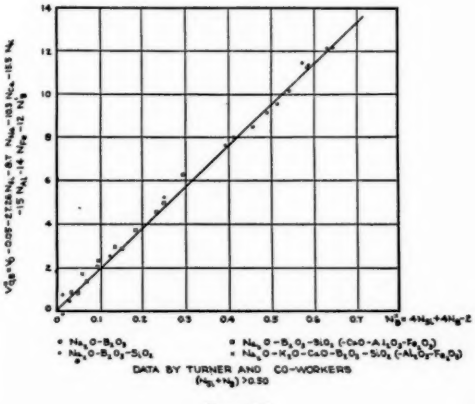

FIG. 23.

changes, for example, at 0.333 and 0.364; $N_{Si}=0.333$ corresponds to the composition $Na_2O \cdot SiO_2$, at which two of the four oxygen atoms around each silicon are shared with others (on the average), as in the crystals containing $(SiO_3^{--})_x$ chains and rings. With smaller N_{Si} values, three or all four of the oxygen atoms around some of the silicons are unshared with other silicons. With larger values of this ratio, some silicons are surrounded by three shared and one unshared oxygen. A possible break at $N_{Si}=0.364$ ($3Na_2O \cdot 4SiO_2$) may be explained as due to a tendency to form $(Si_4O_{11}^{-6})_x$ double chains, as in the asbestos minerals.

Although one might be justified, perhaps, in extending the $V_{O,Si}$ *vs.* N_{Si} curve to $N_{Si}=0.25$, corresponding to $2Na_2O \cdot SiO_2$ or Na_4SiO_4, a break would certainly be expected at that point. For lower values of N_{Si}, the glass would contain O^{--} and SiO_4^{-4} ions, with no oxygens shared between silicons. Between $N_{Si}=0$ and $N_{Si}=0.25$, the $V_{O,Si}$ curve might or might not be straight.

The equations used above in dealing with glasses containing boron can be deduced from the assumptions (1) that an oxygen bonded to but one silicon and a boron bonded to but three oxygens tend to react together, while (2) an oxygen bonded to two silicons and a boron bonded to three oxygens tend *not* to react together:

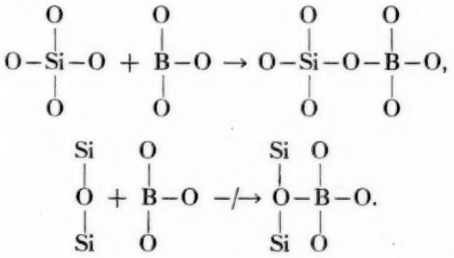

The rather large deviations, already noted, for glasses having $N_{Si}+N_B$ near 0.50, with N_B large, are probably the result of incompleteness of reactions of this first type. Presumably, the better the annealing, the more complete this reaction is, for a given average composition.

The necessity for using $N_{Si}+N_B$ rather than N_{Si} alone, in determining which constants to use for silicon, indicates that (as would be expected) the tetrahedrally surrounded boron atoms enter into the silicon-oxygen framework.

Some of the scattering of the points (Fig. 16) representing glasses in the $Na_2O-Al_2O_3-SiO_2$ system may be the result of the ability of aluminum atoms to be surrounded by either 4 or 6 oxygen atoms, as shown by structure analyses of alumino-silicate crystals. The ratio of the two kinds in a glass would presumably depend, as in the analogous boron case, on the relative amounts of Al, Si, and O atoms and on the adequacy of the annealing. On the other hand, the values of N_{Al} in the glasses studied are quite small, so the absolute magnitudes of the deviations are not large. They may be due almost entirely to experimental error.

If one could extrapolate the lowest segment of the $V_{O,Si}$ *vs.* N_{Si} curve (Fig. 1 or 2) to $N_{Si}=0$, the volume per oxygen in each pure oxide glass (M_mO_n) would be equal to $(m/n)c_M+5.69$ (5.69 is b_{Si} for N_{Si} between 0.27 and 0.345). As has already been pointed out, such extrapolation is certainly not reasonable, for $N_{Si}<0.25$. Nevertheless, it is interesting to compare this quantity, which may be considered loosely as the contribution of the oxide M_mO_n to the total volume per oxygen in a binary glass having $N_{Si}=0.25$ (e.g., one having the composition $2Na_2O \cdot SiO_2$ or $2CaO \cdot SiO_2$), with the volume per oxygen in the pure crystalline oxide. Such a comparison is presented in Table II, columns 3, 4, 8 and 9.

One would expect V_O for the crystalline oxide to be about the same as $(m/n)c_M+5.7$, if the metal atoms have about the same average number of oxygen neighbors in the glass as in the crystal. If the average coordination number of the metal atom is greater in the glass than in the crystalline oxide, the V_O value for the crystal should be larger. This is the case for Na and K, where one would expect an average coordination number of 6 or more in the glass, and for Ba, where one would expect about 8 oxygen neighbors around each metal atom in the glass. On the other hand, the low values of V_O for the crystal, relative to $(m/n)c_M+5.7$ for the glass, indicate a larger coordination number in the crystal than in the glass. This seems to be the state of affairs for Mg, Al, and Ti, suggesting that in the glasses studied most or all of these atoms are surrounded by but four oxygen neighbors, rather than by six as in the crystal.

The low value of V_O for crystalline B_2O_3, computed from the density 2.42 given by McCulloch,[6] suggests a coordination number of six for boron in that crystal.

[6] L. McCulloch, J. Am. Chem. Soc. **59**, 2650 (1937).

ACKNOWLEDGMENT

In conclusion, the author wishes to acknowledge with thanks the aid of Miss Dorothy Owen in performing a large part of the computational work for this paper.

Investigation of Thin Evaporated Silver Films on Glass

JOHN STRONG AND BARRY DIBBLE
California Institute of Technology, Pasadena, California
(Received July 6, 1940)

PRELIMINARY INVESTIGATION

THE work reported in the present paper began with an effort to determine an empirical relationship between the mass of silver evaporated, the distance of a receiving surface from the evaporating source, and the transmission (and reflection) of the resulting film. Such a relationship was originally sought to facilitate the preparation of transmitting silver films such as are used in interferometers, etc.

Several sets of films (42 in all) were prepared. Each set of six films was prepared by evaporating a definite amount of silver from a helical tungsten coil. Microscope slides were used for receiving the evaporated metal. The six microscope slides to receive the silver were arranged in a plane parallel to the axis of the helix. Each slide faced the source. The slides were held by a spider at the following distances (in centimeters) from the source: 22.6, 19.3, 16.6, 14.6, 12.8 and 8.9. Seven sets of films were made evaporating, respectively, 8, 7, 5, 3, 2, 0.95 and 0.475 centimeters of fine silver wire of $\frac{1}{2}$ mm diameter. The transmissivity, T, and the relative reflectivity, R^*, of each film was determined in the manner described later in this paper. The measured reflection and transmission coefficients (for green light only) are plotted in Fig. 1 as a function of the quantity l/r^2, where l is the length of wire evaporated and r is the normal distance from the evaporation source to the slide on which the film was deposited. The results, as represented in Fig. 1, are of little practical value because of the deviations of the observed points from a smooth curve. This is especially true for films which reflect and transmit light in approximately equal amounts.

The reflection and transmission coefficients, R^*, and T, were plotted as shown in Fig. 2 in order to determine which of the observations might be erratic. *When the reflectivity of the films was plotted against the transmissivity, the measurements yielded a definite curve.* In order to elaborate and confirm this result, eighteen new sets of films were more carefully prepared and measured.

EVAPORATION PROCEDURE

The evaporation of the new films was carried out in the usual type of evaporation chamber using a glass bell jar sealed to a steel baseplate with a beeswax-resin compound. Apiezon oil diffusion pumps connecting with the base plate produced the high vacuum. The vacuum as determined by a Knudsen gauge was approximately 10^{-5} mm Hg during the actual evaporation of the silver.

The evaporation of the silver was effected by a small helical heater coil of tungsten (or molybdenum) positioned at the center of a new spider. The plate-to-source distances for the new spider were 10.5, 14.0, 16.5, 18.5, 21.4 and 23.0 cm.

There was no temperature control of the receiving glass plates; evaporation was started with the glass plates at room temperature.

A noticeable contamination results from the use of new tungsten coils; accordingly, the tungsten coils were preheated at high temperature in vacuum before they were loaded with silver.

As before, clear white microscope slides were employed to receive the evaporated silver. As soon as the films were removed from the bell jar they were placed in wooden slide boxes and stored in a vacuum desiccator. The films were measured within a day after they were prepared.

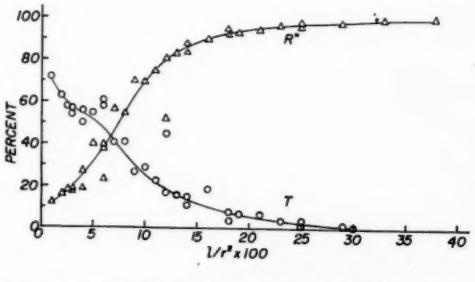

FIG. 1. Reflectivity, R^*, and transmissivity, T, as a function of the amount of evaporated silver and distance of plate from evaporation source. l = centimeters of silver wire of $\frac{1}{2}$ mm diameter, r = distance of plate from evaporating source.

Measurement of the Optical Properties

The transmission and reflection coefficients were measured using red, green and blue light. The rather primitive apparatus employed for these measurements is shown in Fig. 3. L is a galvanometer spotlight containing an automobile headlight lamp. The lamp operated on constant voltage and was assumed to have the color temperature and emission characteristics specified by Forsythe and Worthing for a tungsten filament at 2870 K.[1] T is a shutter and iris diaphragm, used for controlling the light beam. Baffles painted with optical black eliminated the stray radiation. The light, reflected at R by a sample film or by the reference mirror, was passed through a Wratten filter, F_1, and a heat absorbing filter, F_2. (Wratten filters A, B, and C were used to get the red, green and blue light, respectively.) The light was finally received by a type F2 Visitron photo-cell at P. The photo-cell current was determined by a galvanometer of 345 ohms resistance and 10^{-8} ampere per division sensitivity.

The sensitivity curve of the photo-cell was determined by comparison of its response with that of a thermopile using various wave-lengths of monochromatic light obtained with a double quartz monochromator. Also, the spectral transmission curve of each filter was determined. These curves are shown in Fig. 4. These curves, together with the emission characteristic curve of the light source, made possible the calculation of the effective spectral energy distributions of the red, green and blue lights, given in Fig. 4. The effective mean wave-lengths of the three bands employed were 6150, 5400 and 4650A.

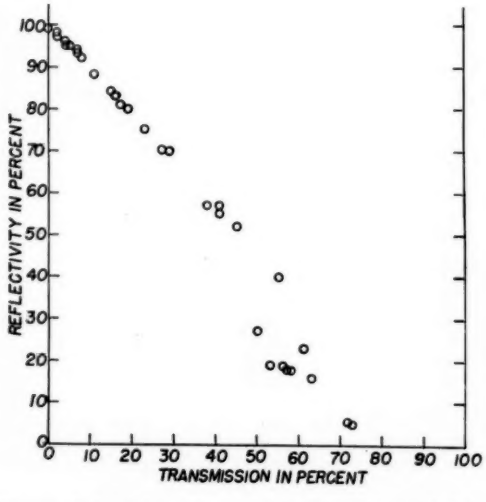

Fig. 2. Reflectivity, R^*, as a function of transmissivity, T, for same films as Fig. 1.

To determine the reflectivity of a film it was placed on the aperture R (silver side down). The reflectivity relative to a fully-polished thick silver comparison film was obtained from the ratio of the galvanometer response for the film to the response obtained with the comparison mirror. To determine the transmissivity of the film, it was placed in the light beam on the camera shutter at T (silver side up). In this case the transmissivity was given by the ratio of the galvanometer response with the film to that when the light beam was unobstructed.

Eighteen sets of six films each were prepared, yielding in all 108 films. Their transmissivities, T, uncorrected for the effect of the backing, and their reflectivities, R^*, referred to a polished silver film as 100 percent, are plotted, respectively, as abscissae and ordinates in Fig. 5. Three complete sets of films were discarded because of miscarriages of technique. Otherwise, *every mirror prepared is represented in Fig. 5*. Also plotted in Fig. 5 is the efficiency, E, of the films, E being the sum of the reflection, R^* and the transmission, T (each measured in the manner described above).

Discussion of the Measurements

It is significant that the data are more consistent when plotted as shown in Fig. 2 and Fig. 5 than when the transmissivity and reflectivity are plotted as functions of the surface density, as in Fig. 1. The inconsistency of the points in Fig. 1 suggests a reason why there have been so many contradictory papers on thin films. Many of the papers on this subject have dealt with a limited group of selected films. It is evident that the results obtained with such selected films will not represent the whole phenomenology. In the present work, a selection was avoided (except as noted above).

The plots of reflectivity *versus* transmissivity

[1] W. E. Forsythe and A. G. Worthing, Astrophys. J. **61**, 146 (1925).

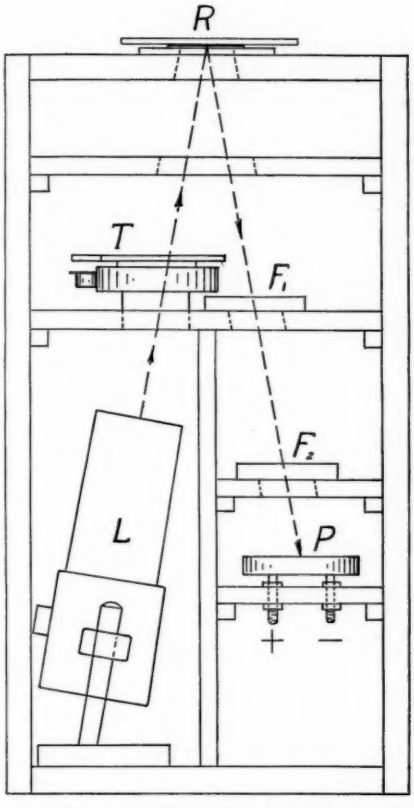

FIG. 3. Apparatus for measuring reflectivity and transmissivity: L—galvanometer spot light; T—shutter and iris diaphragm with microscope slide in position to test transmissivity; R—reflecting mirror; F_1—Wratten filter; F_2—Solex heat filter; and P—Visitron photo-cell.

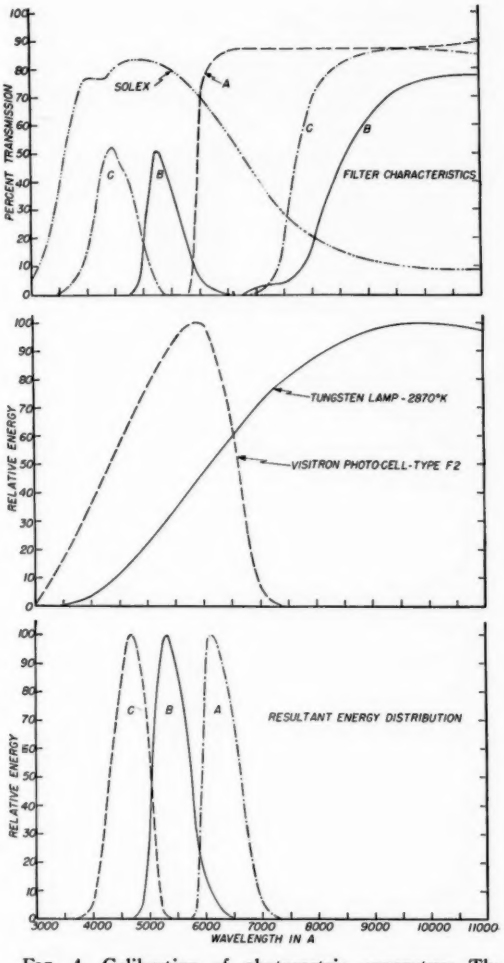

FIG. 4. Calibration of photometric apparatus: The resultant normalized energy distribution curves are shown at the bottom.

(Figs. 2 and 5) expose a general feature of the phenomena of thin silver films; namely, that there are two distinct types. Indeed, these two types of films are so different in their properties as to suggest that they may represent two distinct physical states of the metal. One type of silver film, which we designate as the α-type, exhibits high efficiency, a blue color by transmitted light and freedom from scattered light. As films of greater density are made, α-type films exhibit properties which vary continuously and connect with those of the thick opaque comparison films and presumably with those of massive silver. The second type, the β-type, exhibits low efficiency and variations in color. This type also exhibits scattered light. As the density decreases, this type of film exhibits properties which vary continuously to the values of R^* and, T characteristic of uncoated microscope slides.

The group, α-type or β-type, into which any given film falls, is independent of the color of the light band used. Likewise, the point representing any given film has a position relative to the positions of the points representing the rest of the films which is consistent for the three light bands employed.

Several sets of films were prepared aiming at the density where the discontinuity occurs in order to test the sharpness of the break between the two types of films. It is to be noted that a few

films fall into the region between the two distinct groups. If only *a few selected films had been measured, one might have obtained a set of films which would appear to define a continuous curve.*

In Fig. 6 the logarithm of the reflectivity has been plotted as a function of the logarithm of the calculated surface density. Surface density, in micrograms per sq. cm, was calculated on the basis of uniform molecular radiation from a point evaporation source, using the relationship

$$\sigma = m/4\pi r^2. \tag{1}$$

Here σ is the surface density, m the mass of silver evaporated in grams, and r the distance of the source from the plate in centimeters.

Also, in Fig. 6, the optical density, the logarithm of $1/T$, has been plotted as a function of the logarithm of the calculated surface density.

Surface Density Determination

The optical measurements of R^* and T are accurate to 3 percent or less. Earlier work has shown, however, that the surface density of evaporated metal films may show considerable divergence from the computed values.[2] In order to determine the errors introduced by the assumption of uniform molecular radiation from a point source of evaporation, it was decided to measure directly, by weighing, the amount of metal deposited on a few of the slides. To avoid differential weighings of the relatively heavy coated and uncoated microscope slides, the following method was developed for removing the film and directly weighing the removed silver on a microbalance.

A suitable area of the silver was dissolved by sweeping a small drop of mercury (reagent grade) across the film. A clean glass slide makes an effective manipulator for the mercury. The amalgam drop was then transferred to a previously cleaned and weighed flake of fused quartz. The quartz and its amalgam drop were then heated carefully until all the mercury and other volatile impurities had evaporated, leaving the silver. The flake with its adhering silver was then weighed on a quartz-fiber torsion balance having a sensitivity of 0.12 μg/degree. Simple adhesion between the quartz flake and the hook of the balance ordinarily sufficed to suspend the load; for the largest loads, "moistening" the hook with mineral oil was found to be a satisfactory method of increasing the adhesion.

[2] J. Strong and E. Gaviola, J. Opt. Soc. Am. **26**, 153 (1936).

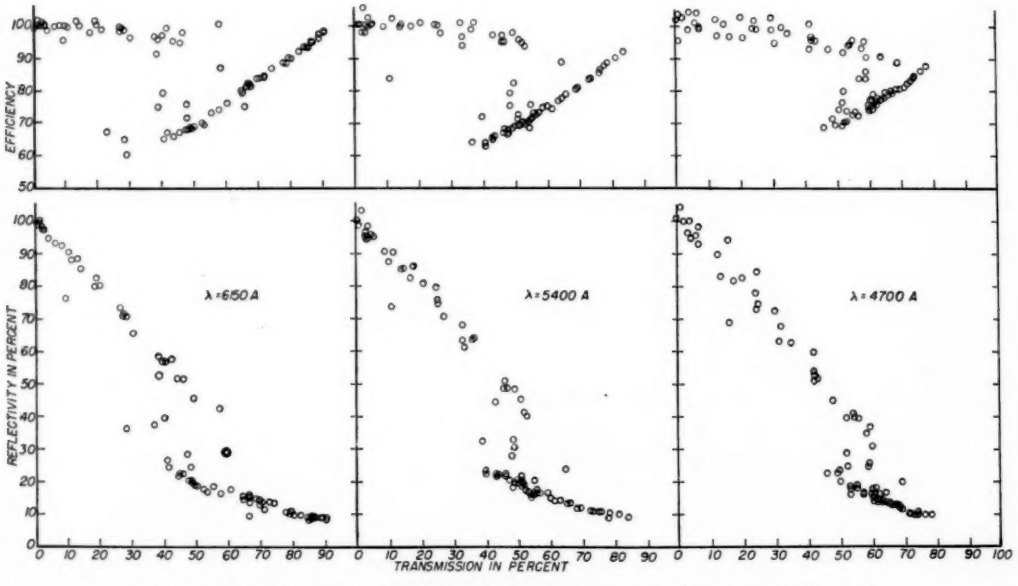

FIG. 5. Reflectivity, R^*, and efficiency, R^*+T, as a function of the transmissivity, T.

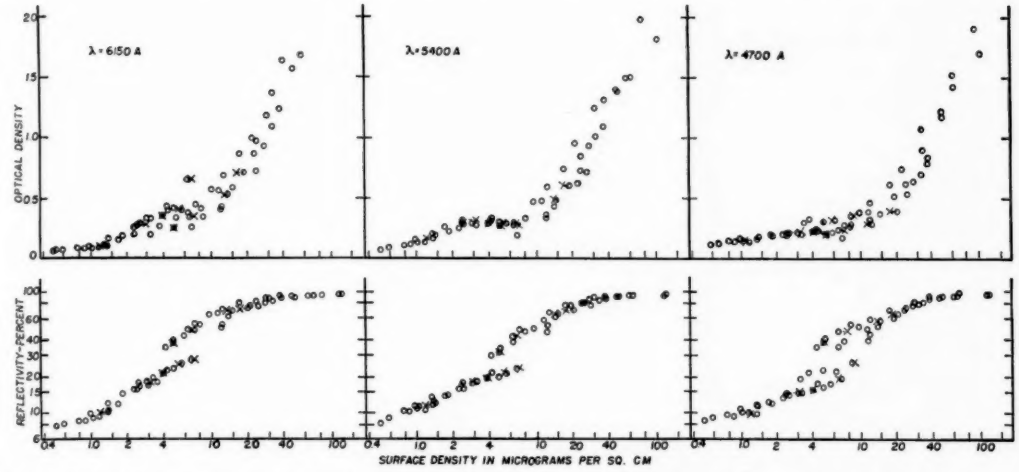

FIG. 6. Reflectivity, R^*, and optical density, $\log 1/T$, as a function of the surface density. o—calculated surface densities, ×—adjusted surface densities, from direct weighings.

Quartz flakes were obtained from a thin bubble of fused quartz blown with an oxyhydrogen flame. Fragments of from 1 to 2 mm on edge weigh from 40 to 250 μg. This is of the same order of magnitude as the weight of the silver.

A drop of mercury of approximately 1 mm diameter was found to be quite sufficient to dissolve up to 200 μg of silver. This amount of reagent grade mercury will introduce less than 0.3 μg of nonvolatile impurities.

Surface Density Results and Discussion

Weighings were made for nine specimens. The surface densities found by weighing divided by those obtained by calculation (Eq. (1)) gave ratios 1.22, 1.50, 1.35, 1.13, 1.14, 1.35, 1.27, 1.45 and 1.75. The ratios were found to depend primarily on the position of the microscope slide on the spider. Certain erratic deviations entered owing to the size of the helix, the amount of metal to be evaporated, the vacuum, etc. Thus the helical evaporation source gives only limited reproducibility of surface densities.

As the weighed surface densities were all larger than the calculated values, the curve resulting from the plotting of the optical properties against the weighed surface densities would lie entirely to the right of those shown in Fig. 6. Therefore, in order to show more clearly the effect of direct determination of surface density on the data shown in Fig. 6, the curve resulting from these new points was shifted to the left by an amount corresponding to the mean of the above ratios. These final values have been shown in Fig. 6 and the corresponding original points indicated. From this it is seen that the corrections to the surface density values are such as to increase the consistency of this observational material.

Scattered Light and Color Effects

All the α-type films appear blue by transmitted light. Also they do not exhibit scattering of light. On the other hand, β-type films appear red by light scattered at large angles. By transmitted light, the thinnest β-type films are a weak reddish-yellow. Films with a greater surface density are red, while even heavier films are a magenta, and finally, at surface densities greater than 6 μg/cm², the films exhibit a more intense blue color than the α-type films.

In Fig. 7 the transmissivity has been plotted as a function of the wave-length for typical films of both the α- and β-type in order to illustrate the degree of saturation of the transmission colors. The approximate surface densities are also given. It is to be noted that the β-type films are more opaque than the α-type films for the same surface density. For example, the transmission for the β-type film characterized by $\sigma = 4$ μg/cm² is approximately the same as for the α-type film

characterized by $\sigma=8$ $\mu g/cm^2$. Also the β-type films show pronounced transmission minima. These transmission minima progress toward longer wave-lengths as the surface density of the film increases.

No compensation for these transmission color effects is found in the reflectivities of the β-type films and the scattered light is insufficient in both quantity and quality to account for the apparent light absorption. It is intended in the future to extend the study of β-type films and to determine the "energy budget" for the light incident upon them.

Ultrapenumbral Deposits

During the evaporation of very thick silver films, a reddish deposit frequently appears on the back side of the receiving plate. Because of the extreme molecular scattering necessary to produce such deposits, they have been termed "ultrapenumbral" deposits. The factors involved in the formation of the ultrapenumbral deposits are not very well understood and no experiments were made to determine the exact mechanism involved. However, the optical properties of the films were studied. It was anticipated that their properties would simulate those of the β-type films.

The same apparatus and general procedure described above were used to prepare the ultrapenumbral films. The slides were attached to the spider in pairs, back to back, and, of course, much larger amounts of silver were evaporated. No surface densities were determined. Six sets of films (thirty-six films) were thus coated by scattered silver molecules.

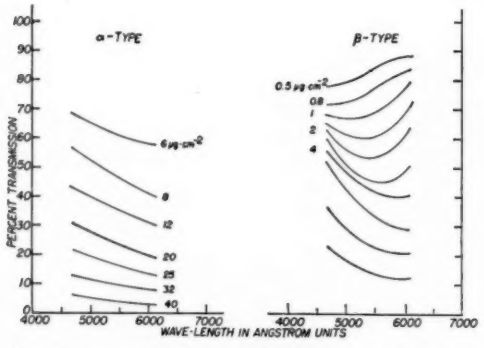

FIG. 7. Transmissivity as a function of wave-length, for α-type and β-type films. (Note: These curves are drawn through only three experimental points.) The lower three curves on the right are for ultrapenumbral deposits.

The R^* and T values for the ultrapenumbral films are plotted in Fig. 8. The points for the thinner specimens fall near the previously obtained curve for the β-type films as was anticipated. And, the points for the thicker specimens appear to extend the curve for the β-type group to the opaque.

As with the β-type films, all the ultrapenumbral films were red by scattered light. Points representing the color effects exhibited by some of the typical specimens are plotted in Fig. 7 in the same column as the β-type films. Here also the color curves representing this group of films are seen to extend the series of curves characteristic of the β-type films to the opaque. While the transmission minima have shifted so far toward the longer wave-lengths as to be less evident, there is a strong depression in the green and red which results in a more intense blue color than is exhibited by α-type films.

Sputtered Silver Films

The reflection and transmission values for sputtered silver films are plotted in Fig. 9. These values are for light of 5870A and are taken from the paper of F. Goos.[3] Inasmuch as Goos' published data were corrected for the effect of the backing material, it was necessary, for comparison, to reduce his values to the case of a silver film on a plate of glass with plane parallel faces. This adjustment was made by the approximate relationships

$$R^*=(R_G+0.04T_G^2)/0.95 \qquad (3)$$

and

$$T=T_G[1-0.04(1-R_G)], \qquad (4)$$

where T_G and R_G are the values given for transmission and reflection by Goos.

Goos' films were prepared by sputtering. It is to be noted that they follow, to a surface density of about 25 $\mu g/cm^2$, the β-type film curve as extended by the measurements on ultrapenumbral films. The optical properties of Goos' thicker sputtered films and our evaporated α-type films are similar for surface densities greater than 30 $\mu g/cm^2$. Likewise, there is good agreement

[3] F. Goos, Zeits. f. Physik **100**, 95 (1936).

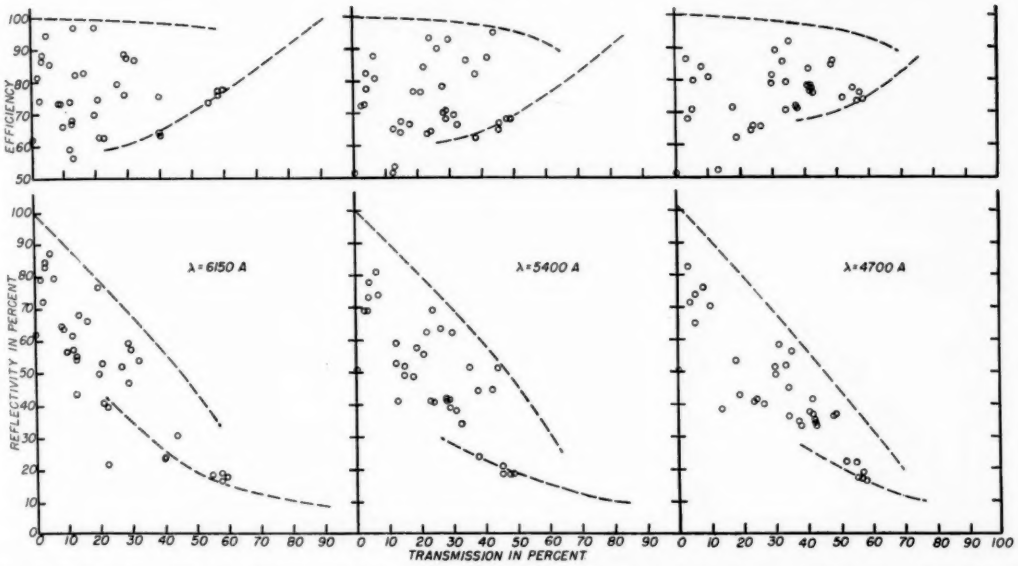

FIG. 8. Reflectivity, R^*, and efficiency, R^*+T, as a function of transmissivity, T, for ultrapenumbral films. Dotted lines show mean of points in Fig. 5.

between Goos' thinner films and our thinner β-type films. But, it would appear that β-type films of greater surface density are formed by sputtering than we obtained by direct evaporation. The fact that these thicker sputtered films are similar in their optical properties to the ultrapenumbral films is a new and pertinent fact to be considered in any theory of sputtering.

MODELS FOR THIN FILMS

A uniform thin film, approximating the massive metal in structure, appears to offer an adequate model for the α-type films.

Because the β-type silver films exhibit optical properties which are distinctly different from those of the α-type films, it is to be expected that the structures are quite different. A tentative model for the β-type silver films, based on the exhibited optical properties, is suggested below.

First, consider the mosaic powder films investigated by A. H. Pfund.[4] They are of interest in this connection because they give qualitatively the same type of color phenomena in transmitted light as was observed for the β-type silver films. Pfund finds that several features of the transmission minima exhibited by his mosaic films are most satisfactorily explained as a mixed plate interference phenomenon. A mixed plate model with random distribution and orientation of the particles gives a satisfactory explanation of the similar results for the β-type films. For example, the wave-lengths at which the transmission minima occur are directly proportional to the surface density and, as with Pfund's films, no halos of complementary color were observed. The absence of halos is a consequence of random distribution. Quantitatively, certain difficulties appear. Thus, reference to Fig. 7 shows that, with a calculated mean thickness of 10A (1 μg/cm^2), the transmission minimum is observed to occur at a wavelength of 5000A. Using the accepted values of the optical constants of the massive metal ($n\sim0.2$, $k\sim4$) no reasonable assumptions as to particle thickness, etc., account for the dissipation from the transmitted beam of 20 percent of the light of that wave-length. However, if the β-type films are considered to represent a physical state distinct from that characterizing the massive metal, the values of the index of refraction and the density may deviate considerably from those characterizing the massive metal. For example, C. V. Kent[5] has found that for molten metals

[4] A. H. Pfund, J. Opt. Soc. Am. **29**, 10 (1939).

[5] C. V. Kent, Phys. Rev. **14**, 459 (1919).

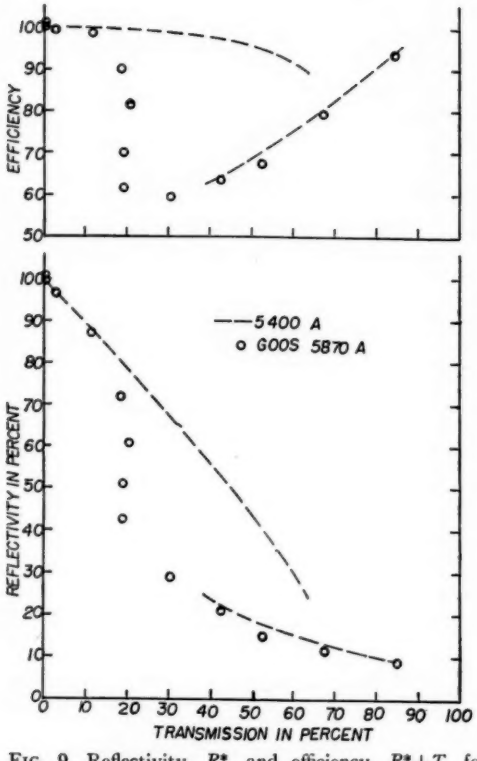

FIG. 9. Reflectivity, R^*, and efficiency, R^*+T, for sputtered silver films. Dotted line shows mean of points in Fig. 5.

there is a close agreement between the optical constants in the visible as determined directly and as computed from the conductivity. Accordingly, an index of refraction of about 15 might be considered reasonable. The observed transmission minimum at 5000A requires the further assumption that the silver granules are about 120A thick and cover about 15 percent of the surface.

Secondly, Gans[6] has shown that for particles small with respect to the wave-length, such as one has in colloidal silver solutions, the amount and quality of the scattered light is strongly dependent on the shape of the particles involved. Let us consider the large angle scattering of red light by the β-type films as being a phenomenon of the same character as that of the scattering of light by a colloidal solution of silver. Spheroids of silver having an ellipticity of about 0.1 are required. The assumption of such small scattering units is reasonable considering the low surface densities prevailing in the β-type films. However, explaining the transmission colors on a basis of scattering is unsatisfactory because: (1) the amount of the scattered light is too small to account for the large losses in transmission (the scattered light can only be seen when the film is viewed against a dark background); (2) the scattered light appears to be in the red for all β-type films while in the thinner films the transmission of red light is not small—it is the blue light which is strongly dissipated. Thus it would appear that the scattered light and the transmission minima arise from different characteristics of the β-type film structure.

At present, on the basis of the optical properties, it appears that the following somewhat complicated qualitative model for the β-type films is required: first, to explain the transmission minima, the film is assumed to have a mosaic structure of relatively large granules exhibiting abnormal physical properties; second, to explain the observed red scattered light, the larger particles are assumed to be made up of smaller elliptically shaped particles, or they may have small elliptical interstices within them. Whether such a model can be experimentally and theoretically justified will be the object of the next series of experiments which we plan to undertake.

[6] R. Gans, Physik. Zeits. **13**, 1185 (1912).

The Prism and the Theory of Optical Resolution

B. P. Ramsay, O. T. Koppius and E. L. Cleveland
Department of Physics, University of Kentucky, Lexington, Kentucky
(Received June 25, 1940)

I. The Prism as an Interferential Device

THE methods of geometrical optics, of interference, and of diffraction may be used as the basis for a theory of optical instruments. Although the results of these three procedures must agree in all gross essentials, the methods themselves may be considered as successively approximate theories. The precision of the methods (and, in general, their complexity also) increases in the order listed above. One might suppose that the method of interference[1] would provide a most satisfactory basis for a theory of optical instruments, since it is more precise than geometrical optics, and less intricate than diffraction methods. This expectation has been confirmed so far as the theory has been developed, but its possibilities have not been exhausted.

One of the chief stumbling blocks in the way of an extensive development of the interferential theory of optical instruments has been the inability of the method to treat effectively such elementary optical devices as lenses, mirrors, and prisms. The reason for this is partly that refinements in the theory of geometrical optics have appeared to make it unnecessary to develop other methods for treating these devices; but equally effective has been the fact that the concepts and notations which were developed for use with multiple beam devices (such as gratings and interferometers) have been defined in a manner too limited to permit general application. Two directions in which the concept of resolving power needs to be extended are indicated in the present discussion of the prism.

II. The Single-Slit Equations

Intuitively, one expects the treatment of the prism as an interferential device to resemble that of the single slit or of the echelon; for it is suggestive in some respects of both of these devices. Here it is preferred to consider the prism as a modification of the single slit, although the other alternative will be discussed.

When the single slit is treated as an interferential instrument, it is a device for superposing an indefinitely large number (k) of beams which differ in phase only. Moreover, γ, the difference in phase between any two adjacent beams is the same as that between every other pair of adjacent beams transmitted by the slit. Thus the phase difference between the extreme beams at the edges of the slit is

$$\beta = k\gamma. \tag{1}$$

Then it is known[2] from what may be called the single-slit theorem that the epoch function in terms of which the intensity pattern may be described is simply

$$\alpha = \beta/2 = k\gamma/2 \tag{2}$$

and the intensity distribution is given by

$$I = (kz)^2 \sin^2 \alpha/\alpha^2. \tag{3}$$

Here z^2 is a constant which is proportional to the intensity of the source.

The minima of the intensity distribution (3) have an intensity value of zero,[3] and occur where

$$\alpha = m\pi, \ m \text{ integral} \tag{4}$$

or

$$\sin i' = m/\sigma a - \sin i. \tag{5}$$

In these relations, m is the order of interference, i is the angle of incidence, i' is the angle of transmission, σ is the wave number, and a is the width of the slit.[4] The separation of minima is given by

$$\sin i_2' - \sin i_1' = 1/\sigma a. \tag{6}$$

The maxima of the intensity function (3) occur where

$$\alpha = \tan \alpha. \tag{7}$$

[1] L. Sturkey and B. P. Ramsay, "A general interferential method." This paper will appear in Phil. Mag.

[2] H. Geiger and K. Scheel, *Handbuch der Physik* (Julius Springer, 1928), Vol. 20, p. 14.

[3] L. W. Taylor, *College Manual of Optics* (Ginn and Company, 1924), Chapter III.

[4] The product, σa, is the width of the slit measured in wave-lengths.

These are the equations which are pertinent for the treatment of the prism as a modification of the single slit.

III. The Epoch Function

According to the wave theory of superposition in optics, only those waves which have originated at a common source can produce observable interferential phenomena.[5] Thus, when two waves, such as

$$s_1 = A_1 \sin (nt - mx), \tag{8}$$

$$s_2 = A_2 \sin (nt - mx - \alpha), \tag{9}$$

are superposed with the aid of a device such as the double slit, the resulting intensity is a function of the phase difference of the two waves. In this simple case, the phase difference is simply the epoch angle, α. The epoch value is introduced by the device itself, and is completely determinable in terms of its geometrical and optical properties. The epoch angle may be expressed either in terms of Δd, the difference in optical path, or in terms of Δt, the difference in time required to traverse these paths. Thus,

$$\alpha = 2\pi\sigma\Delta d \tag{10}$$

or

$$\alpha = 2\pi\nu\Delta t. \tag{11}$$

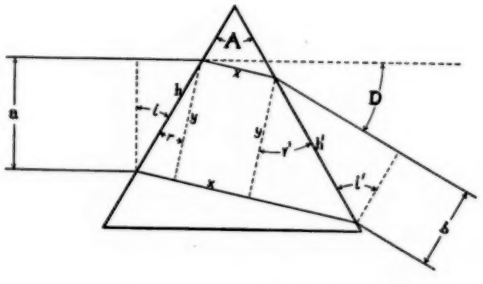

Fig. 1. Diagram for use in calculating the epoch function for the prism.

In more elaborate cases of interference—such as that of the single slit—the concept of phase difference becomes somewhat fictitious, and loses the immediate significance which it holds in the case of the double slit. In these cases, it is convenient to call the argument upon which the intensity distribution depends the epoch function. For the single slit, the epoch function is half the phase difference of the extreme beams which pass through the slit at its edges. This is expressed in (2).

IV. Application to the Prism

When the arguments which are advanced in the discussion of the single slit are applied to the prism, one striking difference is immediately noticeable. The phenomena which are characteristic of the single slit are observable only when a is small; but in the case of the prism, a, the width of the beam defined by the prism is enormously large in comparison with wavelength. Because of this, as may be seen from (6), the separation of the numerous maxima of the intensity pattern is much too small to be observed. The intensity which is observed is the unresolved crowding together of all maxima in one place. Since this is so, it is necessary to ascertain the position of only one of these maxima in order to know the position of all of them to a close approximation. The maximum whose position can be most easily calculated is the one whose order of interference is zero. The position of this maximum is of chief importance, anyway, since its intensity value is approximately twenty times as great as that of any of the other maxima, which rapidly approach zero in intensity value as the order increases.

The epoch function, α, may be calculated by inspection from Fig. 1 with the use of (10). It is

$$\alpha = \pi\sigma[h(\sin i - \mu \sin r) + h'(\sin i' - \mu \sin r')]. \tag{12}$$

For the maximum of zero order,

$$\alpha = 0. \tag{13}$$

This condition is identically fulfilled if

$$\sin i - \mu \sin r = 0 \tag{14}$$

and

$$\sin i' - \mu \sin r' = 0. \tag{15}$$

But these relations are just the applications of Snell's law to the two refracting surfaces of the prism. This conclusion confirms the arguments of geometrical optics.

[5] W. E. Williams, *Applications of Interferometry* (E. P. Dutton and Company, 1930), p. 2.

V. The Rayleigh Resolving Power

The Rayleigh definition of spectroscopic resolving power is

$$\rho=\lambda/\Delta\lambda. \tag{16}$$

The application of this definition to a multiple beam device gives the formula

$$\rho=km, \tag{17}$$

where k is the number of beams, and m is the order of interference. The application of this formula to the prism has been considered by Wood.[6] He visualizes the prism as the physical limit which would result from indefinitely increasing the number of laminae which compose an echelon while decreasing their thickness by such an amount as to keep the physical dimensions of the device constant. Thus he discusses in a pictorial, rather than a mathematical way, the limit of (km) as k approaches infinity and m approaches zero. He finds that the transition in the value of ρ from that of the echelon to that of the prism is not continuous, but changes abruptly at some undetermined point below that at which $m=1$. There is no indication in his discussion as to why the limit is not constant, as to when the analogy breaks down, or as to how one can obtain a consistent understanding of resolving power which is applicable to both echelon and prism.

It will be noted in a subsequent paper[7] that the Rayleigh resolving power is given by

$$\rho=\nu\Delta t. \tag{18}$$

In that paper, this is interpreted as the product of frequency by the uncertainty in time specification of a single photon. From the point of view that is being employed here, a more suitable interpretation may be obtained by paraphrasing a suggestion made by Williams.[8] His interpretation, based on (17), is that resolving power "is the path difference between the beams incident at the ends of the grating measured in wavelengths." That is, (17) may be written as

$$\rho=k(\delta d/\lambda)=(k\delta d)/\lambda=\sigma\Delta d, \tag{19}$$

where $\delta d/\lambda=\sigma\delta d=m$, the order of interference, and $\Delta d=k\delta d$, the path difference of the extreme beams. However, if c is the phase velocity and ν is the frequency, $\nu=c\sigma$, $\Delta d/c=\Delta t$, and (19) becomes identical in form with (18). This suggests that (18) be interpreted as follows: The Rayleigh resolving power of any optical device is the difference in time required to propagate energy over the extreme optical paths, where the unit of time is the period of the wave motion. When paraphrased in this way, the Williams interpretation is applicable to prismatic as well as to multiple beam devices. This can be shown as follows.

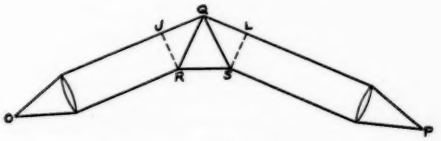

FIG. 2. Diagram for use in calculating the Rayleigh resolving power for the prism.

VI. The Transparent Prism

The extreme geometrical paths of beams traversing the prism shown in Fig. 2 are $OJQLP$ and $ORSP$. Let u be the group velocity of light of frequency ν in the prism, and let v be its group velocity in the surrounding medium. From Fig. 2, it may be seen that the greatest difference in times required for energy to traverse optical paths between O and P is the difference in times required to traverse the optical paths JQL and RS. Let RS be the thickness of the prism, and T be the corresponding optical path. By the principle of Fermat, T is also the length of the optical path JQL. The time required for the energy of frequency ν to traverse the path JQL is

$$t_1=JQL/v=T/v \tag{20}$$

and the time required to traverse RS is

$$t_2=RS/u=T/u. \tag{21}$$

Thus the difference in times is

$$\Delta t=t_2-t_1=T(1/u-1/v). \tag{22}$$

[6] R. W. Wood, *Physical Optics* (The Macmillan Company, 1934), pp. 284–287.

[7] E. L. Cleveland, B. P. Ramsay, and O. T. Koppius, "Optical resolving power and the photon theory," J. Opt. Soc. Am., forthcoming issue.

[8] W. E. Williams, *Applications of Interferometry* (E. P. Dutton and Company, 1930), p. 27.

By relations[9] well known in the study of optics, it may be shown that this may be written as

$$\Delta t = (T/v)(d\mu/d\lambda), \tag{23}$$

where μ is the refractive index of the prism. When this value of Δt is used in (18), the Rayleigh resolving power for the prism is seen to be

$$\rho = -T(d\mu/d\lambda). \tag{24}$$

This is the usual expression.

It thus appears that there is a consistent physical concept of the Rayleigh resolving power, ρ, which is applicable to the prism as well as to other types of interferential devices. It is noteworthy, however, that the discrepancy in the value of ρ noted in Wood's treatment of the prism as the limiting case of the echelon has not been explained by this unifying concept of resolving power. The source of the discrepancy becomes apparent on considering the absorbing prism. This will now be discussed.

VII. The Absorbing Prism

In the usual treatment,[10] it is pointed out that the Rayleigh resolving power varies inversely as the cube of the wave-length. It is because of this that a prism[11] can sometimes afford a greater resolving power than a grating before the short wave-length limit of transmission is reached. Calculations of what resolution is to be expected in this region cannot be satisfactory if they are based solely on the inverse third power rule; for this rule is derived for a perfectly transparent prism, and cannot be expected to apply when resolution is affected by appreciable absorption in the prism.

The intensity for the absorbing prism is given by the equation which has been called[1] the Z constant distribution function. It is

$$I = Z^2 \frac{(1-rk)^2 + 4rk\sin^2(k\gamma/2)}{(1-r)^2 + 4r\sin^2(\gamma/2)}, \tag{25}$$

where $r = e^{-q}$. By a simple trigonometric substitution, this may be seen to be equivalent to the formula given by Sparrow.[12] The principal maxima of this distribution occur where

$$\gamma/2 = m'\pi. \tag{26}$$

The central maximum is that for which $m' = 0$, or

$$\alpha = k\gamma/2 = 0. \tag{27}$$

Thus the condition for the central maximum of the absorbing prism, as well as for the transparent prism, is given by (14) and (15).

The Rayleigh resolving power, as given by (18), is likewise unaffected by the effect of absorption in the prism. It has been shown by Wadsworth,[13] however, that the resolving power in this case is remarkably diminished. It is significant that this decrease in resolving power necessarily follows because the form and width of the spectrum line, as given by (25), differ from that of the transparent prism. For only if

$$q = 0 \tag{28}$$

and

$$r = e^{-q} = 1, \tag{29}$$

can (25) be reduced to (3). Wadsworth shows both numerically and graphically the effect of absorption of various amounts on the intensity distribution.

The fact that the resolving power of the prism[14] is diminished by the effect of absorption makes it clear that the definition of resolving power given in (18) is deficient. What is needed is an explicit statement of the quantities upon which resolving power depends. When this is done, the difficulty encountered in using Wood's conception of the prism as the limiting case of the echelon disappears. One of the quantities which should appear explicitly in the definition of resolving power is discussed in the following section.

VIII. Intensity Gradient and Slope-Visibility

The conclusion that the resolving power of an optical instrument depends upon the width and form of the intensity distribution which it produces can be readily accepted. Ditchburn and

[9] S. Goldman, J. Opt. Soc. Am. **23**, 70–71 (1933).
[10] L. W. Taylor, reference 3, pp. 74–75.
[11] G. Herzberg, *Atomic Spectra and Atomic Structure* (Prentice-Hall, Inc., 1937), p. 2.
[12] C. M. Sparrow, Astrophys. J. **44**, 76–86 (1916).
[13] F. L. O. Wadsworth, Phil. Mag. (6) **5**, 355–374 (1903).
[14] The resolving power of the echelon is likewise diminished by the effect of absorption, as may be seen from the same arguments.

Power-Steele[15] seem willing to consider it the whole physical basis of optical resolving power, for they say: "Obviously the possibility of resolving two close lines should be determined by the pattern produced by a single line." Although no mention is made in their paper of the analytical property of the intensity pattern which should be a measure of resolving power, a discussion by Ditchburn[16] in an earlier paper is suggestive of what they may have had in mind.

Ditchburn comments that whereas the characteristics of the eye as an optical instrument are very incompletely understood, it is a well-established fact that the eye is a very poor judge of intensity but a very good judge of contrast, by which is meant linear intensity (or density) gradient. Thus it might easily be that, in viewing a large area over which the intensity of illumination varies by twenty percent, but never varies suddenly, the eye would fail to distinguish the difference in intensity, whereas—if the intensity gradient were steeper—much smaller differences in intensity might be detected. As an illustration, it is recalled that on a photograph of a spectrum, viewed under a high magnification, faint lines, which are visible to the naked eye under low magnification, disappear, merging into each other and into the background because the "contrast" has been greatly reduced by magnification. Since the eye is sensitive to contrast whereas the microphotometer is sensitive to differences in intensity, the conditions for photometric resolution might be expected to be somewhat different from those for visual measurements. Paradoxically, however, the eye is sometimes able to detect resolution,[17] because of its great sensitiveness to contrast, when the absolute difference in intensity is too small to be measured by the microphotometer. But the microphotometer, in general, detects intensity differences which the eye fails to distinguish.

It appears for both visual observations and measurements with a microphotometer that the "linear intensity (or density) gradient" of a maximum is the analytical property of an intensity distribution upon which resolving power depends. For theoretical purposes, it will be convenient to express this gradient as the average value of the slope, $\Delta I/\Delta\alpha$, of the intensity function over an interval to be chosen later. In experimental measurements, it has been found convenient[7] to express this gradient as a slope-visibility, $\Delta D/\Delta a$, where D is the microphotometer deflection corresponding to an intensity, I, and a is the microphotometer stage reading corresponding to the epoch value, α.

IX. The Intensity-Epoch Slope

Aside from the graphs and numerical calculations of Wadsworth, it is known[18] for all interferential devices in general that the slope of an intensity maximum is dependent both upon r, the ratio of adjacent amplitudes in a compatible set,[1] and on k, the number of beams in the set. Thus for a grating, the epoch interval between a principal maximum, I', and the minimum, I'', by which it is bounded is known to be

$$\Delta\alpha=\Delta\beta/2=\pi/k. \tag{30}$$

This means that the larger the number of beams (or elements in the grating), the narrower the line, and the greater the possibility of resolving two close components. The average value of the slope taken between maximum and minimum is

$$\frac{\Delta I}{\Delta\alpha}=\frac{I'-I''}{\alpha'-\alpha''}=\frac{1}{\pi/k}=\frac{k}{\pi}. \tag{31}$$

Hence, if the resolving power of a grating is proportional to the intensity-epoch slope, it is proportional to the number of rulings on the grating.

This conclusion is not inconsistent with Wood's conception of a prism as the limiting condition of an echelon with an infinity of infinitesimally thin laminae. On the contrary, the problem presented by that point of view can be explained by making the intensity-epoch slope a factor in the definition of resolving power. For the prism, the average value of the slope taken between the central maximum and the first minimum of (3) is

$$\Delta I/\Delta\alpha=1/\pi. \tag{32}$$

[15] R. W. Ditchburn and E. J. Power-Steele, Proc. Roy. Irish Acad. **41**, 137–149 (1933).

[16] R. W. Ditchburn, Proc. Roy. Irish Acad. **39**, 58–72 (1930).

[17] This has been noted also by Sparrow in discussing applications of his "undulation condition" to visual measurements. C. M. Sparrow, Astrophys. J. **44**, 76–86 (1916).

[18] E. Gehrcke, *Dis Anwendung der Interferenzen* (Vieweg and Son, 1906), pp. 39–42 and 66–69.

That is, the intensity-epoch slope (32) for the prism is less than that for the echelon. It is a consequence of this that the resolving power of the prism is less than that for the echelon. Wood's echelon becomes transformed into a prism because the separation (30) between the secondary maxima of the multiple beam interference vanishes as k becomes large.

It is a matter of interest that the effect of absorption on resolving power is automatically included through r when the intensity-epoch slope is included in the definition. However, no discussion will be made here of the manner in which the intensity-epoch slope is to be found in those cases in which $r \neq 1$, and zero minima do not occur. This problem, as well as that of assigning numerical values for the resolving power of optical instruments, will be considered in a subsequent paper. Before this can be done, however, a more complete discussion of the nature of optical resolving power will be necessary.

Experiments to Test the Rebromination Theory of Photographic Solarization*

J. H. Webb and C. H. Evans
Kodak Research Laboratories, Rochester, New York

(Received July 25, 1940)

The rebromination theory of photographic solarization attributes this phenomenon to the latent-image silver being attacked by photolytically formed bromine during great overexposure. With the purpose of testing the validity of this theory, a series of experiments was carried out on a photographic emulsion showing strong solarization. These experiments consisted of exposures at different temperatures over the range +68°C to −196°C, exposures on emulsions treated with various bromine acceptors, tests on emulsions which had been exposed and then treated with silver halide solvents, comparison tests of solarization with physical and chemical development, and experiments with different intensities of exposing radiation. All the experimental results fit in with the rebromination theory of solarization.

Introduction

If a photographic emulsion is exposed to increasing amounts of light, the density obtained on development increases with exposure in accordance with the well-known characteristic H and D curve. This curve, representing density as a function of the logarithm of exposure, rises slowly in the initial stages of exposure, gradually passes into a region where the density increases linearly with the logarithm of exposure, and finally approaches asymptotically to a definite maximum value. If exposure is carried to a point beyond that for which maximum density has been attained, the density is found to decrease again, giving rise to the reversal effect known as solarization. Viewed from the standpoint of an individual grain, this means that after a certain degree of exposure has been reached, further exposure of the photographic grain tends to destroy the developable state induced by the earlier part of the exposure. Different emulsions vary greatly in the extent to which they exhibit this effect and it is only with specially prepared emulsions that large effects can be obtained. Methods for preparing emulsions which show large solarization have been published in papers by Arens,[1] and also in various patents.[2]

Much work has been done in an effort to arrive at an explanation of photographic solarization. According to a study by Trivelli,[3] the latent-image theories which have been proposed to account for this phenomenon can be reduced to two basic types: (a) a *progression theory*, and (b) a *regression theory*. The progression theory attributes solarization to a coagulation of the latent-image silver by continued light action. This theory supposes that the latent-image silver formed in the initial stages of exposure is highly dispersed and acts as a strong catalytic agent for initiating development. Coagulation is assumed to destroy this catalytic power of the silver for development and thereby render the grain inert. The regression theory of solarization, on the other hand, supposes that the latent-image silver specks are so reduced or peptized by continued light action that they are rendered inactive for inducing development. Though other explanations have been suggested, the most generally accepted view as to how this regression takes place is that the latent-image specks are attacked by halogen photochemically liberated during the exposure. For a full discussion of the literature on the subject of solarization covering both the progression and the regression theories, the reader is referred to the excellent survey by Trivelli.[3] Since this paper by Trivelli was written, a series of seven articles have been published by Arens[1] on solarization to which reference may be made for the most recent work on the subject.

The present work was undertaken to investigate the regression theory of solarization in its specific form which attributes this action to rebromination of the latent image by bromine

* Communication No. 775 from the Kodak Research Laboratories.

[1] H. Arens, Zeits. f. wiss. Phot. **28**, 91, 98, 229, 341 (1930); **30**, 127 (1931); **31**, 317 (1932); **33**, 105 (1934).

[2] H. Arens, U.S. Patent 2005837 (1932); I. G. Farbenindustrie A. G., British Patent 443245 (1936); G. Szasz, British Patent 462730 (1937).

[3] A. P. H. Trivelli, J. Frank. Inst. **209**, 373 (1930).

photochemically released during exposure. According to recent theories,[4] the light-absorption in the photographic grain causes ejection of an electron from the energy band belonging to the bromine ions of the crystal into the conduction band. This process leaves one uncharged bromine atom in the crystal. Though bromine atoms cannot diffuse through the silver halide lattice, nevertheless, the location of a bromine atom formed in this way must not be regarded as fixed. This is so because the vacant position left by the ejected electron can move. Thus, by a process of replacement electron conduction, a bromine atom formed by the loss of an electron may pick up an electron from its next neighbor, thereby effectively shifting the position of the bromine atom by one lattice point. By repetition of this process, it is possible for a bromine atom formed originally at one point of the crystal to give rise to a bromine atom at another point in the crystal, without the original atom moving at all. It is by this process that bromine atoms formed at interior points of the photographic grain can diffuse to the grain surface, where they are released. As long as the exposure is small, the amount of bromine liberated over the grain surface in this way remains small and may escape altogether or be absorbed by the gelatin. With large exposures, however, the situation is different. In this case, large amounts of bromine may be liberated, and, if the exposure takes place in a short time, a high concentration of bromine may result in the region immediately surrounding the grain surface. The theory postulates that under these conditions bromine will attack the latent-image specks and form a protective layer of silver halide on their outer surfaces. In this way the latent-image silver specks become inaccessible to the developer and the grain is thereby rendered undevelopable. The rebromination theory of solarization supposes that bromine attacks only the silver formed near the grain surface and not that formed deeper in the grain. Thus, in the solarizing region of exposure, photolytic silver can continue to be formed under the surface.

A number of experiments immediately suggest themselves as a means for testing the rebromination theory of solarization. (Such experiments have been carried out by previous workers and some of these experiments have been repeated many times by different investigators.) If exposures are made at different temperatures, the rate of chemical reaction of bromine and gelatin as well as the reaction between bromine and silver should be altered, thereby giving rise to observable effects.[5–7] The addition of bromine acceptors to the emulsion should alter its solarization characteristics.[8–11] Alteration of the intensity level at which exposures are made would result in different concentrations of bromine around the grain during exposure and should accordingly affect the degree of solarization.[12] Furthermore, if solarization arises from a coating of silver halide on the surface of the latent-image specks in accord with the theory outlined, it should be possible by short treatments with silver halide solvents to render the latent-image silver specks again available for development and thus diminish solarization.[13–17] The experiments just mentioned pertain to the ordinary chemical type of development. If solarization results from rebromination of the latent-image silver, then solarization should also be found for prefixation physical development.[18] On the whole, although contradictions exist, it can be said that results obtained from previous experiments do not refute the rebromination theory and many of them give evidence in its support. In some cases the discrepancies among different workers are merely quantitative differences and can probably be attributed to variations in the emulsions used.

[4] R. W. Gurney and N. F. Mott, Proc. Roy. Soc. **A164**, 151 (1938).

[5] F. Luft, Phot. Korr. **69**, 161 (1933).

[6] W. F. Berg, Trans. Faraday Soc. **35**, 445 (1939).

[7] J. E. Nafe and G. E. M. Jauncey, Phys. Rev. **57**, 1048 (1940).

[8] J. M. Eder, Zeits. f. physik. Chemie **117**, 293 (1925); *Eders Handbuch*, Vol. 2, Part I (1927), p. 585.

[9] H. Arens, Zeits. f. wiss. Phot. **28**, 91 (1930).

[10] H. Kieser, Zeits. f. wiss. Phot. **26**, 321 (1928).

[11] Lüppo-Cramer, *Eders Handbuch*, Vol. 2, Part I (1927), p. 600.

[12] H. Arens, *Veröffentl. Wiss. Zentral-Lab. phot. Abt.* (Agfa, **3**, 64, 1933).

[13] E. R. Bullock, *Monograph of Eastman Kodak Company No. 6* (D. Van Nostrand Company, New York, 1927).

[14] F. Kogelmann, *Ausf. Handbuch Phot.*, Vol. 2 (1895), p. 401.

[15] L. Vidal, Bull. Soc. franç. phot. **14**, 2nd series, 581 (1898).

[16] Lüppo-Cramer, *Die Grundlagen der Negativverfahren* (W. Knapp, Halle, 1927), p. 596.

[17] J. E. Nafe and G. E. M. Jauncey, Phys. Rev. **57**, 1048 (1940).

[18] H. Arens, Zeits. f. wiss. Phot. **30**, 49 (1931–32).

In view of the great amount of discordance among the results of different investigators, some of which may be due to different emulsions and techniques used, it has appeared desirable that a complete set of experiments of the type mentioned be carried out with the factor of emulsion composition held constant. The present work contains a set of experiments made in this way.

Experimental

Intensity scale exposures, made through a photographic step-wedge, were employed throughout this work. The step-wedge used had twenty-one steps, with transmissions increasing progressively by factors of approximately $\sqrt{2}$. Since all exposing radiation passed through the glass walls of a Dewar flask, as will appear below, a piece of Kotava film base, with the emulsion washed off, was placed in front of the step-wedge. This diffused the light and thus prevented marked irregularities in the developed densities which would otherwise have been caused by lens action of inhomogeneities in the glass. In all cases the exposing radiation was obtained from a 500-watt 115-volt projection lamp operated at 4.0 amperes (with a color temperature of approximately 2940°K). Exposures were made by manual operation of a shutter in front of the lamphouse. Timing was done by means of a clock with a sweep second hand. The lamp-to-film distance and the time of exposure varied among the experiments performed and will be found specified in the data accompanying the results.

Three different emulsions, coated on film, were used. For reference each emulsion has been assigned a number, as follows:

I Low speed, blue-sensitive, experimental emulsion showing strong solarization.
II Same as I, but a different batch of emulsion.
III High speed, blue-sensitive, commercial emulsion showing solarization upon gross overexposure.

A strip of film, $\frac{3}{4}$ inch wide and 10 inches long, was used for each exposure.

Except where otherwise noted, emulsions I and II were developed in SD-12 developer, for 3 minutes, at 65°F. Emulsion III was developed in D-19b, for 5 minutes, at 65°F. (After development, the films were fixed, washed, and dried as usual.) The formulas of the developers are given in Table I.

Because it was desired to maintain the film at certain temperatures during exposure for some of the experiments, the apparatus for holding the film (used in all experiments) took the following form:

The film strip to be exposed was held close against a metal surface which could be brought to the desired temperature, the step-wedge was in contact with the film, and the piece of Kotava base was just in front of the step-wedge. The whole assembly was held in an unsilvered Dewar flask. In some of the experiments, the metal against which the back of the film strip pressed formed the wall of a cylindrical container made from thin copper. A suitable liquid in this container was brought to the desired temperature. At low temperatures, petroleum ether was employed, the cooling being accomplished either by dropping small pieces of solid carbon dioxide into the bath, or by sending liquid nitrogen through a copper coil suspended in it.

The petroleum ether went solid around the immersed coil at about −145°C and hence was unsatisfactory for use at temperatures below this point. A fixed temperature point at −196°C could easily be attained, however, by using liquid nitrogen as the bath liquid. For the temperature point at +58°C, water heated by an immersion electric heater was used.

In other experiments, the film was held against a flat surface milled along the length of a solid cylinder of aluminum, 2.5 inches in diameter and 10 inches long, suspended in the Dewar flask. This whole piece of aluminum was cooled by

Table I.

SD-12	
Elon	4 grams
Sodium sulfite	160 "
Hydroquinone	12 "
Kodalk	160 "
Potassium bromide	4 "
Benzotriazole	0.8 "
Water to	4 liters
D-19b	
Elon	8.8 grams
Hydroquinone	35.2 "
Sodium sulfite	288.0 "
Sodium carbonate	192.0 "
Potassium bromide	16.0 "
Water to	4 liters

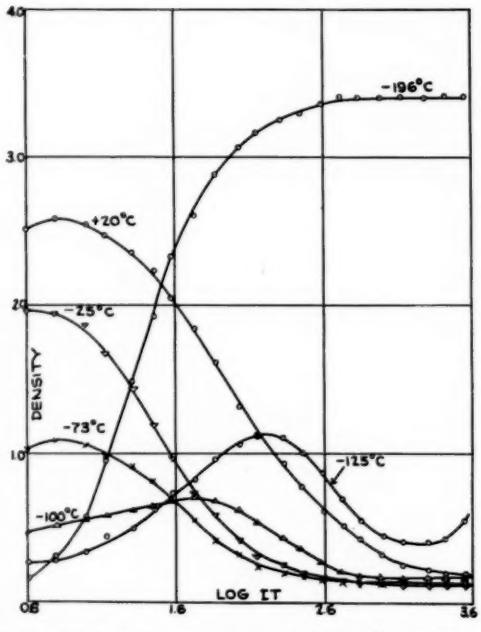

FIG. 1. Effect of temperature on solarization for emulsion I.

introducing liquid nitrogen into a chamber bored along the axis. By proper manipulation this apparatus could be easily maintained at any temperature between room temperature and that of liquid nitrogen.

Low temperatures were measured by means of a pentane thermometer inserted in the bath or into a hole drilled into the aluminum cylinder. Room temperature and +58°C were measured with a mercury thermometer.

For exposures at temperatures other than room temperature, three minutes was allowed after the film was slipped into the apparatus, between the step-wedge and the metal, before starting the exposure. High accuracy is not claimed for the determination of temperature, but, because of the low heat capacity of the film strip, its temperature was undoubtedly very close to that of the metal.

RESULTS

The results of the various experiments will be presented in the form of density *vs.* log exposure curves. Units of exposure are purely relative but are the same for all experiments. Exposures were always extended over the region of solarization but the negative sides of the curves, where density increases with exposure, are, in most cases, not shown.

Effect of temperature on solarization

The first experiments in this study consisted of exposures with the emulsion maintained at different temperatures during the exposure. The range of temperatures covered extends from +58°C to −196°C. The results obtained on the three emulsions I, II, and III are shown in Figs. 1, 2, and 3, respectively. The exposure conditions for these emulsions are given in Table II.

The results obtained for emulsions I and II being qualitatively similar, only the results of emulsion I will be discussed in detail. In Fig. 1, the curve marked 20°C is the normal solarization curve at room temperature. As a result of exposures made on this emulsion at the various temperatures −25°C, −73°C, −100°C, −125°C, and −196°C, the curves shown in Fig. 1 were obtained. As the temperature is lowered below room temperature, the first effect observed is a lowering of the maximum density value. As the temperature drops below −73°C, a shift of this maximum toward higher exposure values takes place. Both of these effects continue with lower temperature until a temperature of about −100°C is reached. Below −100°C, the curve rises again and the solarization decreases. At −196°C a full negative characteristic curve is obtained with no solarization remaining at all. While it is fairly certain that this complicated evolution in the characteristic curve with temperature is due to a variety of causes arising from the effect of temperature on various processes connected with latent-image formation, nevertheless it is believed that the results can be interpreted to give some information concerning the mechanism of solarization. Briefly, it can be said that lowering the temperature sufficiently (−196°C) eliminates solarization entirely.* This

TABLE II.

EMULSION	LAMP DISTANCE *m*	EXPOSURE TIME MIN.
I	1.0	6
II	0.6	2
III	0.6	6

* This result is in agreement with results obtained by Berg (reference 6) and by Nafe and Jauncey (reference 7).

is shown by the results with all three emulsions, as may be seen from Figs. 1, 2, and 3. Accordingly, it appears that whatever the mechanism of solarization may be, sufficiently low temperature renders it inoperative.

Relative to the alteration in shape of the characteristic curve at intermediate temperatures between 20°C and −196°C, certain further remarks can perhaps be made at this point. The great drop with temperature of the negative side of the H and D curve for emulsions I and II, as shown by the fall in maximum density, must be attributed in part to a temperature effect on the regular latent-image process through lowering of the silver ion conductivity of the silver halide grain. However, the very large magnitude of this drop over the range between 25°C and −100°C makes it appear probable that part of this drop in the curve may be due to increase of solarization and to a shift of solarizing action

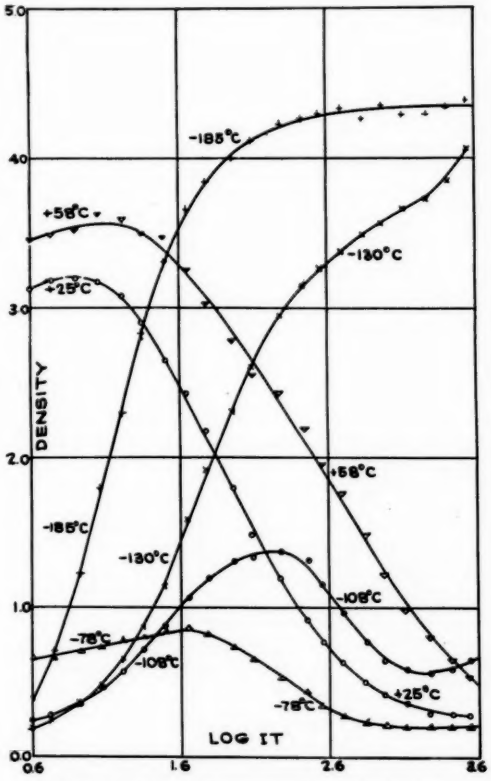

FIG. 2. Effect of temperature on solarization for emulsion II.

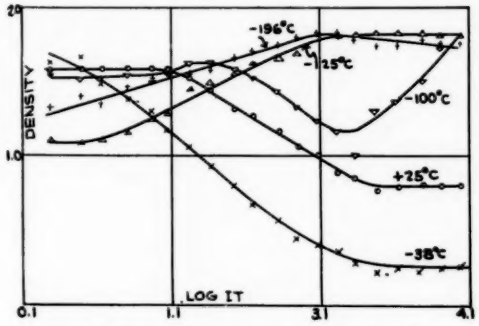

FIG. 3. Effect of temperature on solarization for emulsion III.

into the region of the negative side of the curve. Such an increase of solarization with lowered temperature may be readily understood on the rebromination theory, if it is assumed that gelatin acts as an acceptor for photochemically released bromine during exposure. Lowering the temperature would decrease the reactivity of the gelatin for the bromine and there would result a higher concentration of bromine around the grain to attack the latent-image silver specks. Evidence to support this view is to be found later in this paper in connection with experiments on emulsions to which bromine acceptors were deliberately added. At room temperature these emulsions showed no solarization, but when the temperature was lowered, solarization appeared. When the temperature was lowered still further, however, the solarization again disappeared, which presumably must be attributed to a lessened reactivity of bromine with the latent-image silver. The curves for emulsion III shown in Fig. 3 also seem to be in line with this explanation. Here, the solarization is increased by lowering the temperature from 25°C to −38°C. However, further decrease of temperature below −38°C reduces the solarization, finally eradicating it altogether. This emulsion differs from emulsions I and II in that much greater amounts of exposure relative to that required in the negative region are required to produce solarization. Thus, the solarizing region and the negative region of the curve are widely separated and the conditions are not complicated by solarization shifting over into the negative region.

It is to be noted that the foregoing explanation of the effect of temperature upon solarization is

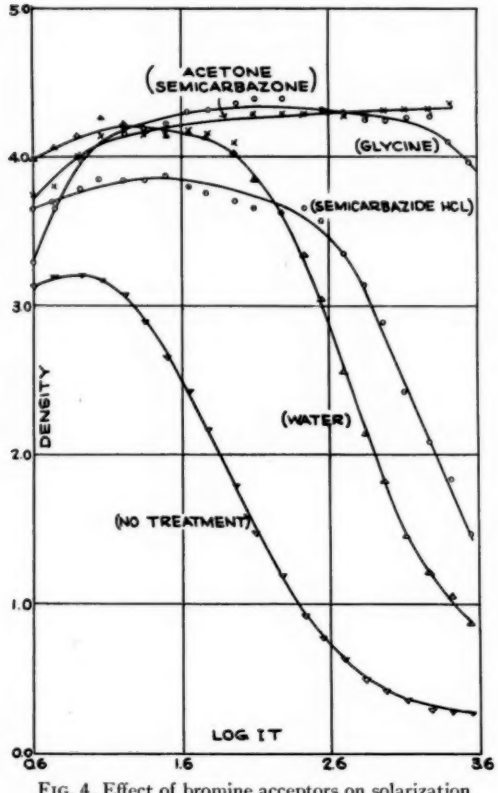

FIG. 4. Effect of bromine acceptors on solarization (emulsion II).

based on the assumption of two chemical reactions of bromine (one with gelatin and the other with silver) with different temperature coefficients.

In discussing the curves of Figs. 1 and 2 for exposure at −196°C, it is not only necessary to account for the absence of solarization at this low temperature, but also to account for the fact that such large maximum densities can be obtained at all for this temperature. The high densities obtained signify that practically all the grains of the emulsion have been rendered developable. According to the Gurney-Mott[4] theory of latent-image formation based on trapping of electrons at the sensitivity specks followed by silver-ion conduction, it is difficult to see how this can take place at such extremely low temperatures. A satisfactory answer seems to have been given by Berg[6] for this. According to Berg, the photographic grain can store up electrons in shallow traps throughout the crystal at low temperatures and these electrons can be liberated when the temperature of the emulsion is raised for development, thereby permitting the latent-image formation to be completed at a higher temperature than that at which the exposure was made. That the silver halide grain can store up electrons at low temperature in the manner outlined appears very plausible in the light of observations on large single crystals of silver halide at low temperature. Below −100°C, it is found that gross illumination of these crystals changes them from insulators into semiconductors. This means that electrons are stored in energy levels lying so closely below the conduction band of the crystal that temperature motion suffices to eject them into the conduction band where they become available for movement through the crystal under an electric field. If this view is correct, then the absence of solarization at extremely low temperatures may be due to the fact that no silver is actually formed during the exposure period, when the bromine is being freed. Thus, the bromine liberated combines with gelatin or diffuses away. When the emulsion is warmed, the latent-image silver then forms after the bulk of the photochemically liberated bromine has escaped. The rather sudden change in the characteristic curve in the region around −100°C makes this explanation appear very plausible.

Whether the absence of solarization at low temperature is due to the nonreactivity of bromine and silver at low temperature or whether it is due to the fact that silver is not formed and therefore is not available for attack by the bromine at the low temperature, is not important for the present discussion. Either mechanism alone or a combination of them fits in with the general rebromination theory of solarization.

TABLE III. *Treatment with bromine acceptors.*

SHEET	SOLUTION CONTAINING BROMINE ACCEPTOR
1 (check)	(untreated)
2 (check)	(distilled water only)
3	1 percent semicarbazide HCl, brought to *p*H of emulsion
4	1 percent acetone semicarbazone
5	saturated solution of *p*-hydroxyphenol glycine, brought to *p*H of emulsion
6	1 percent sodium nitrite

An analysis of the large and small grains of emulsion I was made. It was found, after fractionation by centrifuging, that the largest grains (2 percent of the total) had the same silver halide content as the smallest grains (2 percent of the total). This fact eliminates interpretations based upon chemical differences in the halide content of the grains as a function of grain size.

Action of Bromine Acceptors

As was apparent in the previous section on solarization as a function of temperature, it is probable that at room temperature some of the photolytic bromine which might otherwise be utilized for rebromination is taken up by the gelatin of the emulsion, thus reducing the degree of solarization attained. This hypothesis appears to be supported by the behavior of an emulsion treated with chemicals known to be good bromine acceptors.

Several of these chemicals were added (singly) to emulsion II by bathing sheets of the coated emulsion for 5 minutes in solutions at 65°F, as shown in Table III. After being bathed, the sheets were dried before exposure.

Strips from sheets 1–5, inclusive, were exposed at +25°C for 2 minutes with the lamp at 0.6 meter, and then processed as usual. Curves

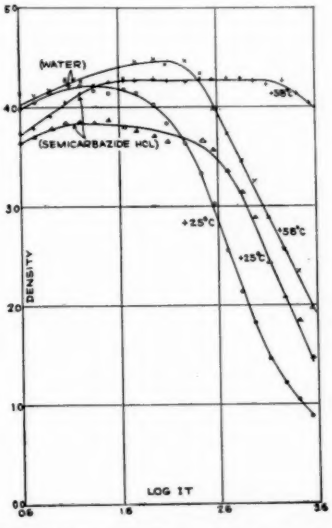

Fig. 5. Effect of temperature variation on solarization in an emulsion treated previously with a bromine acceptor.

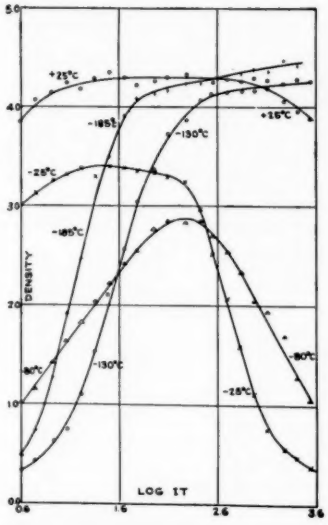

Fig. 6. Effect of temperature variation on solarization for an emulsion treated previously with $NaNO_2$.

plotted from the resulting densities are shown in Fig. 4. Each curve is labeled with the name of the compound used to treat the emulsion before exposure. Curves labeled "No Treatment" and "Water" are for comparison. The difference between these two curves is probably due to the removal of soluble halide by the water treatment. At +25°C the film strips bathed in acetone semicarbazone and glycine no longer exhibit solarization in the region of exposure where it appears on the untreated emulsion. Semicarbazide HCl was not very effective in reducing solarization at +25°C, but it became so at +58°C, as can be seen from Fig. 5. Here are shown curves obtained at +25°C and at +58°C for strips treated with this compound and also for check strips treated with water alone. Exposure conditions were the same as those given above.

In accordance with the rebromination theory of solarization, these facts may be explained as follows: At +25°C the bromine acceptors acetone semicarbazone, and glycine, when incorporated in the emulsion as indicated above, have sufficient acceptor action to prevent photolytic bromine from reaching and combining with the silver of the development centers. According to this point of view, the beginning of solarization seen at the high exposure end of the curve for the emulsion treated with glycine is to be

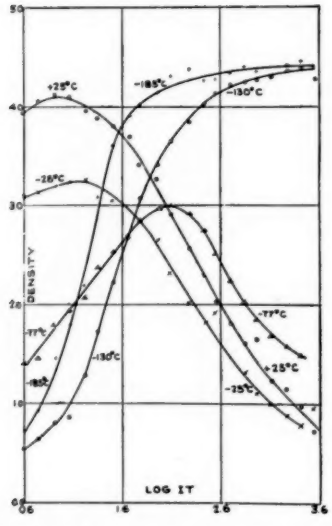

FIG. 7. Effect of temperature variation on solarization for an emulsion treated previously with water. (To be compared with Fig. 6.)

attributed to the exhaustion of the glycine by combination with bromine. Photolytic bromine formed thereafter would be available for rebromination of latent-image silver.

Semicarbazide HCl, on the other hand, appears to be a less efficient bromine acceptor at +25° than the other compounds. When the emulsion containing this acceptor is warmed to +58°C, however, solarization disappears, indicating an increase in the rate of reaction of the bromine with semicarbazide HCl. That the observed effect is not due to gelatin alone can be seen in Fig. 5, from which it appears, nevertheless, that the acceptor action of gelatin is also greater at +58°C than at +25°C.

A more detailed picture of the effect of temperature upon the solarization of an emulsion treated with a bromine acceptor is shown in Fig. 6, which pertains to strips from sheet 6 of Table III (treatment with sodium nitrite). Exposures of two minutes' duration, with the lamp at 0.6 meter were made at various temperatures from +25°C to −185°C. These temperatures are marked on the corresponding curves. For comparison, results for the same emulsion treated with water only are shown in Fig. 7.

At +25°C sodium nitrite prevents solarization of this emulsion, but with decreasing temperature solarization appears. According to the rebromination theory, this would be caused by a decreasing rate of reaction of bromine and gelatin, with falling temperature. This lowered rate of reaction makes bromine available for rebromination of development centers while the temperature is still high enough for this rebromination to occur. Thus, for example, there is pronounced solarization at −80°C. In fact, this curve is very similar to the curve obtained at −77°C for the emulsion treated with water alone, which indicates that the sodium nitrite has become practically inactive at −80°C. At −130°C and −185°C the curves for the emulsion with nitrite added are practically identical with those for the water-treated emulsion.

The similarity in the results for the emulsion treated with a bromine acceptor (Fig. 6) and for the same emulsion treated with water alone (Fig. 7) is very striking. The only difference appears to be in the degree of bromine acceptor action at the higher temperatures. In both cases this action decreases as the temperature decreases, with a resultant increase in solarization. Below a certain temperature, however, solarization again decreases, and finally disappears because of the factors discussed previously in connection with the effect of temperature upon the solarization of the untreated emulsion (Fig. 2).

TREATMENT WITH DILUTE SOLUTION OF HYPO AFTER EXPOSURE BEFORE CHEMICAL DEVELOPMENT

This experiment was undertaken to find out whether or not the solarization of an emulsion could be removed, for chemical development, by treating it with a silver bromide solvent after exposure and before development. The solvent chosen was a dilute solution of hypo of the

TABLE IV.

STRIP	BATHED IN DISTILLED WATER AT 65°F	BATHED IN DILUTE HYPO AT 65°F	WASHED IN RUNNING WATER
	MIN.	MIN.	MIN.
1 (check)	5.0	—	2.5
2	4.5	0.5	2.5
3	1.0	4.0	2.5

following composition:

Dilute Hypo
16.0 grams $Na_2S_2O_3$
1.0 gram Na_2SO_3
Water to make 1.0 liter.

Emulsion I was used. Three strips were exposed for 30 seconds each, with the lamp at 0.6 meter distance. Table IV below summarizes the subsequent treatment of these strips. For each strip treatment followed the sequence from left to right in the table.

The strips were subsequently developed without first being dried.

The results are shown in the curves of Fig. 8, each of which is marked with the time of treatment in dilute hypo. The curve marked "Water Only" is the control, showing that treatment with water alone after exposure does not destroy the solarization. A time of only half a minute in the dilute hypo, however, was sufficient to reduce strongly the solarization of the emulsion. Bathing for four minutes removed all but a trace of the solarization but also greatly reduced the maximum density.

On the basis of the rebromination theory, these results may be explained as follows: Dilute hypo removes the protective coating of silver bromide which has formed during exposure upon the surfaces of some of the development centers

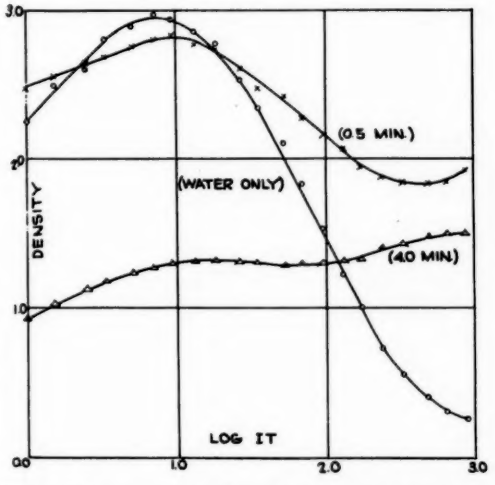

FIG. 8. Effect on solarization of bathing an exposed and solarized emulsion in dilute hypo solution.

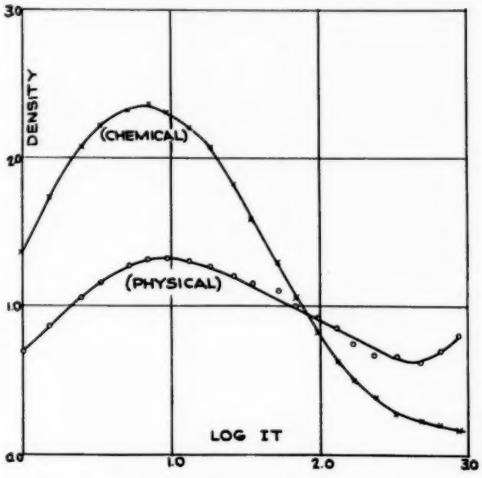

FIG. 9. Solarization compared for chemical and physical development.

formed during the earlier stages of exposure. These centers are thus made accessible to the developer again, and hence regain their developability. This results in the disappearance of solarization. Brief treatment in the hypo does not allow time for the protective layers to be removed from all of the solarizing grains, so that solarization is not thereby completely removed. Treatment prolonged sufficiently to make all solarizing grains developable once more dissolves so much of the silver bromide of the original grains that the maximum density is reduced.

SOLARIZATION WITH PREFIXATION PHYSICAL DEVELOPER

If solarization is caused by rebromination of silver on the surfaces of what would otherwise be development centers, it should occur for both chemical and prefixation physical development, since presumably the protective layer would act against both kinds of developers.

Figure 9 shows the behavior of emulsion I in a chemical developer and in a physical developer. Solarization appears in the same region for both types of development.

The film strips used were each exposed for 30 seconds with the lamp at 0.6 meter. Chemical development was for 3 minutes in SD-12 developer at 65°F. Physical development was for

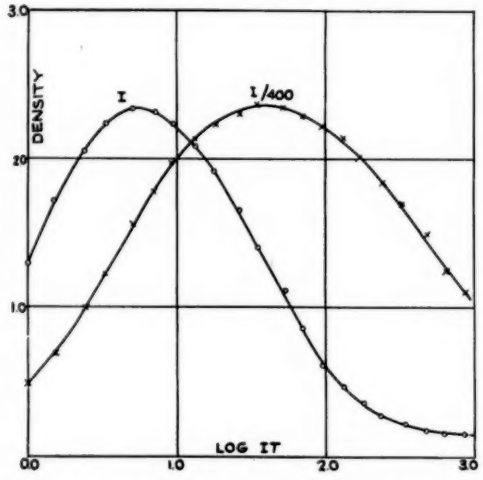

FIG. 10. Curves showing the effect of intensity of light during exposure on solarization.

30 minutes in the developer whose formula is given in Table V, at 45°F.

TABLE V. *Physical developer.*

SOLUTION A	SOLUTION B
20 grams elon	10% $AgNO_3$
100 grams citric acid	
5 grams gum arabic	
Water to make 1.0 liter	
Use 291 cc of solution A+9 cc of solution B.	

EFFECT OF INTENSITY LEVEL ON SOLARIZATION

If solarization is caused by rebromination of the latent image by halogen liberated during overexposure, then it would appear that exposures made at different intensity levels would show different degrees of solarization. The reasoning here is that if an exposure is made at high intensity, the bromine would reach a higher concentration immediately surrounding the grain than if the exposure were made at a low intensity.

To test this hypothesis, solarizing exposures were made on emulsion I, using two different intensity levels in the ratio 1 : 400. The high intensity exposure was made with the lamp at 0.6 meter, $t=30$ seconds. The times of the exposures were varied reciprocally so that the total exposure in the two cases remained the same. The results are shown in Fig. 10. It may be seen that much greater exposures are required to produce the same degree of solarization with the low intensity exposure than with the high intensity exposure. There is a shift in the negative side of the curve which is to be attributed to reciprocity law failure. In spite of this, however, the shift in the solarizing part of the curve has changed by an amount greater in log units by 0.5. Thus, it appears that the shift in solarization region with lowered intensity is in the direction to be expected on the basis of the rebromination theory.

SUMMARY

Experiments were carried out to test the regression theory of solarization in its specific form which attributes this action to rebromination of the development centers by photochemically released bromine during gross overexposure. The experiments consisted of the following:

1. Exposures at various temperatures from +58°C to −196°C.
2. Experiments to test the effect of bromine acceptors on solarization.
3. Effect on solarization of treatment by silver halide solvents.
4. Measurement of solarization with prefixation physical development.
5. Measurement of solarization with different intensity levels of exposure.

One complete set of the above experiments was carried out on one particular type of emulsion. The temperature experiments were checked on a second emulsion.

It is thought that all the results of the above series of experiments are in agreement with the rebromination theory of solarization.

ACKNOWLEDGMENT

The authors wish to express their appreciation to Dr. B. H. Carroll, Mr. R. M. Evans, Dr. W. T. Hanson, Dr. J. A. Leermakers, Dr. C. J. Staud, and Dr. H. C. Yutzy, for valuable discussion in connection with the experimental work and the interpretation of the results given in the present paper. The authors also desire to thank Dr. Staud and Dr. Yutzy for their collaboration in preparing the two experimental emulsions used in this work.

There is System in Color Preferences

J. P. GUILFORD
University of Southern California, Los Angeles, California
(Received July 29, 1940)

IT is frequently said that preferences for colors are a purely personal matter, and even when it is admitted that there is agreement among individuals it is often maintained that conformities are imposed by the culture in which we live. These views are often held in the face of results which show that different races, living in different parts of the world, hold color preferences in common. There is agreement, in the main, that blue, green, and red stand high on the scale of preferences while yellow, orange, and violet are generally less preferred, as shown in the experimental findings.

The mass of repeated results has failed to win complete conviction for several reasons. Most investigators have used only a small number of color samples, usually from 6 to 10. What is more serious, they have almost invariably failed to control the factor of *lightness* (tint, brightness, or brilliance) and the factor of *saturation* (chroma, or purity) when drawing conclusions about the effects of *hue* (color tone; determined primarily by dominant wave-length). Two investigators may report the use of a "red" sample, but there are hundreds of reds; which particular red did each one use? Even supposing that they did employ the red of the same lightness and saturation, was the yellow they also used equal to the red in lightness and saturation? This is a serious matter if these two attributes of color are determining factors for likes and dislikes. Divergences among previous results may well be due to the disregard of these two attributes of color.

A few years ago the writer attempted to correct these defects in technique by employing 40 colors which were selected and evaluated with regard to lightness and saturation as well as hue.[1] Evaluations for hue, lightness, and saturation were made for the samples in terms of the *Munsell Book of Color*,[2] which offers quantitative descriptions of colors in psychologically equal steps with respect to the three attributes of color. From a sub-group of 18 samples of approximately equal lightness and saturation, but varying in hue, it was discovered that the average affective value[3] (as determined by a rating-scale method with 10 adult judges) varied as a continuous function of hue. Three maxima occurred, at red, green, and blue, and three minima, at yellow, blue-green, and violet, somewhat in accord with earlier results. The regression curve gave the appearance of a sine-cosine function and so a Fourier analysis was made. A Fourier series including only the first and third harmonics fitted the relationship very well. From all 40 samples it was found that in general the affective value increased with increasing lightness of the color and also with increasing saturation. The affective value of a color could then be described as a function of a linear combination of lightness and saturation and a sine-cosine function of hue.

For several reasons it was decided to undertake a much more intensive examination of the relationships that were only suggested in the study of 40 colors. It was deemed necessary to sample systematically the entire surface-color solid. For this purpose, samples of every degree of Munsell chroma (saturation) and of alternate degrees of Munsell value (lightness) were selected from alternate hues of the *Munsell Book of Color*. From available colored papers as many of the selected samples as possible were obtained, giving nearly 300. In addition, a series of grays was obtained, with 21 samples between the limits of black and white. The total list included 316 specimens.

These specimens were cut into 2-inch squares and glued to gray cards which had a Munsell rating of *N* 5, or medium gray. The samples were exposed to observers in an enclosure that was built to fit a table top 30″×48″ and which was

[1] J. P. Guilford, "The affective value of color as a function of hue, tint, and chroma," J. Exper. Psych. **17**, 342–370 (1934).

[2] *Munsell Book of Color* (Munsell Color Company, Baltimore, 1929).

[3] By "affective value" is meant the numerical position of a stimulus on the psychological continuum that extends from extreme unpleasantness to extreme pleasantness.

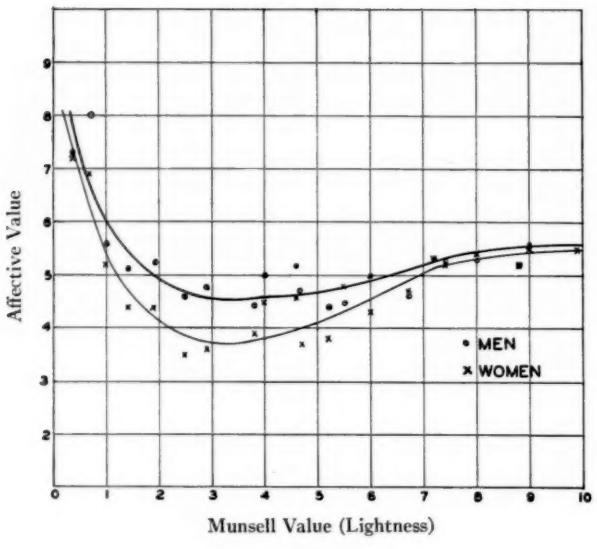

FIG. 1. Relationship between affective value (preferences) and Munsell value (lightness) for achromatic samples. The indifference point is at 5.5 on the affective scale. Pleasant samples exceed this value while unpleasant ones are below it.

lined with gray paper rating *N* 5. The interior was illuminated by means of four 60-w Mazda daylight lamps which were shielded from the direct view of the observers. The observer's head was kept at a constant position at one end of the enclosure and the color samples were exposed singly for only 5 sec. each at the opposite end. A rating scale of 11 numerical points was provided, extending from 0 (defined as "the most unpleasant imaginable") to 10 (defined as "the most pleasant imaginable") with a rating of 5 (defined as "indifferent; neither pleasant nor unpleasant") at the middle. The judges were 40 university students, 20 men and 20 women of normal color vision, each of whom made two independent sets of judgments on two different days.[4] The self-consistency of the judgments is indicated by self-correlations of 0.62 to 0.81 for the individual men, and 0.53 to 0.84 for individual women. Average ratings for the colors were obtained by computing medians. The reliabilities of the pooled ratings were estimated by correlating two random sets. These self-correlations were 0.94 for the men's averages and 0.93 for the women's.

The relationship of affective value to lightness for the gray samples is shown in Fig. 1. The curves, for men and women separately, were fitted freehand to the data and they show that while men and women differ slightly, the two functions are continuous and similar in type. The grays are slightly to moderately unpleasant between Munsell *N* 1 and *N* 8, a median rating of 5.5 being at the indifference point.[5] The darkest blacks are moderately pleasant, while the very light grays and white are near the indifference point. It should be remembered that, as far as we know, these functions, and the others to be mentioned later, hold only for the conditions of the experiment; 2-inch squares of surface colors on a background of medium gray when viewed in daylight in sequence with a great variety of color samples. The goodness of fit of the data to the freehand curves is indicated by correlations of 0.87 for the men and 0.94 for the women. It is interesting to note that many observers reported an ambivalent attitude toward the black specimens. The same individual might waver between strong liking and strong disliking during the same observation, or report strong liking at one

[4] I am deeply indebted to Mrs. Ada P. Jorgensen and to Miss Patricia Cain for obtaining the data upon which this brief report is based. More complete details as to procedure and results will be published elsewhere (see, for example, J. P. Guilford, "A study in psychodynamics," Psychometrika **4**, 1–21 (1939)).

[5] The indifference point is at 5.5 rather than at 5.0 because in computing medians it was assumed that a rating of five represented an internal extending from 5.0 to 5.99 inclusive, and similarly with other numerical ratings.

time and strong disliking at another. The reasons for this have not as yet been determined.

It must not be supposed that the curves in Fig. 1 serve as the prototype for the relation of affective value to lightness when the samples are chromatic. For very unsaturated samples there was some resemblance, but for the saturated colors the regressions were very different. In no case, with hue and saturation held constant, were the regressions linear. They were usually curves of the second degree, in other words without inflection points. The general rule held that for warm colors (red to yellow) the curves were concave upward, and for cool colors (green to blue) they were concave downward. The significance of this rule has not been determined, except that it is true that the cool colors have their maximum saturations at the more moderate lightnesses whereas the warm colors, particularly orange and yellow, have their greatest saturations at high levels of lightness.

The regressions of affective value upon saturation, when hue and lightness are held constant, were also curved, almost always concave upward and without inflection points. For every hue considered, the regression of affective value upon lightness and saturation simultaneously would be represented by a continuous curved surface. There were no attempts to fit mathematically-defined surfaces to the data for any hue. A graphic smoothing process was used, taking into consideration both lightness and saturation, until consistent, continuous regressions both ways were obtained.

While keeping lightness and saturation constant at various combinations of levels for both, a series of curves of relationship between affective value and hue were determined. A family of such curves, derived from the judgments of the women for Munsell chroma 6, is given in Fig. 2. While these curves, and the others, could probably be described as trigonometric functions, no Fourier analysis has as yet been attempted for any of them. By means of successive smoothings, these curves have been made consistent with the regressions on lightness and saturation. The goal was to find graphically a means of predicting affective value from the Munsell notations of a color.

As a more practical device for showing these relationships, and also for making quick predictions, *isohedon* charts were prepared for each of the 10 hues, treating judgments of men and women separately. An isohedon chart for any hue shows the lines of equal affective value or preference. Figure 3 exhibits such a chart for men's judgments of reds. For any color sample whose hue is red, having determined its Munsell value and chroma, one can easily read off its most probable average value for liking or disliking. Thus, a red of Munsell value 7 and chroma 10 (briefly designated as R 7/10) would have an expected affective value of 6.8, and Munsell R 3/12 would have an expected affective

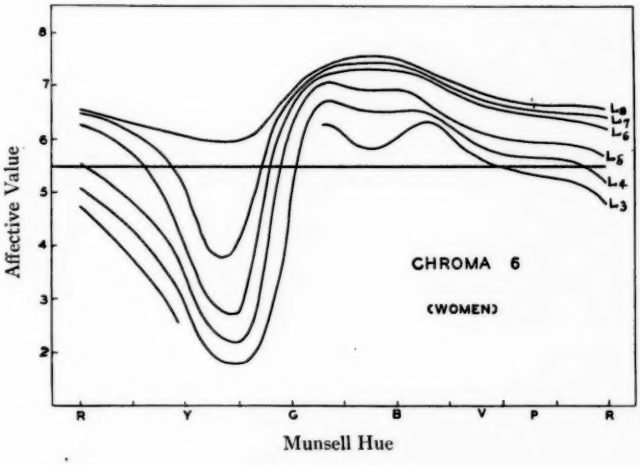

FIG. 2. Relationship between affective value and Munsell hue of color samples for Munsell chroma (saturation) constant at 6.0. The relationship is indicated for Munsell value (lightness) ranging between 3 (L_3) and 8 (L_8).

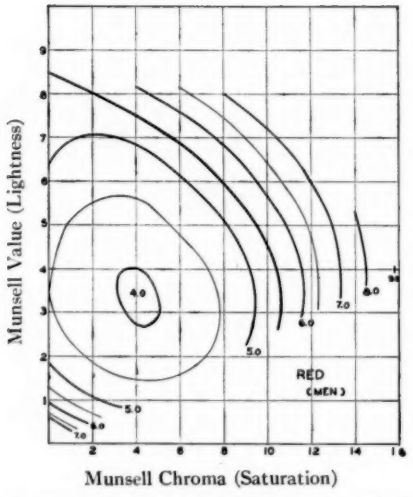

FIG. 3. An *isohedon* chart showing lines of equal affective value for colors of red hue as judged by men.

value of 6.3. The heavy line at 5.5 indicates the division between likes and dislikes. Color samples to the right of it are all pleasant; those to the left, with the exception of the colors very close to black, are unpleasant. The isohedon lines cover only that portion of the entire rectangular chart in which colors actually occur; other positions represent impossible combinations of hue, lightness and saturation. The isohedon lines at the extreme lower left are suggested entirely by the ratings of the gray samples and by the rest of the configuration of the chart. These lines are therefore largely extrapolations.

The goodness of fit of these much-smoothed graphic predictions of affective value was tested by the correlation method. The expected preference value for every color sample was determined from the proper isohedon chart. For every chart a coefficient of correlation was computed for the relation between observed and predicted values. The results are given in Table I. From the inspection of Table I it will be seen that in general the predictions were closer for men than for women and that the correlations were mostly above 0.90. Predictions appear to be least valid for the hues of orange (Munsell's yellow-red), for green-yellow, and for purple. This result held true for both men and women. The purples, in particular, gave quite variable results.

The correlations between observed and predicted values for all colors combined were 0.93 for the men and 0.88 for the women. When these coefficients are corrected for attenuation in the judgments of color alone they become 0.96 and 0.92, respectively. These coefficients indicate a very strong determination of average preferences for colors when other factors than hue, lightness, and saturation have been ruled out of the picture. The prediction of preferences of individuals, would of course, be less accurate when made on the basis of the common isohedons. There is some possibility that average preferences of other groups of judges would be less accurately predicted on the basis of the system derived from these particular judges. In spite of these qualifications, the results point very strongly to a basic communality of color preferences among individuals. This communality probably rests upon biological factors, since it is hard to see how cultural factors could produce by conditioning the continuity and system that undoubtedly exists.

Some indication as to sex differences in preferences is given in the last row of Table I, in which are shown the correlations between ratings of men and women for the colors belonging to each of the 10 hues. The correlations are in general very high, in fact about as high as the self-consistency with each sex, at least within the range of hues from yellow to purple-blue. The lowest correlation is 0.27, for the red-purples, and the next lowest is for the yellow-reds. In general, the agreement between the sexes is lowest where the predictability is lowest and probably where the reliabilities of judgments are also lowest.

It is possible that the purples are judged less consistently because of the peculiar spectral composition of their stimuli. Though none of our samples approaches spectral homogeneity, many

TABLE I. *Correlations between observed and predicted affective values for the ten hues, and the correlations between preferences of men and women.*

HUE	R	YR	Y	GY	G	BG	B	PB	P	RP	ALL 10 HUES
Men	0.96	0.83	0.97	0.86	0.97	0.93	0.95	0.94	0.81	0.87	0.93
Women	.93	.80	.90	.79	.92	.92	.96	.91	.77	.90	.88
M. and W.	.88	.67	.94	.92	.93	.96	.95	.91	.70	.27	.84

R = red, Y = yellow, G = green, B = blue, P = purple.

of them probably have wave-length distributions of reflected energy that are unimodal, whereas purples result from a combination of long wave and short wave energy. The relation of affective value to wave-length as such is unknown and can only be suggested by our results. We chose to use the variable of hue rather than that of wave-length for the reason that an observed hue is a constant psychological event (at least cognitively) that may be produced by a variety of spectral compositions to which, as such, we are oblivious when observing the color. Another reason is that the variable of hue includes the purples whereas the variable of wave-length does not include them in the spectrum. It may be that affective reactions are more discriminating with regard to the spectral composition of chromatic stimuli than are cognitive reactions, that wave-lengths as such have a more direct and unique influence upon our feelings than upon our awareness of color as such. This could be true because cognitive and affective reactions depend upon different cerebral levels of functioning. This is, to say the least, an interesting hypothesis to be followed up. The question of sex differences in color preferences will be more fully analyzed and reported elsewhere. It has been the purpose of this short article merely to point out the kind of system that exists when color preferences are related to the attributes of color.

New Polaroid Study Lamp

THE Polaroid Corporation of Cambridge, Massachusetts, is now manufacturing for the first time a popularly priced Polaroid study lamp that gives promise of being the modern successor to the old-fashioned type of "gooseneck" lamp. Designed to fit a student's budget, the new lamp offers glareless Polaroid light for only $2.95.

The outward simplicity of the lamp belies the difficulty of the engineering problems that had to be solved before a successful attempt could be made at mass production, the reason for its extremely low cost. This method of manufacture places the new Polaroid study lamp in the same class with refrigerators, electric irons, and other modern products that similarly reach a vast public at a popular price as a result of mass production.

FIG. 1.

Advantages of glare-free light are well recognized. Black type may actually disappear from a white printed page under certain glare conditions. But even under the most severe glare condition, it has been determined that the proper introduction of Polaroid sheeting in the light path completely dissipates the undesirable glare element, and restores the print-to-paper contrast that is necessary for effortless seeing.

Typical of all Polaroid light is the fact that its glareless quality makes the intensity unapparent. Light meter readings prove that the new Polaroid study lamp produces adequate illumination over the working area of a desk.

A walnut-finished Bakelite stem and base with a shining copper trim, and an eggshell-brown parchment type shade combine to make a sturdy lamp that is both functional and pleasing in appearance.

Light from a hundred-watt bulb is projected through the Polaroid antiglare material by a mirror-like reflector under the lamp shade. This projecting device produces the desired direction, intensity, and uniformity of the light over the working surface of a desk. No diffusing devices are necessary in Polaroid lamps; the Polaroid light-control material under the lamp shade removes all glare.

Specially designed ventilation slots dissipate the heat produced by the bulb; the lower half of the column remains cool to the touch after many consecutive hours of operation.